Development of a Methodology for Comprehensive Analysis of Lipid-Membrane Protein Interactions Using Lipid-Immobilized Beads

森藤, 将之

Doctoral Thesis

Development of a Methodology for Comprehensive Analysis of Lipid-Membrane Protein Interactions Using Lipid-Immobilized Beads

Masayuki MORITO

Department of Chemistry

Graduate School of Science

Kyushu University

Contents

Chapter 1
General Introduction

1.1 Biological Membranes and Membrane Proteins

Biological membranes act as critical boundaries that separate cells and organelles from their external environments. They are composed fundamentally of lipid bilayers and their associated membrane proteins (MPs), which limit the free diffusion of substances across the membrane. However, the inner space enclosed by biological membranes is not completely isolated; MPs facilitate the functional and selective transport of substances across membranes and signal transduction. In mammals, approximately 30% of all proteins are MPs,[1] which localize to the appropriate membranes, such as plasma membranes and intracellular membranes, to perform various cellular functions. For example, the sodium-potassium pump, localized in the plasma membrane, actively transports sodium and potassium ions across the cell membrane to maintain the membrane potential of cells (**Figure 1.1a**).[2] Additionally, the adrenergic receptor, a G protein-coupled receptor, undergoes a structural change upon binding extracellular adrenaline, activating G proteins and transmitting signals into the cell (**Figure 1.1b**).[3] Thus, biological membranes not only separate the interior of the cell from the outside but also serve as platforms on which various membrane proteins function to maintain vital activities.

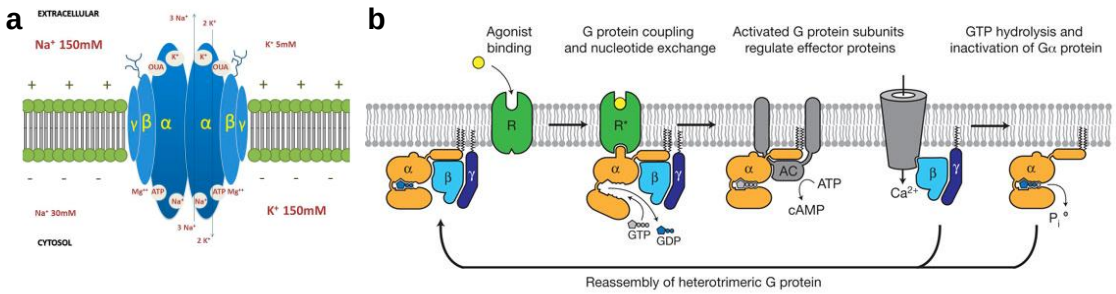

Figure 1.1. (**a**) An illustration of sodium-potassium pump inserted in plasma membranes. Ionic transport is accomplished by ATP hydrolysis to maintain the concentration gradients of ions inside and outside the cell. This figure is cited from ref 2. (**b**) Signaling pathway through the adrenergic receptor. The binding of extracellular agonists, including adrenaline, to the receptor induces structural changes, leading to signal transduction mediated by G-proteins. This figure is cited from ref 3 with permission from SNCSC.

1.2 Membrane structure and lipid diversity

The structure of biological membranes is described by the fluid mosaic model, proposed by Singer and Nicholson in 1972 (**Figure 1.2**).[4] In this model, lipid molecules form lipid bilayers, which are described as a two-dimensional fluid. Membrane proteins are embedded in and diffuse freely within lipid bilayers. Thus, lipids have been thought to be the medium in which membrane proteins float. On the other hand, the lipids that constitute lipid bilayers have diverse structures. The lipid database, Lipid Maps,[5, 6] is divided into eight categories (Fatty acyls, Glycerolipids, Glycerophospholipids, Sphingolipids, Sterol lipids, Prenol lipids, Saccharolipids, and Polyketides), each of which has its own subcategory. It is estimated that more than 40,000 lipid species, including predicted structures, exist in the biological world. However, such lipid diversity would not be necessary, if the lipid bilayer is merely a medium in which membrane proteins float, as was assumed in the classical fluid mosaic model. This lipid diversity is one of the important challenges in life sciences.

As research into biological membranes has progressed, the fluid mosaic model has been revised. Recent findings showed that lipids were not uniformly mixed within biological membranes but are distributed heterogeneously. Biological membranes contain microdomains called lipid rafts (**Figure 1.3**).[7, 8] Lipid rafts are defined as heterogeneous and highly dynamic membrane domains rich in sterols and sphingolipids, with diameters ranging from 10–200 nm.[9] It has been reported that GPI-anchored proteins,[10, 11] and several receptors[12, 13] and channels,[14, 15] localize to lipid rafts. Lipid rafts function as platforms for signal transduction by facilitating the localization and association of these proteins.[16] Interestingly, the interior of lipid rafts is not uniform, suggesting the presence of nano-subdomains,[17] which may determine the properties of lipid rafts. In addition to this lateral asymmetry, biological membranes also exhibit vertical asymmetry. The distribution of lipids differs between the inner and outer leaflets of the cell membrane,[18-21] with sphingomyelin (SM) and phosphatidylcholine (PC) being more abundant in the outer leaflet, and phosphatidylethanolamine (PE), phosphatidylserine (PS), and phosphatidylinositol (PI) in the inner leaflet. In apoptotic cells, PS that should be localized in the inner leaflet is exposed on the cell surface, and macrophages recognize the outer PS, resulting in phagocytosis.[22, 23] In this way, diverse membrane lipids contribute to the nanoscale heterogeneous structure of biological membranes and play crucial roles in the complex regulation of various cellular functions.

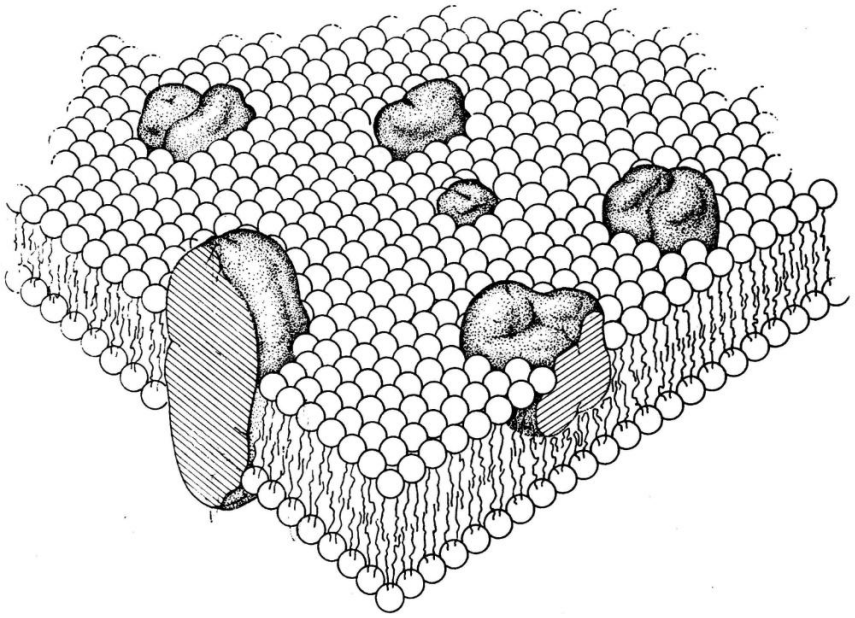

Figure 1.2. Biological membrane described as fluid mosaic model. This figure is cited from ref 4 with permission conveyed through Copyright Clearance Center, Inc.

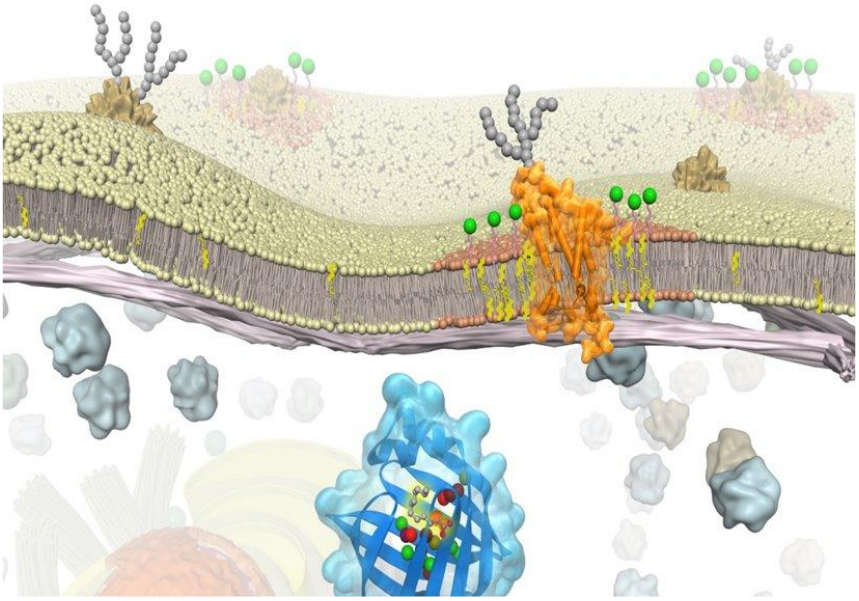

Figure 1.3. Schematic diagram of the raft structure in a biological membrane. This figure is cited from ref 17 with permission conveyed through Copyright Clearance Center, Inc.

1.3 Lipid-MP Interaction

Numerous proteins are expressed within a cell and are involved in various physiological functions. To sustain cellular activities, *specific MPs* must function at *specific times* and *specific locations*. This intricate regulation of MP functions in the cell can be explained by "lipid-MP interactions." Namely, specific membrane lipids interact with certain MPs, regulating their function and structure. This would require the heterogeneity and diversity of lipids. Supporting this hypothesis, many specific lipid-MP interactions have been identified in recent years.[24-27] For instance, it was shown that sphingomyelin (SM) contributes to the dimerization and activation of p24, an MP present in COPI vesicles involved in Golgi transport (**Figure 1.4a**),[28] and that cholesterol (Chol) activates a bitter taste receptor (**Figure 1.4b**).[29] Therefore, lipid-MP interactions are essential for understanding the regulation of cellular life functions.

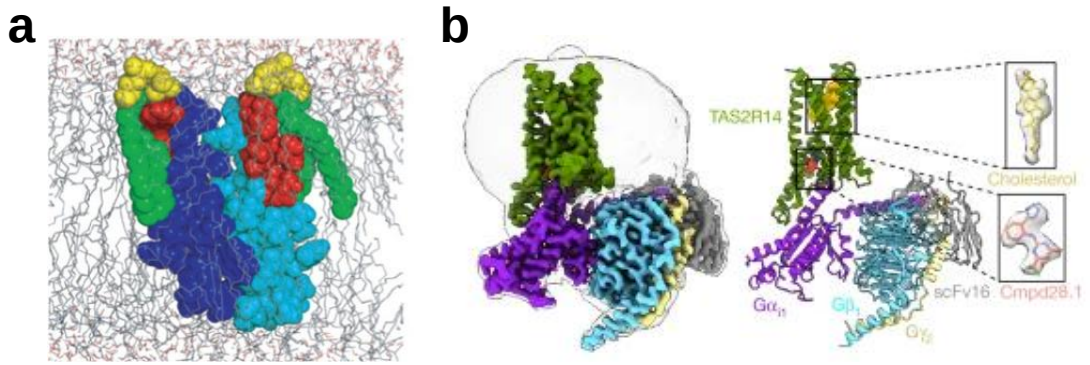

Figure 1.4. (**a**) SM–p24 interaction. The interacting lipid and residues of p24 are highlighted. Blue and light blue, transmembrane domain of p24; red, sphingomyelin-binding pocket; yellow, SM 18:0 head group; green, SM 18:0 backbone and *N*-acylated fatty acid. This figure is cited from ref 28 with permission from SNCSC. (**b**) The interaction between type 2 taste receptors (TAS2R, green) and cholesterol (yellow). This figure is cited from ref 29 with permission from SNCSC.

1.4 Analysis of Lipid-MP Interaction

The detailed investigation on the allosteric action of lipids towards MPs requires "lipid-MP interaction analysis," but methods for this are limited. For example, complex structures of MPs and lipids have been reported by X-ray crystallography[24, 25, 30] and recent single-particle analysis using cryo-EM.[26, 31, 32] Such structural analysis clearly demonstrated the binding sites and interaction modes of lipids, as exemplified in **Figure 1.4b**, and triggered the recognition of the importance of the interactions between lipids and MPs. However, the throughput for those complex structure analyses is not high, and lipids are not always observed in the structure due to their disorders. On the other hand, a technique called native MS, which ionizes proteins without denaturing them, has enabled measurements of mass spectrometry of lipid-MP complexes.[33-36] However, application of this method requires the highest level of mass spectrometry equipment and optimization of surfactants and ionization conditions.

These methods aim to identify "MP-binding lipids"; however, methods for identifying "lipid-binding MPs" are further scarce and limited. A conventional method for the identification of lipid-binding MPs is liposome coprecipitation (**Figure 1.5a**).[37-40] This method has revealed, for example, that coronin1A, a critical regulator of branched actin network, binds to phosphatidylinositol 4,5-bisphosphate.[41] However, this method is incompatible with the presence of surfactants, rendering it unsuitable for screening detergent-solubilized MPs. Several chemical biology-based methods have also been reported for detecting lipid-specific MPs using photoaffinity-labeled lipids (**Figure 1.5b**)[42, 43] but their application is still limited due to problems such as intracellular metabolism of photoaffinity-labeled lipids and/or competition with native lipids existing in large amounts in the cell.

So far, the methods described above have been applied to a limited number of lipids and MPs by a limited number of research groups because of their low versatility and throughput. The lack of practical methodologies is a major reason for the slow progress in this research field. To overcome this situation, a systematic method with high throughput, comprehensiveness, and ease of use is required.

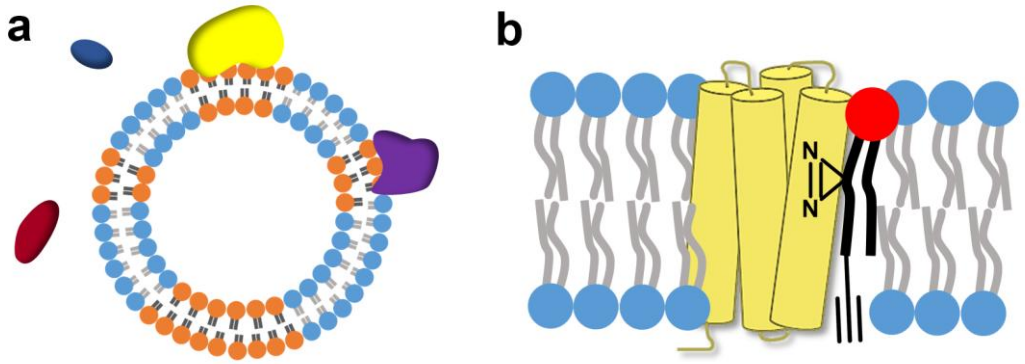

Figure 1.5. (**a**) Liposome coprecipitation.[37-40] Liposomes are incubated with a protein mixture, and the binding proteins are then centrifuged together with the liposomes. (**b**) Photoaffinity labeling method.[42, 43] Photoaffinity-labeled lipids are introduced into the cells. After UV irradiation, diazirines form reactive carbene species, which covalently capture nearby proteins. The captured proteins are collected using a click-chemistry method with the alkyne group contained in the probe.

1.5 Purpose and Contents of this Study

Diverse lipids regulate the function of MPs through interactions with them. Assuming that lipids and MPs have co-evolved, such allosteric regulations of lipids on MPs are considered reasonable and universal. To investigate this regulation in detail, lipid-MP interaction analysis is required, but methods for this are limited, especially in the analysis of lipid-binding MPs. To solve this issue, the author developed a comprehensive and systematic approach for identification of lipid-binding MPs with high-density lipid-immobilized beads. In this study, lipid molecules were covalently

immobilized onto beads at high density, enabling the beads to mimic lipid membranes, even under surfactant conditions typically required to solubilize MPs. By achieving a high-throughput and comprehensive lipid-MP interaction analysis method, it may be possible to reveal lipid-mediated regulation of MPs and, ultimately, the significance of lipid diversity.

Chapter 2 describes the development of high-density lipid-immobilized beads for identification of lipid-binding MPs (**Figure 1.6**). SM and ceramide (Cer) were immobilized to demonstrate the utility of the beads. After confirming the ability to obtain known lipid-binding proteins, a screening for lipid-binding proteins was performed using lysates from mouse neuroblastoma cells.

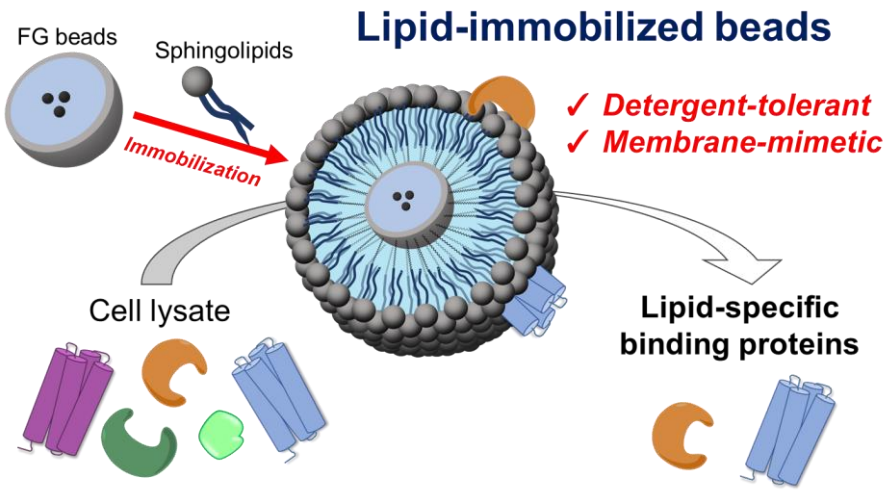

Figure 1.6. Screening of lipid-specific binding proteins with lipid-immobilized beads.

In **Chapter 3,** the author conducted more comprehensive identification of lipid-binding MPs with combination of in-depth proteomics and extended lipid-immobilized beads (**Figure 1.7**). To achieve a more comprehensive analysis of lipid-binding proteins, this bead-based method was improved from two aspects. First, the mixture of the obtained

lipid-binding proteins was directly digested into peptides and detected using a nano-LC-MS/MS system without SDS-PAGE separation. Second, dihydrosphingomyelin (DHSM), dihydroceramide (DHCer), phosphatidylcholine (PC), and cholesterol (Chol) were additionally immobilized to extend the variety of lipid-immobilized beads.

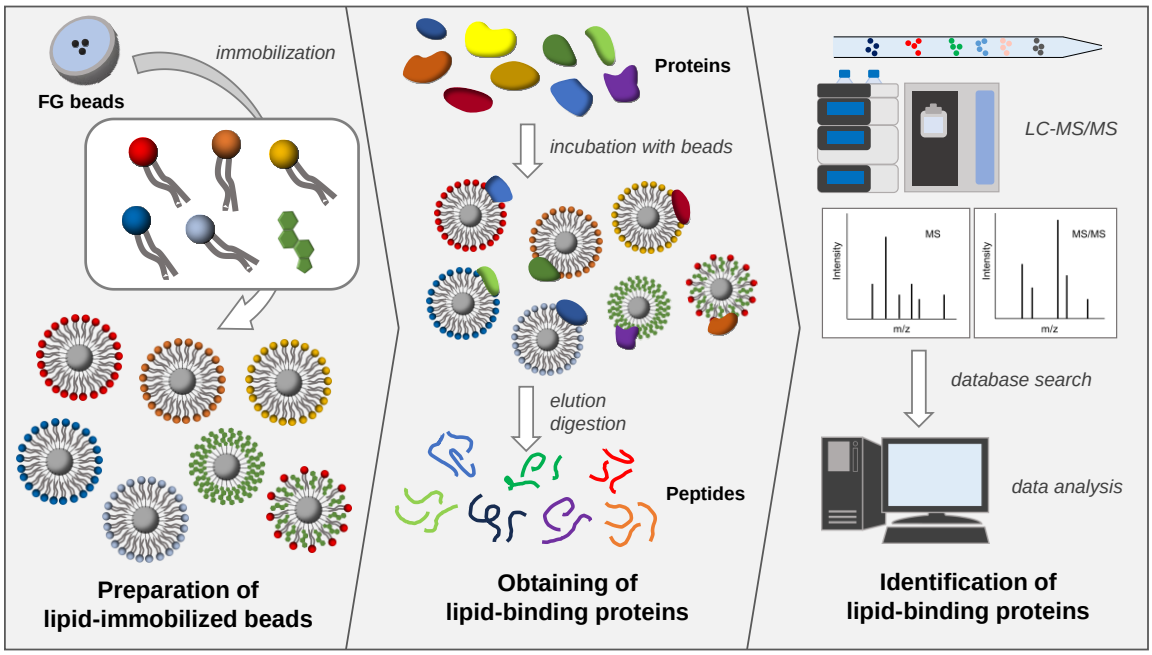

Figure 1.7. Comprehensive and systematic identification of lipid-specific binding proteins achieved by methodological improvements.

In **Chapters 4 and 5**, the author tried to extend this approach by the subsequent interaction analysis and functional analysis. In **Chapter 4**, by using yeast cells, which facilitate genetic and biochemical approaches, investigation on the physiological roles of the identified lipid-protein interactions would be much easier. Yeast-derived ceramide species were immobilized on beads, and a screening for binding proteins was demonstrated. Vacuolar-type ATPase was identified as one of the candidates, and interaction analysis using fluorescently labeled lipids and proteins was then carried out. In **Chapter 5**, a quantitative lipid-MP interaction analysis was conducted using the

surface plasmon resonance (SPR) system. The previously reported self-assembled monolayer (SAM)-modified SPR sensor chip method[44] was combined with single-cycle kinetics (SCK) analysis, enabling improved quantitative analysis of lipid-MP interactions. The author demonstrated the interaction between lipids and KcsA potassium channels,[45] which is from the soil bacteria *Streptomyces lividans* and has been studied extensively in ion channel research.[46, 47] As a result, the author identified strong binding of cardiolipin (CL) to the KcsA channel and As a result, the author identified strong binding of cardiolipin (CL) to the KcsA channel and demonstrated the utility of this method for the quantitative analysis of lipid-MP interactions.

In **Chapter 6**, the author concludes this thesis and discusses future perspectives on lipid-MP interactions and their analysis.

References

(1) Fagerberg, L.; Jonasson, K.; von Heijne, G.; Uhlén, M.; Berglund, L. Prediction of the human membrane proteome. *PROTEOMICS* **2010**, *10* (6), 1141-1149. DOI: https://doi.org/10.1002/pmic.200900258.
(2) Felippe Gonçalves-de-Albuquerque, C.; Ribeiro Silva, A.; Ignácio da Silva, C.; Caire Castro-Faria-Neto, H.; Burth, P. Na/K Pump and Beyond: Na/K-ATPase as a Modulator of Apoptosis and Autophagy. *Molecules* **2017**, *22* (4), 578.
(3) Rasmussen, S. G. F.; DeVree, B. T.; Zou, Y.; Kruse, A. C.; Chung, K. Y.; Kobilka, T. S.; Thian, F. S.; Chae, P. S.; Pardon, E.; Calinski, D.; Mathiesen, J. M.; Shah, S. T. A.; Lyons, J. A.; Caffrey, M.; Gellman, S. H.; Steyaert, J.; Skiniotis, G.; Weis, W. I.; Sunahara, R. K.; Kobilka, B. K. Crystal structure of the β2 adrenergic receptor–Gs protein complex. *Nature* **2011**, *477* (7366), 549-555. DOI: 10.1038/nature10361.
(4) Singer, S. J.; Nicolson, G. L. The fluid mosaic model of the structure of cell membranes. *Science* **1972**, *175* (4043), 720-731. DOI: 10.1126/science.175.4023.720.
(5) Fahy, E.; Subramaniam, S.; Murphy, R. C.; Nishijima, M.; Raetz, C. R. H.; Shimizu, T.; Spener, F.; van Meer, G.; Wakelam, M. J. O.; Dennis, E. A. Update of the LIPID MAPS comprehensive classification system for lipids1. *J. Lipid Res.* **2009**, *50*, S9-S14. DOI: https://doi.org/10.1194/jlr.R800095-JLR200.
(6) Liebisch, G.; Fahy, E.; Aoki, J.; Dennis, E. A.; Durand, T.; Ejsing, C. S.; Fedorova, M.; Feussner, I.; Griffiths, W. J.; Köfeler, H.; Merrill, A. H.; Murphy, R. C.; O'Donnell, V. B.; Oskolkova, O.; Subramaniam, S.; Wakelam, M. J. O.; Spener, F. Update on LIPID MAPS classification, nomenclature, and shorthand notation for MS-derived lipid structures. *J. Lipid Res.* **2020**, *61* (12), 1539-1555. DOI: https://doi.org/10.1194/jlr.S120001025.
(7) Simons, K.; Ikonen, E. Functional rafts in cell membranes. *Nature* **1997**, *387* (6633), 569-572. DOI: 10.1038/42408.
(8) Levental, I.; Levental, K. R.; Heberle, F. A. Lipid Rafts: Controversies Resolved, Mysteries Remain. *Trends Cell Biol.* **2020**, *30* (5), 341-353. DOI: 10.1016/j.tcb.2020.01.009.
(9) Pike, L. J. Rafts defined: a report on the Keystone symposium on lipid rafts and cell function. *J. Lipid Res.* **2006**, *47* (7), 1597-1598. DOI: https://doi.org/10.1194/jlr.E600002-JLR200.
(10) Kasahara, K.; Watanabe, K.; Kozutsumi, Y.; Oohira, A.; Yamamoto, T.; Sanai, Y. Association of GPI-anchored protein TAG-1 with src-family kinase Lyn in lipid rafts of cerebellar granule cells. *Neurochem. Res.* **2002**, *27* (7-8), 823-829. DOI: 10.1023/a:1020265225916.
(11) Wang, Y.; Murakami, Y.; Yasui, T.; Wakana, S.; Kikutani, H.; Kinoshita, T.; Maeda, Y. Significance of glycosylphosphatidylinositol-anchored protein enrichment in lipid rafts for the control of autoimmunity. *J. Biol. Chem.* **2013**, *288* (35), 25490-25499. DOI: 10.1074/jbc.M113.492611.
(12) Janes, P. W.; Ley, S. C.; Magee, A. I. Aggregation of lipid rafts accompanies signaling via the T cell antigen receptor. *J. Cell Biol.* **1999**, *147* (2), 447-461. DOI:

10.1083/jcb.147.2.447.
(13) Varshney, P.; Yadav, V.; Saini, N. Lipid rafts in immune signalling: current progress and future perspective. *Immunology* **2016**, *149* (1), 13-24. DOI: 10.1111/imm.12617.
(14) Martens, J. R.; O'Connell, K.; Tamkun, M. Targeting of ion channels to membrane microdomains: localization of KV channels to lipid rafts. *Trends Pharmacol. Sci.* **2004**, *25* (1), 16-21. DOI: https://doi.org/10.1016/j.tips.2003.11.007.
(15) Dart, C. Lipid microdomains and the regulation of ion channel function. *J. Physiol.* **2010**, *588* (Pt 17), 3169-3178. DOI: 10.1113/jphysiol.2010.191585.
(16) Simons, K.; Toomre, D. Lipid rafts and signal transduction. *Nature Reviews Molecular Cell Biology* **2000**, *1* (1), 31-39. DOI: 10.1038/35036052.
(17) Murata, M.; Matsumori, N.; Kinoshita, M.; London, E. Molecular substructure of the liquid-ordered phase formed by sphingomyelin and cholesterol: sphingomyelin clusters forming nano-subdomains are a characteristic feature. *Biophys. Rev.* **2022**, *14* (3), 655-678. DOI: 10.1007/s12551-022-00967-1.
(18) Bretscher, M. S. Phosphatidyl-ethanolamine: Differential labelling in intact cells and cell ghosts of human erythrocytes by a membrane-impermeable reagent. *J. Mol. Biol.* **1972**, *71* (3), 523-528. DOI: https://doi.org/10.1016/S0022-2836(72)80020-2.
(19) Zachowski, A. Phospholipids in animal eukaryotic membranes: transverse asymmetry and movement. *Biochem. J.* **1993**, *294 (Pt 1)* (Pt 1), 1-14. DOI: 10.1042/bj2940001.
(20) Kobayashi, T.; Menon, A. K. Transbilayer lipid asymmetry. *Curr. Biol.* **2018**, *28* (8), R386-R391. DOI: https://doi.org/10.1016/j.cub.2018.01.007.
(21) Pabst, G.; Keller, S. Exploring membrane asymmetry and its effects on membrane proteins. *Trends Biochem. Sci.* **2024**, *49* (4), 333-345. DOI: https://doi.org/10.1016/j.tibs.2024.01.007.
(22) Nagata, S.; Suzuki, J.; Segawa, K.; Fujii, T. Exposure of phosphatidylserine on the cell surface. *Cell Death Differ.* **2016**, *23* (6), 952-961. DOI: 10.1038/cdd.2016.7.
(23) Nagata, S. Apoptosis and Clearance of Apoptotic Cells. *Annu. Rev. Immunol.* **2018**, *36* (Volume 36, 2018), 489-517. DOI: https://doi.org/10.1146/annurev-immunol-042617-053010.
(24) Cherezov, V.; Rosenbaum, D. M.; Hanson, M. A.; Rasmussen, S. G.; Thian, F. S.; Kobilka, T. S.; Choi, H. J.; Kuhn, P.; Weis, W. I.; Kobilka, B. K.; Stevens, R. C. High-resolution crystal structure of an engineered human beta2-adrenergic G protein-coupled receptor. *Science* **2007**, *318* (5854), 1258-1265. DOI: 10.1126/science.1150577.
(25) Long, S. B.; Tao, X.; Campbell, E. B.; MacKinnon, R. Atomic structure of a voltage-dependent K+ channel in a lipid membrane-like environment. *Nature* **2007**, *450* (7168), 376-382. DOI: 10.1038/nature06265.
(26) Yuan Gao and Erhu Cao and David Julius and Yifan, C. TRPV1 structures in nanodiscs reveal mechanisms of ligand and lipid action. *Nature 2016 534:7607* **2016**, *534*, 347-351 , pmid = 27281200 , publisher = Nature Publishing Group. DOI: 10.1038/nature17964.
(27) Corradi, V.; Sejdiu, B. I.; Mesa-Galloso, H.; Abdizadeh, H.; Noskov, S. Y.; Marrink, S. J.; Tieleman, D. P. Emerging Diversity in Lipid-Protein Interactions. *Chem. Rev.* **2019**,

119 (9), 5775-5848. DOI: 10.1021/acs.chemrev.8b00451.
(28) Contreras, F. X.; Ernst, A. M.; Haberkant, P.; Bjorkholm, P.; Lindahl, E.; Gonen, B.; Tischer, C.; Elofsson, A.; von Heijne, G.; Thiele, C.; Pepperkok, R.; Wieland, F.; Brugger, B. Molecular recognition of a single sphingolipid species by a protein's transmembrane domain. *Nature* **2012**, *481* (7382), 525-529. DOI: 10.1038/nature10742.
(29) Kim, Y.; Gumpper, R. H.; Liu, Y.; Kocak, D. D.; Xiong, Y.; Cao, C.; Deng, Z.; Krumm, B. E.; Jain, M. K.; Zhang, S.; Jin, J.; Roth, B. L. Bitter taste receptor activation by cholesterol and an intracellular tastant. *Nature* **2024**, *628* (8008), 664-671. DOI: 10.1038/s41586-024-07253-y.
(30) Gimpl, G. Interaction of G protein coupled receptors and cholesterol. *Chem. Phys. Lipids* **2016**, *199*, 61-73. DOI: 10.1016/j.chemphyslip.2016.04.006.
(31) Chi, X.; Li, X.; Chen, Y.; Zhang, Y.; Su, Q.; Zhou, Q. Cryo-EM structures of the full-length human KCC2 and KCC3 cation-chloride cotransporters. *Cell Res.* **2021**, *31* (4), 482-484. DOI: 10.1038/s41422-020-00437-x.
(32) Guo, H.; Courbon, G. M.; Bueler, S. A.; Mai, J.; Liu, J.; Rubinstein, J. L. Structure of mycobacterial ATP synthase bound to the tuberculosis drug bedaquiline. *Nature* **2021**, *589* (7840), 143-147. DOI: 10.1038/s41586-020-3004-3.
(33) Cong, X.; Liu, Y.; Liu, W.; Liang, X.; Laganowsky, A. Allosteric modulation of protein-protein interactions by individual lipid binding events. *Nat Commun* **2017**, *8* (1), 2203. DOI: 10.1038/s41467-017-02397-0.
(34) Gupta, K.; Li, J.; Liko, I.; Gault, J.; Bechara, C.; Wu, D.; Hopper, J. T. S.; Giles, K.; Benesch, J. L. P.; Robinson, C. V. Identifying key membrane protein lipid interactions using mass spectrometry. *Nat. Protoc.* **2018**, *13* (5), 1106-1120. DOI: 10.1038/nprot.2018.014.
(35) Gault, J.; Liko, I.; Landreh, M.; Shutin, D.; Bolla, J. R.; Jefferies, D.; Agasid, M.; Yen, H. Y.; Ladds, M.; Lane, D. P.; Khalid, S.; Mullen, C.; Remes, P. M.; Huguet, R.; McAlister, G.; Goodwin, M.; Viner, R.; Syka, J. E. P.; Robinson, C. V. Combining native and 'omics' mass spectrometry to identify endogenous ligands bound to membrane proteins. *Nat Methods* **2020**, *17* (5), 505-508. DOI: 10.1038/s41592-020-0821-0.
(36) Norris, C. E.; Keener, J. E.; Perera, S.; Weerasinghe, N.; Fried, S. D. E.; Resager, W. C.; Rohrbough, J. G.; Brown, M. F.; Marty, M. T. Native Mass Spectrometry Reveals the Simultaneous Binding of Lipids and Zinc to Rhodopsin. *Int J Mass Spectrom* **2021**, *460*, 116477. DOI: 10.1016/j.ijms.2020.116477.
(37) Capriotti, A. L.; Caracciolo, G.; Caruso, G.; Cavaliere, C.; Pozzi, D.; Samperi, R.; Lagana, A. Analysis of plasma protein adsorption onto DC-Chol-DOPE cationic liposomes by HPLC-CHIP coupled to a Q-TOF mass spectrometer. *Anal. Bioanal. Chem.* **2010**, *398* (7-8), 2895-2903. DOI: 10.1007/s00216-010-4104-y.
(38) Pattipeiluhu, R.; Crielaard, S.; Klein-Schiphorst, I.; Florea, B. I.; Kros, A.; Campbell, F. Unbiased Identification of the Liposome Protein Corona using Photoaffinity-based Chemoproteomics. *ACS Cent Sci* **2020**, *6* (4), 535-545. DOI: 10.1021/acscentsci.9b01222.
(39) Frick, M.; Schwieger, C.; Schmidt, C. Liposomes as Carriers of Membrane-Associated Proteins and Peptides for Mass Spectrometric Analysis. *Angew. Chem. Int. Ed.*

Engl. **2021**, *60* (20), 11523-11530. DOI: 10.1002/anie.202101242.
(40) Tanaka, M.; Arakaki, A.; Matsunaga, T. Identification and functional characterization of liposome tubulation protein from magnetotactic bacteria. *Mol. Microbiol.* **2010**, *76* (2), 480-488. DOI: 10.1111/j.1365-2958.2010.07117.x.
(41) Tsujita, K.; Itoh, T.; Kondo, A.; Oyama, M.; Kozuka-Hata, H.; Irino, Y.; Hasegawa, J.; Takenawa, T. Proteome of acidic phospholipid-binding proteins: spatial and temporal regulation of Coronin 1A by phosphoinositides. *J. Biol. Chem.* **2010**, *285* (9), 6781-6789. DOI: 10.1074/jbc.M109.057018.
(42) Zhu, Z.; Chen, J.; Wang, G.; Elsherbini, A.; Zhong, L.; Jiang, X.; Qin, H.; Tripathi, P.; Zhi, W.; Spassieva, S. D.; Morris, A. J.; Bieberich, E. Ceramide regulates interaction of Hsd17b4 with Pex5 and function of peroxisomes. *Biochim Biophys Acta Mol Cell Biol Lipids* **2019**, *1864* (10), 1514-1524. DOI: 10.1016/j.bbalip.2019.05.017.
(43) Yu, W.; Baskin, J. M. Photoaffinity labeling approaches to elucidate lipid-protein interactions. *Curr. Opin. Chem. Biol.* **2022**, *69*, 102173. DOI: 10.1016/j.cbpa.2022.102173.
(44) Inada, M.; Kinoshita, M.; Sumino, A.; Oiki, S.; Matsumori, N. A concise method for quantitative analysis of interactions between lipids and membrane proteins. *Anal. Chim. Acta* **2019**, *1059*, 103-112. DOI: 10.1016/j.aca.2019.01.042.
(45) Heginbotham, L.; Odessey, E.; Miller, C. Tetrameric Stoichiometry of a Prokaryotic K+ Channel. *Biochemistry* **1997**, *36* (33), 10335-10342. DOI: 10.1021/bi970988i.
(46) Doyle, D. A.; Morais Cabral, J.; Pfuetzner, R. A.; Kuo, A.; Gulbis, J. M.; Cohen, S. L.; Chait, B. T.; MacKinnon, R. The structure of the potassium channel: molecular basis of K+ conduction and selectivity. *Science* **1998**, *280* (5360), 69-77. DOI: 10.1126/science.280.5360.69.
(47) Zhou, Y.; Morais-Cabral, J. H.; Kaufman, A.; MacKinnon, R. Chemistry of ion coordination and hydration revealed by a K+ channel-Fab complex at 2.0 A resolution. *Nature* **2001**, *414* (6859), 43-48. DOI: 10.1038/35102009.

Chapter 2
Identification of Lipid-Specific Proteins with High-Density Lipid-Immobilized Beads

Abstract

In biological membranes, lipids often interact with membrane proteins (MPs), regulating the localization and activity of MPs in cells. Although elucidating lipid–MP interactions is critical to comprehend the physiological roles of lipids, a systematic and comprehensive identification of lipid-binding proteins has not been adequately established. Therefore, the author reported the development of lipid-immobilized beads where lipid molecules were covalently immobilized. Owing to the detergent tolerance, these beads enable screening of water-soluble proteins and MPs, the latter of which typically necessitate surfactants for solubilization. Herein, two sphingolipid species—ceramide and sphingomyelin—which are major constituents of lipid rafts, were immobilized on the beads. The author first showed that the density of immobilized lipid molecules on the beads was as high as that of biological lipid membranes. Subsequently, the author confirmed that these beads enabled the selective pulldown of known sphingomyelin- or ceramide-binding proteins (lysenin, p24, and CERT) from protein mixtures, including cell lysates. In contrast, commercial sphingomyelin beads, on which lipid molecules are sparsely immobilized through biotin–streptavidin linkage, failed to capture lysenin, a well-known protein that recognizes clustered sphingomyelin molecules. This clearly demonstrates the applicability of these beads for obtaining proteins that recognize not only a single lipid molecule but also lipid clusters or lipid membranes. Finally, the author demonstrated the screening of lipid-binding proteins from Neuro2a cell lysates using these beads. This method is expected to significantly contribute to the understanding of interactions between lipids and proteins and to unravel the biological significance of lipid diversity.

2.1 Introduction

In biological membranes, lipids often interact with MPs, regulating the localization and activity of MPs in cells.[1-5] Therefore, elucidation of lipid–MP interactions is critical to understanding the physiological roles of lipids. However, due to the lack of analytical methods, the understanding remains insufficient. Therefore, methods for analyzing lipid-protein interactions are required.

As mentioned in **Chapter 1**, X-ray crystallography, cryo-EM, and native MS are powerful techniques for identifying lipid-MP interactions, but they require complex sample preparation and expensive analytical equipment, making comprehensive and high-throughput analysis challenging. Additionally, while these methods can identify "MP-binding lipids," they are not suitable for identifying "lipid-binding proteins." Conventionally, liposome coprecipitation[6-9] and photoaffinity labeling techniques[10, 11] have been adapted to identify lipid-binding proteins. However, the former cannot be applied in the presence of surfactants, and the latter is limited due to the intracellular metabolism of photoaffinity-labeled lipids, which restricts their applications for comprehensive analysis.

Besides, affinity beads are used to identify target proteins of small molecules, including pharmaceuticals.[12-16] This method is highly valuable for identifying binding proteins because it can be applied to various immobilized ligands and protein sources. This method has been applied to identifying binding proteins of bioactive lipids, including ceramide[17, 18] and PI(4,5)P_2.[19, 20] In those studies, conventional immobilization methods used for small molecules, where ligands are immobilized sparsely on the bead surface, have been employed for lipid immobilization. In fact, commercially available lipid-coated beads[21] are prepared based on the biotin–streptavidin binding, and thus, the density of

immobilized lipids is relatively low (**Figure 2.1a**). This would be suitable for identifying proteins that recognize a single lipid molecule, but identifying proteins that bind to or are embedded in lipid membranes through lipid-MP interactions is challenging.

In this chapter, to mimic lipid membranes on the bead surface, the author developed lipid-immobilized affinity beads, on which lipid molecules were densely immobilized (**Figure 2.1b**). The lipid-immobilized beads were designed so that the acyl chains of the lipid molecules are covalently bound to the bead surface and the hydrophilic head of the lipid is exposed to the outside. To achieve this, lipid derivatives featuring aminated acyl chain termini were synthesized and immobilized on magnetic nanobeads with high capacity for ligand immobilization. The covalent immobilization of lipid molecules enables screening of not only water-soluble proteins, but also MPs, which typically necessitate the use of surfactants for solubilization. The prepared beads were used to capture lipid-binding proteins from cell lysates and identified several lipid-specific protein candidates.

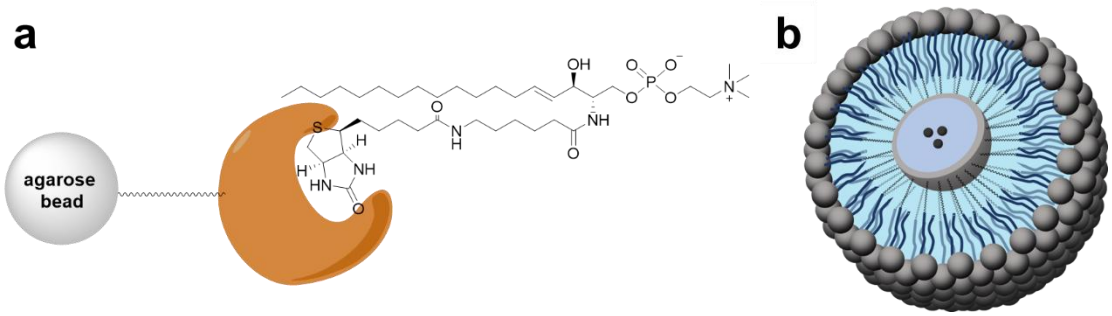

Figure 2.1. (a) Commercially available lipid-coated beads. Lipid molecules are immobilized via biotin–streptavidin binding. (b) Lipid-immobilized beads prepared in this study. Lipid molecules are covalently immobilized at high density.

2.2 Identification of Proteins in Proteomics

Mass spectrometry (MS)-based proteomics is widely used to identify binding proteins obtained through the photoaffinity labeling method and affinity purification. In this approach, 1) proteins are digested into peptides using amino acid residue-specific endopeptidases, 2) the mass spectra of the fragment peptides are measured using tandem mass spectrometry (MS/MS), and then 3) the obtained mass spectrum data is used to search protein sequence databases, where the sequence data that most closely matches the measured data is identified (**Figure 2.2**).

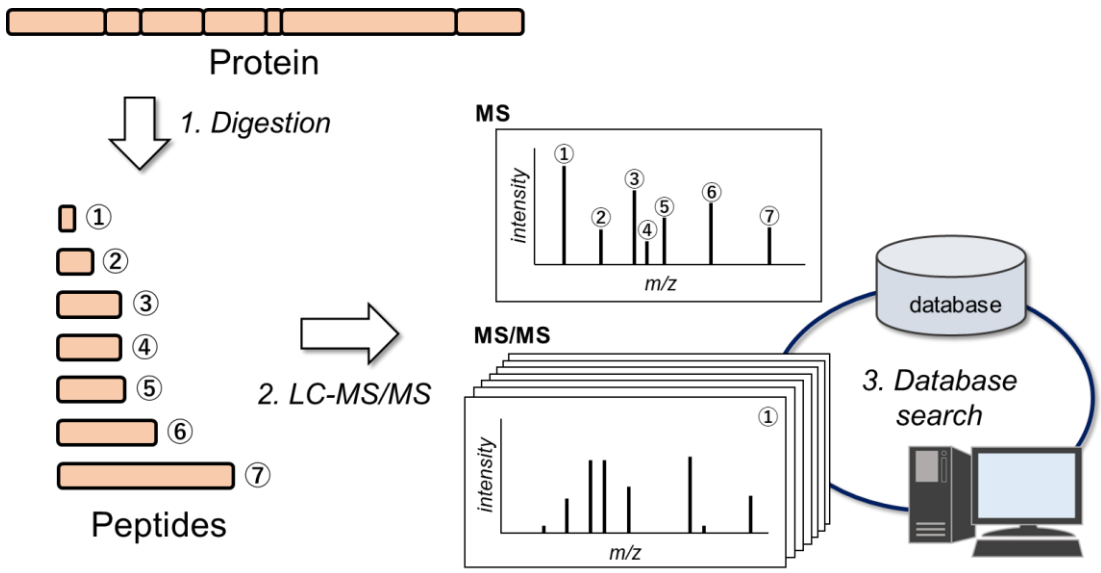

Figure 2.2. The outline of protein identification in MS-based proteomics.

The peptides derived from proteins are separated typically using a Nano-LC system and then ionized by electrospray ionization. In the first MS, each ionized peptide is separated, and specific ions (precursor ions) are directed into the collision cell. In the collision cell, ions are subjected to collisions with inert gases such as argon or helium, leading to fragmentation and the generation of product ions. In the second MS, product

ions are measured for each precursor ion, and the sequence is determined from the fragmentation patterns. These patterns correspond to ions formed by the cleavage of the peptide chain[22] (**Figure 2.3**). The amino acid sequence of each peptide is identified based on the degree of match between the obtained MS/MS data and the theoretical data from the protein sequence database. Finally, the proteins containing the matched sequences are identified.

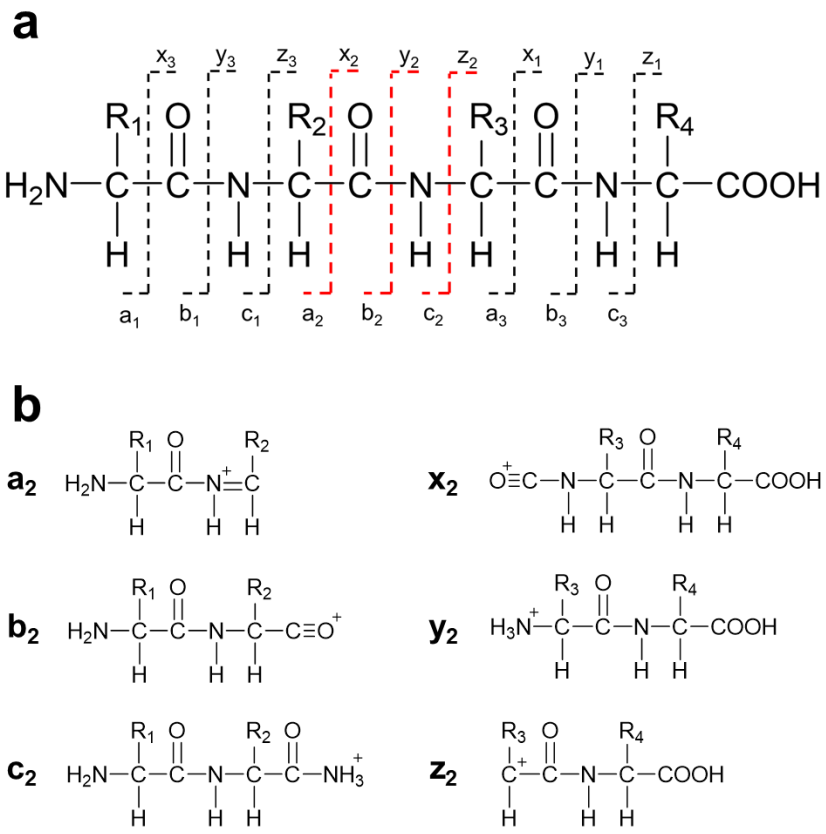

Figure 2.3. The cleavage sites in the peptide chain (**a**) and the fragment ions generated by the cleavage (**b**). The sequences that retain the N-terminal of the precursor ion are denoted as a, b, and c, while the sequences that retain the C-terminal are denoted as x, y, and z.

2.3 Experimental Section

2.3.1 Materials and Methods

General

NHS-activated FG beads were purchased from Tamagawa Seiki Co., Ltd. (Nagano, Japan). SM coated beads were purchased from Echelon Biosciences (Salt Lake City, UT, USA). Antibodies were purchased from Proteintech Group, Inc. (Rosemont, IL, USA). All other reagents were purchased from FUJIFILM Wako Pure Chemical Corp. (Osaka, Japan), Tokyo Chemical Inc. (Tokyo, Japan), Nacalai Tesque Inc. (Kyoto, Japan), or Sigma-Aldrich (St. Louis, MO, USA). For details of the synthesis of compounds **1**–**7**, see Supporting Information.

Preparation of lipid-immobilized beads

NHS-activated beads (1.0 mg) were washed three times with 200 μL of DMF and incubated with 10 mM triethylamine and 1 mM aminated lipids in 200 μL of DMF overnight at room temperature. The beads were washed three times with 200 μL of DMF, and unreacted NHS ester groups were masked with 1.0 M ethanolamine in DMF. After washing three times with 50% MeOH, these beads were resuspended in 50 μL of 50% MeOH, and stored at 4°C. Negative control beads were prepared by reacting with 1 mM dodecylamine in DMF, instead of aminated lipids.

Phosphorus quantification

The amount of phosphorus on SM beads was quantified using the molybdenum blue method.[29] 25% H_2SO_4 (225 μL) was added to 0.2 mg of SM and control beads, respectively. Each suspension was heated at 200°C for 25 min, cooled for 5 min, mixed

with 75 μL of H_2O_2, and heated at 200°C for 30 min. After cooling for 5 min, Milli-Q water (1950 μL), 10% ascorbic acid (250 μL), and 2.5% hexaammonium heptamolybdate (250 μL) were sequentially added to the suspension and the mixture was heated at 100°C for 7 min. Absorbance of the supernatant was measured at 820 nm using a JASCO V-730BIO (JASCO Corporation, Tokyo, Japan).

STEM and EDS analysis

SM and control beads were washed with water twice and resuspended in 50 μL of Milli-Q water. An aliquot of 7 μL suspension was placed on a carbon-coated copper grid (Okenshoji, Tokyo, Japan), excess water was removed, and the sample was dried in vacuo overnight. STEM images were observed using a JEM-ARM200F instrument equipped with a JED-2300T (JEOL, Tokyo, Japan) at an acceleration voltage of 200 kV. The JEOL Analysis Station software was used to control STEM-EDS mapping.

Neuro-2a cell lysate preparation

Neuro-2a cells were cultured in E-MEM supplemented with 10% fetal bovine serum and 1% penicillin-streptomycin at 37°C with 5% CO_2. Cells were suspended in lysis buffer (50 mM Tris [pH 8.0], 150 mM NaCl, and 1% Nonidet P-40) containing protease inhibitor cocktail (Nacalai Tesque Inc., Kyoto, Japan), incubated on ice for 1 h, and centrifuged at 1,5000 rpm, for 20 min at 4°C. The supernatant was collected to prepare the lysate. The protein content in the lysate was quantified with BCA Protein Assay Kit (Takara Bio Inc., Shiga, Japan), and the lysate was diluted to a concentration of 1 mg mL^{-1}.

Pulldown with lipid-immobilized beads

Each type of bead (0.5 mg) was washed with 200 μL of lysis buffer before use, followed by dispersion in 50 μL of protein solution. After incubation at 4°C for 4 h, the supernatant was removed through magnetic separation. The beads were washed twice with 200 μL of lysis buffer and then boiled in SDS sample buffer (240 mM Tris-HCl [pH6.8], 8% SDS, 40% glycerol, 0.1% bromophenol blue, and 20% 2-mercaptoethanol). The eluted proteins were applied to 4%–20% SDS-PAGE. Proteins were detected by silver staining or western blotting.

Lysenin pulldown with lipid-immobilized beads and commercial beads

SM-immobilized beads (0.2 mg) were incubated with a protein mixture (10 μg mL^{-1} RFP-lysenin and 1 mg mL^{-1} BSA in lysis buffer, 50 μL). The subsequent procedure was the same as above. By contrast, commercial SM beads (Echelon Bioscience, 40 μL) were washed with 200 μL of lysis buffer before use, followed by dispersion in 50 μL of the same protein mixture. After incubation at 4°C for 4 h, the supernatant was removed by centrifugation at 800 × g for 4 min. The beads were washed twice with 200 μL of lysis buffer, boiled in SDS sample buffer, and centrifuged at 800 × *g* for 4 min. The supernatant was applied to a 4%–20% SDS-PAGE gel, followed by silver staining.

Western blotting

Proteins were electrophoretically transferred from SDS-PAGE gels to PVDF membranes (Bio-Rad, Hercules, CA, USA). The membranes were blocked with 2% BSA in PBS containing 0.05% Tween-20 (PBS-T) for 1 h at room temperature, incubated with primary antibodies (anti-p24 antibody and anti-CERT antibody) in PBS-T containing 2% BSA

overnight at 4°C, washed three times with PBS-T, incubated with HRP-conjugated secondary antibodies for 1 h, and washed three times with PBS-T. Signals were detected with an imaging system (ImageQuant LAS 4000 mini, Cytiva, Marlborough, MA, US).

Proteomic analysis

Each selected band was cut into pieces and subjected to LC-MS/MS analysis. The gel fragments were destained and digested with mass spectrometry-grade trypsin (PROMEGA, Madison, WI, USA) in 25 mM ammonium bicarbonate. nLC-MS/MS analysis was conducted using Advance UHPLC (Bruker, Billerica, MA, USA) and Orbitrap Velos Pro (Thermo Fisher Scientific, Waltham, MA, USA). Trypsin-digested samples were separated by SilicaTip (0.100 mm i.d. × 15 cm, Nikkyo Technos, Japan) packed with a 3-μm C18 L-column (Chemical Evaluation and Research Institute, Japan) using a linear gradient (30 min, acetonitrile/0.1% formic acid) at a flow rate of 320 nL min^{-1}. The resulting MS and MS/MS data were searched against the Swiss-Prot database using the Mascot search engine software (ver. 2.8.0.1, Matrix Science, Boston, MA, USA). Significance threshold was set to $p < 0.05$. The proteins with at least three peptide matches were listed. Nonspecific proteins identified in control samples were excluded from the list of identified proteins.

2.4 Result

2.4.1 Preparation of lipid-immobilized beads

Because lipid rafts—functional domains of biological membranes enriched in sphingolipids and cholesterol—are proposed to be platforms for the accumulation and functioning of MPs,[23-26] sphingomyelin (SM) and ceramide (Cer), which are major players in lipid rafts, were chosen for immobilization.[27] Because proteins localized in lipid rafts potentially recognize not only the rigidity but the constituent lipid molecules of the rafts, these beads are expected to identify raft-related proteins. First, derivatives of SM and Cer were synthesized by introducing amino groups at the acyl chain terminals of lipid molecules (**Scheme 2.1**). Synthesis of aminoSM **5** commenced with deacylation of eggSM in methanolic HCl to yield lysosphingomyelin **3**. Subsequent introduction of the azido acyl chain to **3**, followed by reduction of the azido group through the Staudinger reaction yielded the desired product **5**. AminoCer **7** was synthesized according to a similar scheme utilizing sphingosine as a substrate instead of lysosphingomyelin. The synthesized lipid derivatives were immobilized on FG beads (**Scheme 2.2**). Because FG beads (nanomagnetic beads) have a high density of functional groups on their surface,[28] they would be well-suited for mimicking lipid membranes. The aminated lipids were immobilized by mixing with NHS-activated FG beads, where carboxy groups were activated as *N*-hydroxysuccinimide (NHS) ester groups. Subsequently, unreacted NHS ester groups were masked with aminoethanol. In addition to these lipid-immobilized beads, negative control beads were prepared by reacting with dodecylamine.

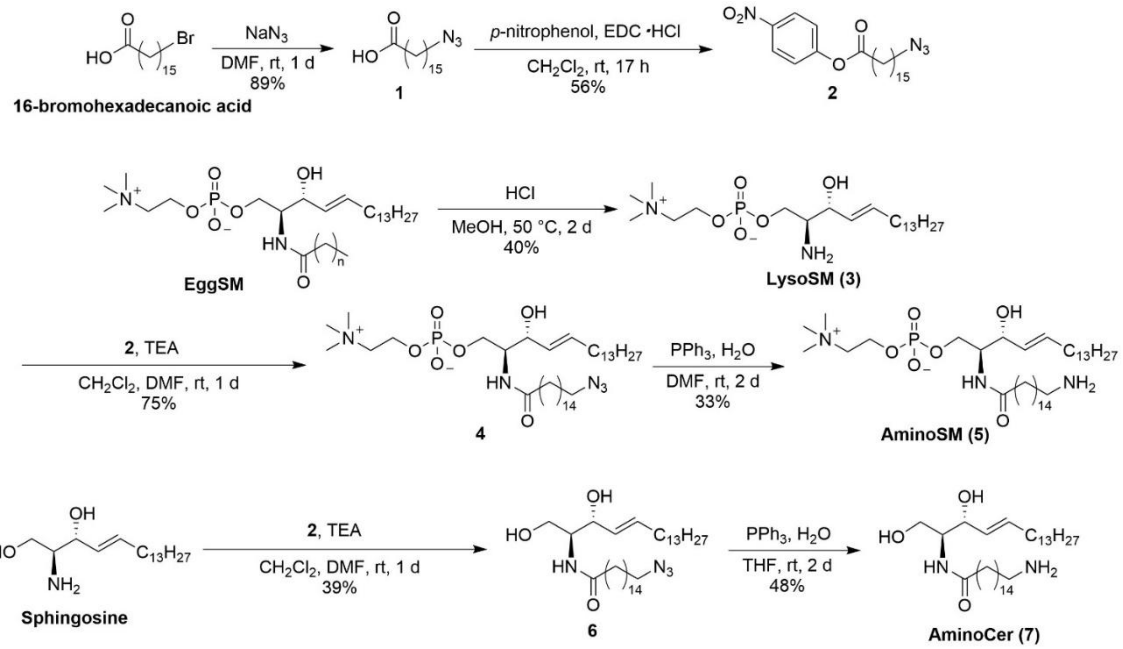

Scheme 2.1. Syntheses of aminoSM and aminoCer.

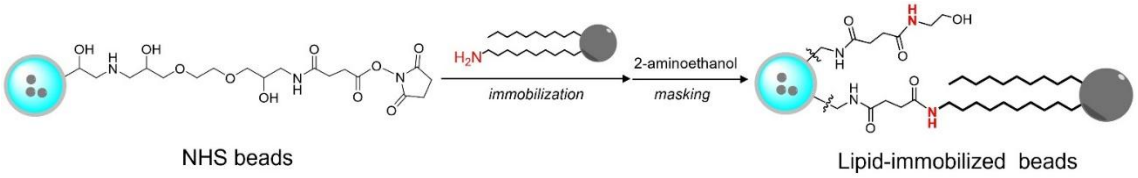

Scheme 2.2. Immobilization of aminosphingolipids on beads.

2.4.2 Lipids were densely immobilized on the beads

To confirm the dense immobilization of lipid molecules on the bead surface, phosphorus atoms present in the head of SM were used to quantify immobilized lipid. Because phosphorus atoms are not contained in either the bead carrier or linker, the distribution and quantification of lipid molecules on the beads was simultaneously estimated through phosphorus detection.

Initially, scanning transmission electron microscopy (STEM) and energy-dispersive X-ray spectroscopy (EDS) analyses were conducted to confirm secure immobilization of SM molecules. In addition to carbon and Fe atoms, which were present

in FG beads, phosphorus atoms were detected and distributed on SM beads (**Figure 2.4a**). In the case of SM beads, a 2.0 keV peak, derived from phosphorus atoms, was detected in the EDS spectrum (**Figure 2.4b**), whereas no phosphorus atoms were detected in control beads (**Figure 2.4c**).

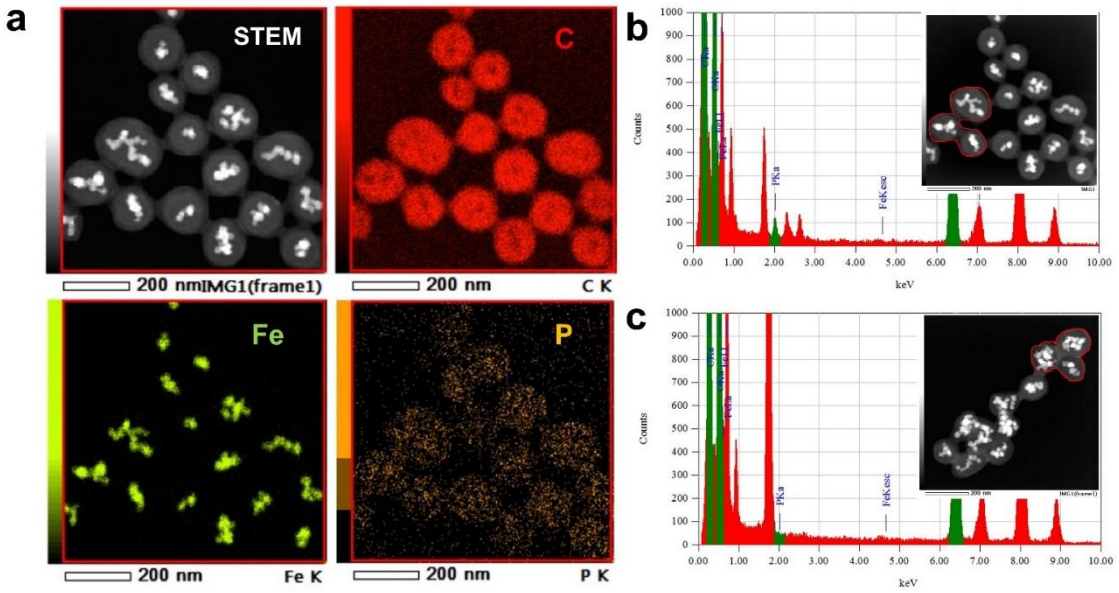

Figure 2.4. (**a**) STEM and EDS mapping images of SM beads; (**b**) an extracted EDS spectrum of SM beads in the area enclosed by the red line; a 2.0-keV peak derived from phosphorus atoms is detected; (**c**) an extracted EDS spectrum of control beads in the area enclosed by the red line; a 2.0-keV peak is not detected.

Next, the amount of immobilized SM was determined through phosphorus quantification. The beads were decomposed with sulfuric acid and hydrogen peroxide. The phosphoric acid formed was quantified by the molybdenum blue method.[29] The amount of immobilized SM molecules per milligram of beads was determined as 73.2 ± 3.0 nmol mg^{-1}, indicating an occupation area of 51.4 ± 2.1 $Å^2$ per SM molecule on the bead surface (**Table 2.1**). This value is comparable to that of an authentic lipid bilayer (40–60 $Å^2$),[30, 31] suggesting that a lipid membrane structure is reproduced on the bead surface.

Taken together, these results confirmed uniform immobilization of lipid molecules at high density on the bead surface mimicking a lipid membrane structure.

Table 2.1. Amount of immobilized SM molecules per milligram of beads (x) and an occupation area per SM molecule on the bead surface (s).

	$\boldsymbol{x}$ (nmol mg^{-1})	$\boldsymbol{s}$ (Å^2)
1	76.6	49.1
2	72.5	51.8
3	70.6	53.2
Average	73.2	51.4
SD	3.0	2.1

2.4.3 Lipid-binding proteins interacted with the beads

To validate the efficacy of lipid-immobilized beads in obtaining lipid-specific binding proteins, pulldown experiments were conducted using known lipid-binding proteins. Initially, a pulldown assay was executed using lysenin, which is a toxic protein sourced from earthworms and specifically recognizes and binds SM clusters.[32-34] SM-, Cer-, and control beads were incubated with a solution containing red-fluorescent protein (RFP)-labelled lysenin and bovine serum albumin (BSA) and washed. Fluorescence microscopy showed that RFP-lysenin bound specifically to SM beads and not the other beads (**Figure 2.5**). Bead-bound proteins were recovered through heat treatment and visualized using silver-stained SDS-PAGE. Lysenin exhibited specific binding to SM beads (**Figure 2.6a**). Then, these lipid-immobilized beads were compared with commercially available lipid-coated beads (Echelon Biosciences), on which lipids are sparsely immobilized through biotin–streptavidin linkage. SM-immobilized beads prepared in this study and commercial SM-coated beads were incubated with a mixture

of lysenin and BSA, and subjected to pulldown experiments. Consequently, SM-immobilized beads had a markedly higher affinity for lysenin than the commercial beads (**Figure 2.6b**).

To further demonstrate the capacity of lipid-immobilized beads, we examined whether known lipid-binding proteins could be pulled down from complex protein mixtures such as cell lysates. The cell lysate of Neuro2a was incubated with the beads and the recovered proteins were identified through western blotting with antibodies targeting p24,[35] an SM-specific binding protein, and START domain of CERT,[36, 37] a Cer-specific binding domain. The results revealed the specific binding of p24 to SM beads (**Figure 2.7, top**) and the START domain to Cer beads (**Figure 2.7, bottom**). Thus, the author confirmed the applicability of lipid-immobilized beads in isolating lipid-binding proteins from complex protein mixtures and identifying lipid-specific proteins.

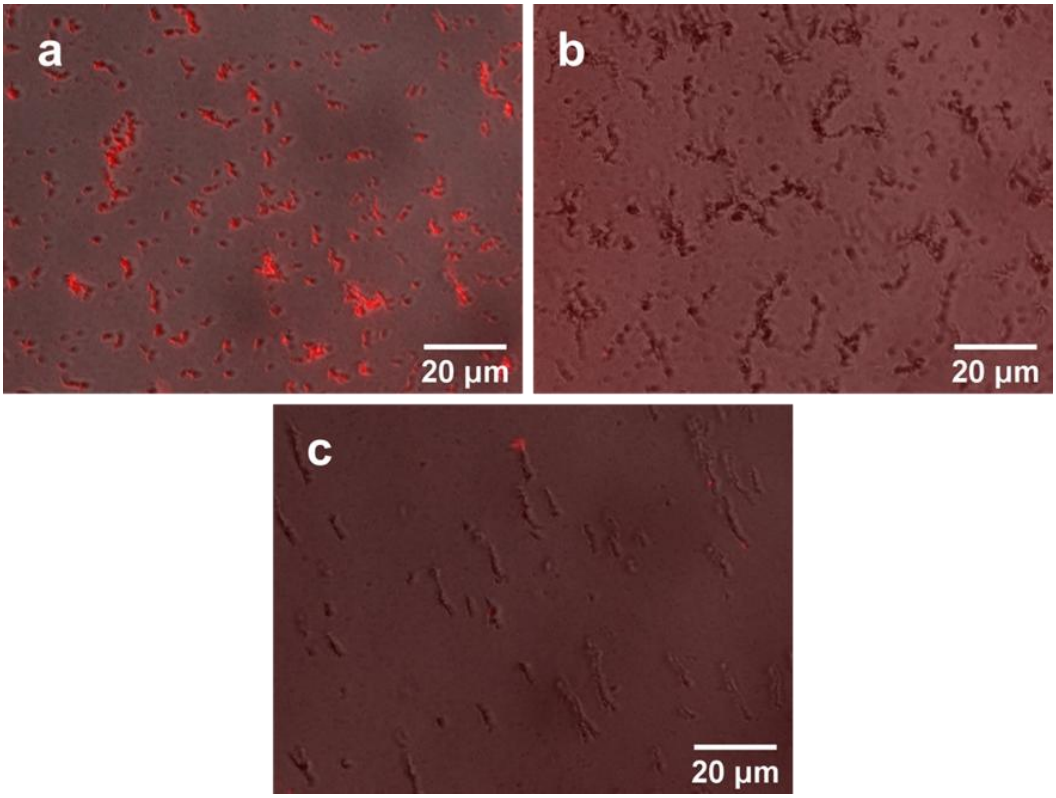

Figure 2.5. RFP-lysenin bound to each type of beads (a: SM beads, b: Cer beads, c: control beads). After incubation with RFP-lysenin and washing with PBS, the beads were resuspended in PBS and observed using a fluorescence microscope (BZ-X700, Keyence, Osaka, Japan). RFP-lysenin specifically bound to SM beads and not to the other beads. The brightness and contrast were adjusted for clarity.

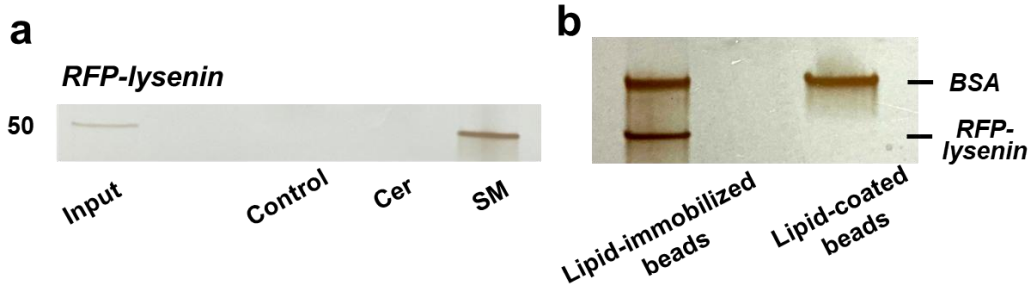

Figure 2.6. (**a**) Pulldown assay of lysenin with SM, Cer, and control beads. Each lipid-immobilized bead (0.2 mg) was incubated with 30 μg mL^{-1} RFP-lysenin solution. Lysenin specifically bound to SM beads; (**b**) comparison of the performance between SM-immobilized beads prepared in this study and commercial lipid-coated beads. SM-immobilized beads and commercial SM beads were dispersed in a protein mixture containing RFP-lysenin and BSA.

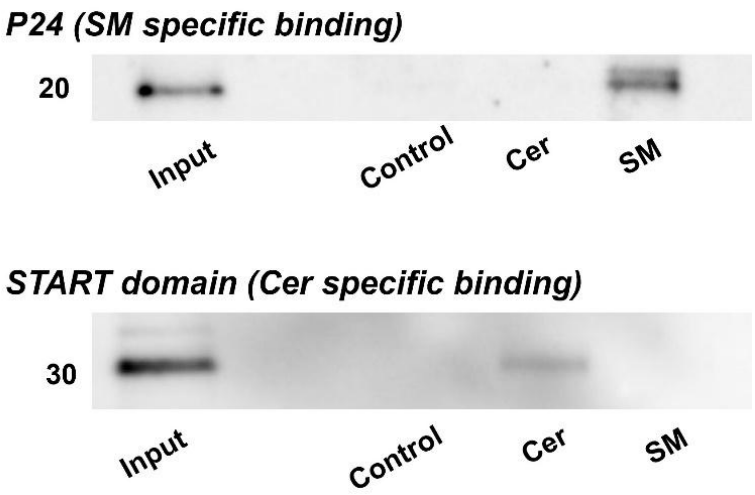

Figure 2.7. Western blotting of endogenous lipid-binding proteins from Neuro2a cell lysates; P24, a protein specific to SM, exhibited specific binding to SM beads (**top**); START domain of CERT, a domain that specifically binds Cer, was detected with Cer beads (**bottom**).

2.4.4 Screening lipid-specific binding proteins from Neuro2a cells

To demonstrate screening of lipid-binding proteins, proteins recovered from lipid-immobilized beads incubated with Neuro2a cell lysates were separated with SDS-PAGE, to obtain several distinctive bands (indicated by arrows, **Figure 2.8**). The proteins in these bands were identified by proteomic analysis (**Table S2.1** in Supporting Information). For each band, proteins with top three Mascot scores are presented in **Table 2.2**, and proteins from control beads were excluded as nonspecific bindings. the author focused on tumor protein D54 (TPD54), an SM-binding protein, identified in band **#3**. Pulldown experiments with authentic TPD54 were performed, confirming the specific binding of TPD54 to SM beads (**Figure 2.9**).

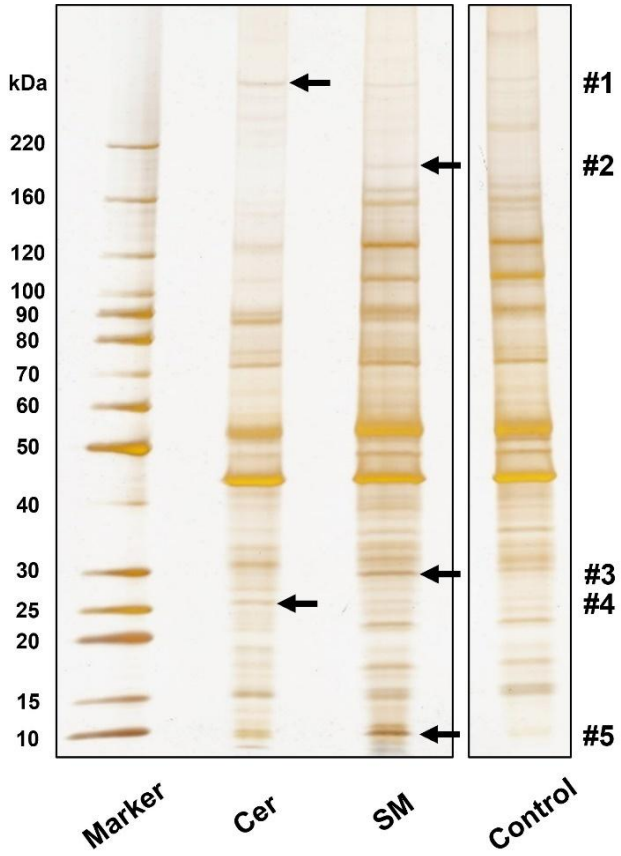

Figure 2.8. SDS-PAGE separation of lipid-binding proteins obtained from Neuro2a cell lysate using lipid-immobilized beads (0.5 mg); proteins were visualized with silver staining; numbered bands were excised and subjected to LC-MS/MS analyses; lanes not involved in this experiment have been removed.

Figure 2.9. Pulldown assay of recombinant TPD54 using SM, Cer and control beads; each type of lipid-immobilized beads (0.25 mg) was incubated with 25 μg mL^{-1} TPD54 in lysis buffer; TPD54 specifically bound to SM beads.

Table 2.2. Candidate lipid-specific proteins from Neuro2a cells in each band

Band	*Lipid*	*Protein name*	*Mascot score*	*Mass*	*Number of peptides*
#1	Cer	Keratin, type I cytoskeletal 42	123	50,444	4
		Bone marrow stromal antigen 2	91	19,311	3
		Nesprin-2	87	787,997	5
#2	SM	Proline-, glutamic acid- and leucine-rich protein 1	99	119,306	4
		YLP motif-containing protein 1	80	155,146	4
		GRB10-interacting GYF protein 2	79	149,387	3
#3	SM	Tumor protein D54	805	24,085	32
		MICOS complex subunit Mic19	229	26,546	6
		Vimentin	222	53,712	11
#4	Cer	Protein FAM3C	200	25,022	8
		Protein SCO2 homolog, mitochondrial	183	29,097	7
		Bone marrow stromal antigen 2	167	19,311	4
#5	SM	ATP synthase subunit g	273	11,417	13
		Dynein light chain 1	160	10,530	4
		ATP synthase subunit e	144	8,230	6

2.5 Discussion

In this study, lipid-immobilized beads were developed to identify lipid-binding proteins. To mimic lipid membranes, sphingolipid derivatives with aminated acyl chain terminals were synthesized from lysosphingolipids (**Scheme 2.1**). These derivatives were subsequently amide-linked to the beads such that their hydrophilic heads were directed outward. EDS analysis and phosphorus quantification not only confirmed secure immobilization, but also revealed a high density of immobilized lipids equivalent to authentic lipid membranes, suggesting that the bead surface imitates lipid membranes (**Figure 2.4**). Thus, the author succeeded in preparing of ***detergent-tolerant and membrane-mimetic lipid-immobilized beads*** for screening membrane-associated proteins.

Pulldown of a known SM-binding protein, lysenin, showed specific binding to SM beads (**Figures 2.5 and 2.6a**). Comparison of the performance between these beads and commercially available beads further demonstrated the superiority of SM-immobilized beads in recognizing lysenin (**Figure 2.6b**). Lysenin recognizes and binds SM domains rather than a single SM molecule.[34] Thus, the commercial beads with sparse SM immobilization likely failed to capture lysenin. This result further supports the formation of a lipid membrane-like structure on the surface of lipid-immobilized beads. Additionally, p24 and START domain of CERT in Neuro2a cell lysates exhibited specific binding to SM and Cer beads, respectively (**Figure 2.7**), demonstrating that endogenous lipid-binding proteins can be detected from complex protein mixtures. The START domain is thought to be produced by proteolysis of CERT. These findings underscore the utility of this approach in obtaining lipid-specific binding proteins. Furthermore, the author conducted a screening from cell lysates as a demonstration experiment, and

identified interesting proteins as candidate lipid-binding proteins (**Figure 2.8, Table 2.2**). These candidates included transmembrane proteins, indicating that lipid-immobilized beads were suitable not only for soluble proteins but also for membrane proteins, due to the linker being sufficiently long to allow the insertion of transmembrane proteins onto the beads. ATP synthase subunit g was identified as an SM-specific protein at band **#5**. Given that ATP synthase was reported to localize in lipid rafts,[38] SM recognition of ATP synthase may be attributed to its preference for lipid rafts. Protein FAM3C, identified as a Cer-binding protein in this study, is a biomarker for Alzheimer's disease and known to reduce the production of amyloid β (Aβ) protein.[39] Besides, Cer is involved in the elevation of Aβ.[40, 41] Therefore, the interaction between Cer and FAM3C might control the production of Aβ.

TPD54 was confirmed as SM-specific by the pulldown experiments (**Figure 2.7**). TPD54 is one of the most abundantly expressed proteins in cancer cells, and quantitative proteomics of HeLa cells revealed that TPD54 is the 180th most abundant of 8,804 identified proteins.[42] Recently, the presence of a membrane transport pathway facilitated by intracellular nanovesicles (diameter: ~30 nm) was revealed. TPD54 was reported to bind to the surface of the nanovesicles by inserting an amphipathic lipid-packing sensor (ALPS) motif.[43, 44] Because the ALPS motif senses lipid packing,[45] TPD54 likely recognizes and binds densely-packed SM membranes, and not individual SM molecules, through the ALPS motif. This again indicates the applicability of lipid-immobilized beads for obtaining proteins that recognize lipid membranes, which is otherwise difficult with conventional approaches.

2.6 Conclusion

Thus far, sparsely immobilized lipid-coated beads have been employed for screening lipid-binding proteins. However, these approaches face serious challenges when screening under conditions reflective of biological membranes, as evidenced by the pulldown of lysenin (**Figure 2.4b**). In this context, membrane-mimetic lipid-immobilized beads have opened a new avenue for identifying lipid-specific MPs that recognize not only a single lipid molecule but also lipid clusters or lipid membranes. Additionally, magnetic beads enable efficient pulldown through magnetic force, facilitating high-throughput analysis and potential automation. The synthesis of aminated derivatives allows for the immobilization of diverse lipid species and development of a variety of lipid-immobilized beads. With an expanded repertoire of immobilized lipid species, high-throughput analysis of various lipid–protein interactions becomes feasible. The comprehensive analysis of lipid-binding proteins can significantly contribute to understanding lipid–protein interactions and the significance of lipid diversity.

Reference

(1) Lee, A. G. Lipid-protein interactions in biological membranes: a structural perspective. *Biochim. Biophys. Acta* **2003**, *1612* (1), 1-40. DOI: 10.1016/s0005-2736(03)00056-7.
(2) Janmey, P. A.; Kinnunen, P. K. Biophysical properties of lipids and dynamic membranes. *Trends Cell Biol.* **2006**, *16* (10), 538-546. DOI: 10.1016/j.tcb.2006.08.009.
(3) Hunte, C.; Richers, S. Lipids and membrane protein structures. *Curr. Opin. Struct. Biol.* **2008**, *18* (4), 406-411. DOI: 10.1016/j.sbi.2008.03.008.
(4) Phillips, R.; Ursell, T.; Wiggins, P.; Sens, P. Emerging roles for lipids in shaping membrane-protein function. *Nature* **2009**, *459* (7245), 379-385. DOI: 10.1038/nature08147.
(5) Yeagle, P. L. Non-covalent binding of membrane lipids to membrane proteins. *Biochim. Biophys. Acta* **2014**, *1838* (6), 1548-1559. DOI: 10.1016/j.bbamem.2013.11.009.
(6) Capriotti, A. L.; Caracciolo, G.; Caruso, G.; Cavaliere, C.; Pozzi, D.; Samperi, R.; Lagana, A. Analysis of plasma protein adsorption onto DC-Chol-DOPE cationic liposomes by HPLC-CHIP coupled to a Q-TOF mass spectrometer. *Anal. Bioanal. Chem.* **2010**, *398* (7-8), 2895-2903. DOI: 10.1007/s00216-010-4104-y.
(7) Pattipeiluhu, R.; Crielaard, S.; Klein-Schiphorst, I.; Florea, B. I.; Kros, A.; Campbell, F. Unbiased Identification of the Liposome Protein Corona using Photoaffinity-based Chemoproteomics. *ACS Cent Sci* **2020**, *6* (4), 535-545. DOI: 10.1021/acscentsci.9b01222.
(8) Frick, M.; Schwieger, C.; Schmidt, C. Liposomes as Carriers of Membrane-Associated Proteins and Peptides for Mass Spectrometric Analysis. *Angew. Chem. Int. Ed. Engl.* **2021**, *60* (20), 11523-11530. DOI: 10.1002/anie.202101242.
(9) Tanaka, M.; Arakaki, A.; Matsunaga, T. Identification and functional characterization of liposome tubulation protein from magnetotactic bacteria. *Mol. Microbiol.* **2010**, *76* (2), 480-488. DOI: 10.1111/j.1365-2958.2010.07117.x.
(10) Zhu, Z.; Chen, J.; Wang, G.; Elsherbini, A.; Zhong, L.; Jiang, X.; Qin, H.; Tripathi, P.; Zhi, W.; Spassieva, S. D.; Morris, A. J.; Bieberich, E. Ceramide regulates interaction of Hsd17b4 with Pex5 and function of peroxisomes. *Biochim Biophys Acta Mol Cell Biol Lipids* **2019**, *1864* (10), 1514-1524. DOI: 10.1016/j.bbalip.2019.05.017.
(11) Yu, W.; Baskin, J. M. Photoaffinity labeling approaches to elucidate lipid-protein interactions. *Curr. Opin. Chem. Biol.* **2022**, *69*, 102173. DOI: 10.1016/j.cbpa.2022.102173.
(12) Kuramori, C.; Azuma, M.; Kume, K.; Kaneko, Y.; Inoue, A.; Yamaguchi, Y.; Kabe, Y.; Hosoya, T.; Kizaki, M.; Suematsu, M.; Handa, H. Capsaicin binds to prohibitin 2 and displaces it from the mitochondria to the nucleus. *Biochem. Biophys. Res. Commun.* **2009**, *379* (2), 519-525. DOI: 10.1016/j.bbrc.2008.12.103.
(13) Hirota, T.; Lee, J. W.; St. John, P. C.; Sawa, M.; Iwaisako, K.; Noguchi, T.; Pongsawakul, P. Y.; Sonntag, T.; Welsh, D. K.; Brenner, D. A.; Doyle, F. J.; Schultz, P. G.; Kay, S. A. Identification of Small Molecule Activators of Cryptochrome. *Science* **2012**, *337* (6098), 1094-1097. DOI: doi:10.1126/science.1223710.
(14) Rosania, G. R.; Chang, Y.-T.; Perez, O.; Sutherlin, D.; Dong, H.; Lockhart, D. J.; Schultz, P. G. Myoseverin, a microtubule-binding molecule with novel cellular effects.

Nat. Biotechnol. **2000**, *18* (3), 304-308. DOI: 10.1038/73753.
(15) Khersonsky, S. M.; Jung, D.-W.; Kang, T.-W.; Walsh, D. P.; Moon, H.-S.; Jo, H.; Jacobson, E. M.; Shetty, V.; Neubert, T. A.; Chang, Y.-T. Facilitated Forward Chemical Genetics Using a Tagged Triazine Library and Zebrafish Embryo Screening. *J. Am. Chem. Soc.* **2003**, *125* (39), 11804-11805. DOI: 10.1021/ja035334d.
(16) Ito, T.; Ando, H.; Suzuki, T.; Ogura, T.; Hotta, K.; Imamura, Y.; Yamaguchi, Y.; Handa, H. Identification of a Primary Target of Thalidomide Teratogenicity. *Science* **2010**, *327* (5971), 1345-1350. DOI: doi:10.1126/science.1177319.
(17) Kota, V.; Szulc, Z. M.; Hama, H. Identification of C6-ceramide-interacting proteins in D6P2T Schwannoma cells. *Proteomics* **2012**, *12* (13), 2179-2184. DOI: 10.1002/pmic.201100527.
(18) Kong, J. N.; Zhu, Z.; Itokazu, Y.; Wang, G.; Dinkins, M. B.; Zhong, L.; Lin, H. P.; Elsherbini, A.; Leanhart, S.; Jiang, X.; Qin, H.; Zhi, W.; Spassieva, S. D.; Bieberich, E. Novel function of ceramide for regulation of mitochondrial ATP release in astrocytes. *J. Lipid Res.* **2018**, *59* (3), 488-506. DOI: 10.1194/jlr.M081877.
(19) Lewis, A. E.; Sommer, L.; Arntzen, M. O.; Strahm, Y.; Morrice, N. A.; Divecha, N.; D'Santos, C. S. Identification of nuclear phosphatidylinositol 4,5-bisphosphate-interacting proteins by neomycin extraction. *Mol. Cell. Proteomics* **2011**, *10* (2), S1-S15. DOI: 10.1074/mcp.M110.003376.
(20) Kim, S. K.; Kim, H.; Yang, Y. R.; Suh, P. G.; Chang, J. S. Phosphatidylinositol phosphates directly bind to neurofilament light chain (NF-L) for the regulation of NF-L self assembly. *Exp. Mol. Med.* **2011**, *43* (3), 153-160. DOI: 10.3858/emm.2011.43.3.019.
(21) Rao, V. R.; Corradetti, M. N.; Chen, J.; Peng, J.; Yuan, J.; Prestwich, G. D.; Brugge, J. S. Expression cloning of protein targets for 3-phosphorylated phosphoinositides. *J. Biol. Chem.* **1999**, *274* (53), 37893-37900. DOI: 10.1074/jbc.274.53.37893.
(22) Johnson, R. S.; Martin, S. A.; Biemann, K.; Stults, J. T.; Watson, J. T. Novel fragmentation process of peptides by collision-induced decomposition in a tandem mass spectrometer: differentiation of leucine and isoleucine. *Anal. Chem.* **1987**, *59* (21), 2621-2625. DOI: 10.1021/ac00148a019.
(23) Pike, L. J. The challenge of lipid rafts. *J. Lipid Res.* **2009**, *50 Suppl* (Suppl), S323-328. DOI: 10.1194/jlr.R800040-JLR200.
(24) Lingwood, D.; Simons, K. Lipid rafts as a membrane-organizing principle. *Science* **2010**, *327* (5961), 46-50. DOI: 10.1126/science.1174621.
(25) Levental, I.; Levental, K. R.; Heberle, F. A. Lipid Rafts: Controversies Resolved, Mysteries Remain. *Trends Cell Biol.* **2020**, *30* (5), 341-353. DOI: 10.1016/j.tcb.2020.01.009.
(26) Sezgin, E.; Levental, I.; Mayor, S.; Eggeling, C. The mystery of membrane organization: composition, regulation and roles of lipid rafts. *Nat. Rev. Mol. Cell Biol.* **2017**, *18* (6), 361-374. DOI: 10.1038/nrm.2017.16.
(27) van Meer, G.; Hoetzl, S. Sphingolipid topology and the dynamic organization and function of membrane proteins. *FEBS Lett.* **2010**, *584* (9), 1800-1805. DOI: 10.1016/j.febslet.2009.10.020.
(28) Nishio, K.; Masaike, Y.; Ikeda, M.; Narimatsu, H.; Gokon, N.; Tsubouchi, S.;

Hatakeyama, M.; Sakamoto, S.; Hanyu, N.; Sandhu, A.; Kawaguchi, H.; Abe, M.; Handa, H. Development of novel magnetic nano-carriers for high-performance affinity purification. *Colloids Surf B Biointerfaces* **2008**, *64* (2), 162-169. DOI: 10.1016/j.colsurfb.2008.01.013.
(29) Murphy, J.; Riley, J. P. A modified single solution method for the determination of phosphate in natural waters. *Anal. Chim. Acta* **1962**, *27*, 31-36. DOI: 10.1016/S0003-2670(00)88444-5.
(30) Niemela, P. S.; Ollila, S.; Hyvonen, M. T.; Karttunen, M.; Vattulainen, I. Assessing the nature of lipid raft membranes. *PLoS Comput. Biol.* **2007**, *3* (2), e34. DOI: 10.1371/journal.pcbi.0030034.
(31) Leftin, A.; Molugu, Trivikram R.; Job, C.; Beyer, K.; Brown, Michael F. Area per Lipid and Cholesterol Interactions in Membranes from Separated Local-Field 13 C NMR Spectroscopy. *Biophys. J.* **2014**, *107* (10), 2274-2286. DOI: 10.1016/j.bpj.2014.07.044.
(32) Sekizawa, Y.; Hagiwara, K.; Nakajima, T.; Kobayashi, H. A NOVEL PROTEIN, LYSENIN, THAT CAUSES CONTRACTION OF THE ISOLATED RAT AORTA: ITS PURIFICATION FROM THE COELOMIC FLUID OF THE EARTHWORM, *EISENIA FOETIDA*. *Biomedical Research* **1996**, *17* (3), 197-203. DOI: 10.2220/biomedres.17.197.
(33) De Colibus, L.; Sonnen, A. F.; Morris, K. J.; Siebert, C. A.; Abrusci, P.; Plitzko, J.; Hodnik, V.; Leippe, M.; Volpi, E.; Anderluh, G.; Gilbert, R. J. Structures of lysenin reveal a shared evolutionary origin for pore-forming proteins and its mode of sphingomyelin recognition. *Structure* **2012**, *20* (9), 1498-1507. DOI: 10.1016/j.str.2012.06.011.
(34) Ishitsuka, R.; Yamaji-Hasegawa, A.; Makino, A.; Hirabayashi, Y.; Kobayashi, T. A lipid-specific toxin reveals heterogeneity of sphingomyelin-containing membranes. *Biophys. J.* **2004**, *86*, 296-307. DOI: 10.1016/S0006-3495(04)74105-3.
(35) Contreras, F. X.; Ernst, A. M.; Haberkant, P.; Bjorkholm, P.; Lindahl, E.; Gonen, B.; Tischer, C.; Elofsson, A.; von Heijne, G.; Thiele, C.; Pepperkok, R.; Wieland, F.; Brugger, B. Molecular recognition of a single sphingolipid species by a protein's transmembrane domain. *Nature* **2012**, *481* (7382), 525-529. DOI: 10.1038/nature10742.
(36) Hanada, K.; Kumagai, K.; Tomishige, N.; Yamaji, T. CERT-mediated trafficking of ceramide. *Biochim. Biophys. Acta* **2009**, *1791* (7), 684-691. DOI: 10.1016/j.bbalip.2009.01.006.
(37) Kumagai, K.; Hanada, K. Structure, functions and regulation of CERT, a lipid-transfer protein for the delivery of ceramide at the ER-Golgi membrane contact sites. *FEBS Lett.* **2019**, *593* (17), 2366-2377. DOI: 10.1002/1873-3468.13511.
(38) Bae, T. J.; Kim, M. S.; Kim, J. W.; Kim, B. W.; Choo, H. J.; Lee, J. W.; Kim, K. B.; Lee, C. S.; Kim, J. H.; Chang, S. Y.; Kang, C. Y.; Lee, S. W.; Ko, Y. G. Lipid raft proteome reveals ATP synthase complex in the cell surface. *Proteomics* **2004**, *4* (11), 3536-3548. DOI: 10.1002/pmic.200400952.
(39) Zhu, Y.; Pu, Z.; Wang, G.; Li, Y.; Wang, Y.; Li, N.; Peng, F. FAM3C: an emerging biomarker and potential therapeutic target for cancer. *Biomark. Med.* **2021**, *15* (5), 373-384. DOI: 10.2217/bmm-2020-0179.
(40) Jembrek, M. J.; Hof, P. R.; Simic, G. Ceramides in Alzheimer's Disease: Key Mediators of Neuronal Apoptosis Induced by Oxidative Stress and Abeta Accumulation.

Oxid. Med. Cell. Longev. **2015**, *2015*, 346783. DOI: 10.1155/2015/346783.
(41) Chowdhury, M. R.; Jin, H. K.; Bae, J. S. Diverse Roles of Ceramide in the Progression and Pathogenesis of Alzheimer's Disease. *Biomedicines* **2022**, *10* (8), 1956. DOI: 10.3390/biomedicines10081956.
(42) Hein, M. Y.; Hubner, N. C.; Poser, I.; Cox, J.; Nagaraj, N.; Toyoda, Y.; Gak, I. A.; Weisswange, I.; Mansfeld, J.; Buchholz, F.; Hyman, A. A.; Mann, M. A human interactome in three quantitative dimensions organized by stoichiometries and abundances. *Cell* **2015**, *163* (3), 712-723. DOI: 10.1016/j.cell.2015.09.053.
(43) Larocque, G.; Penelope, J. L.-B.; Clarke, N. I.; Carter, N. J.; Royle, S. J. Tumor protein D54 defines a new class of intracellular transport vesicles. *J. Cell Biol.* **2020**, *219*, e201812044. DOI: 10.1083/JCB.201812044/VIDEO-6.
(44) Reynaud, A.; Magdeleine, M.; Patel, A.; Gay, A. S.; Debayle, D.; Abelanet, S.; Antonny, B. Tumor protein D54 binds intracellular nanovesicles via an extended amphipathic region. *J. Biol. Chem.* **2022**, *298* (7), 102136. DOI: 10.1016/j.jbc.2022.102136.
(45) Vanni, S.; Vamparys, L.; Gautier, R.; Drin, G.; Etchebest, C.; Fuchs, P. F.; Antonny, B. Amphipathic lipid packing sensor motifs: probing bilayer defects with hydrophobic residues. *Biophys. J.* **2013**, *104* (3), 575-584. DOI: 10.1016/j.bpj.2012.11.3837.

Chapter 3
Comprehensive Identification of Lipid-Membrane Protein Interactions via Advanced Proteomics and Extended Lipid-Immobilized Bead Technology

Abstract

In biological membranes, lipids interact with membrane proteins (MPs) and play an important role in allosterically regulating their structure and function. Analyzing lipid-MP interactions is necessary for understanding these regulatory mechanisms; however, there have been few comprehensive and systematic studies to date. To address this, the author developed a high-sensitivity, high-throughput platform that integrates lipid-immobilized beads with advanced proteomics to analyze lipid-MP interactions in detail. The author prepared six types of lipid-immobilized beads, including sphingomyelin (SM), ceramide (Cer), dihydrosphingomyelin (DHSM), dihydroceramide (DHCer), phosphatidylcholine (PC), and cholesterol (Chol). In addition, the author introduced a novel type of beads that immobilized SM and Chol (SM/Chol beads) to mimic lipid rafts. The author first demonstrated that SM/Chol beads co-precipitated with Nakanori, a protein that specifically recognizes and binds to SM-Chol complexes, whereas beads immobilized with SM or Chol alone did not co-precipitate. This indicates the effectiveness of SM/Chol beads for the identification of raft-associated proteins. Next, the cell lysates were incubated with the seven types of lipid-immobilized beads and the recovered proteins were analyzed using shotgun proteomics. This approach successfully identified over 7000 lipid-binding proteins. Filtering based on fold-change values and subsequent enrichment analysis revealed distinct binding protein profiles for each lipid, highlighting the functional diversity of lipid-MP interactions and their roles in cellular processes. In summary, this methodology enables an unprecedented large-scale exploration of lipid-MP interactions. This platform provides a versatile tool for examining the lipid-mediated regulation of MPs and offers new insights into the physiological significance of the lipidome and its implications for health and disease.

3.1 Introduction

In **Chapter 2**, a systematic analysis of "lipid-binding proteins" was developed using detergent-tolerant and membrane-mimetic lipid-immobilized beads. Thus, this method will provide a long-awaited advance in the analysis of lipid-MP interactions; however, the use of SDS-PAGE makes it still difficult to perform a comprehensive analysis of MPs.

In this chapter, the author has improved this method in three ways. First, shotgun proteomics replaced SDS-PAGE, enabling the comprehensive and quantitative screening of lipid-binding proteins. Proteins bound to lipid-immobilized beads were eluted by heat denaturation with SDS, and the recovered proteins were digested with trypsin and analyzed by nanoflow liquid chromatography tandem mass spectrometry (nano-LC/MS/MS) with data-independent acquisition (DIA). Second, to gain insight into the biological context of the lipid-protein interactions, the identified proteins were annotated to biological processes using an enrichment analysis. Third, the author expanded the variation of the lipid-immobilized beads. Since lipid rafts, domains of biological membranes enriched in sphingolipids and Chol, have been proposed to serve as platforms for the accumulation and function of MPs,[1-4] raft-related lipid species were selected for immobilization. In addition to the previously prepared SM- and Cer-beads, the author newly immobilized dihydrosphingomyelin (DHSM), dihydroceramide (DHCer), phosphatidylcholine (PC), and cholesterol (Chol) on the beads (**Figure 3.1**). DHSM and DHCer, in which the double bond at C4–C5 in the sphingosine base is hydrogenated to a single-bond, are known to form domain more efficiently than their normal counterparts, SM and Cer, respectively,[5, 6] but their specific physiological functions are less clear. Furthermore, SM/Chol beads were prepared by immobilizing a mixture of SM and Chol

in order to better reproduce lipid rafts on the beads surface. Using shotgun proteomics and these beads, more than 7,000 lipid-specific binding protein candidates were successfully identified from cell lysates.

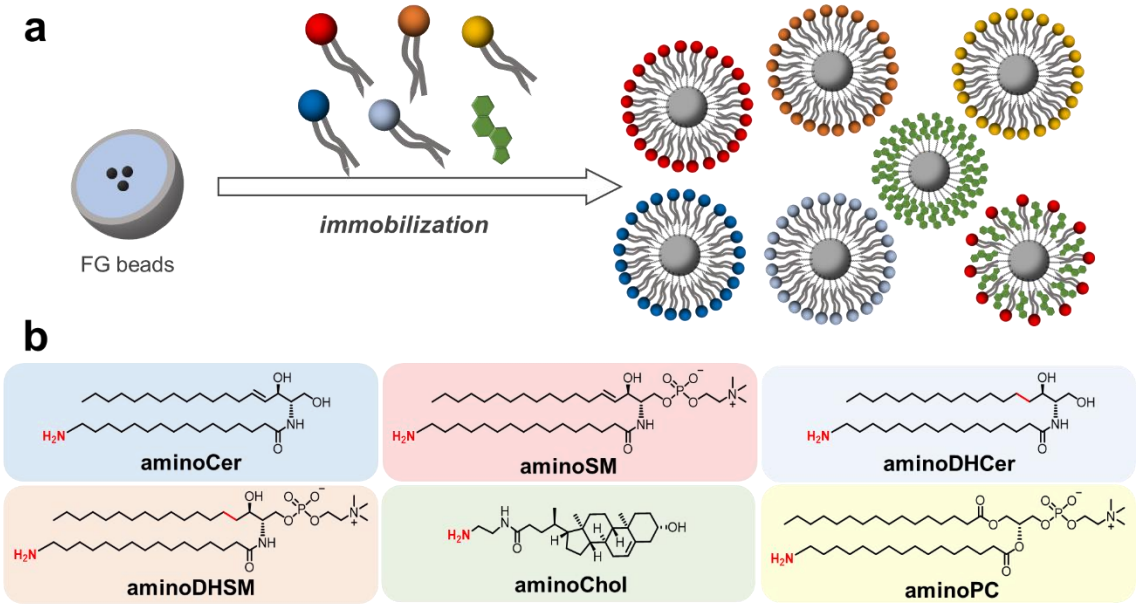

Figure 3.1. (a) Various lipids were immobilized on the beads. (b) The synthesized lipid derivatives have an amino group for covalent immobilization through amide bond formation.

3.2 Gene Ontology Analysis

Gene Ontology (GO) is a standardized terminology used to describe the functions of genes, and each term defined within GO is referred to as a GO term. GO terms are organized in a hierarchical structure and are broadly classified into three categories: Biological Process (BP), Cellular Component (CC), and Molecular Function (MF). BP describes the metabolic or signaling pathways in which gene products are involved, such as apoptosis. CC describes the subcellular locations of gene products, such as mitochondria. MF describes the biochemical activities of gene products, such as ligand

binding. Each gene is assigned GO terms that represent its functions, and this information is stored in databases. For example, the GO terms assigned to ATP synthase subunit a are shown in **Table 3.1**.

Table3.1. the GO terms assigned to ATP synthase subunit a

Biological Process (BP)

GO ID	GO term
GO: 0001937	negative regulation of endothelial cell proliferation
GO: 0006629	lipid metabolic process
GO: 0006754	ATP biosynthetic process
GO: 0014850	response to muscle activity
GO: 0015986	proton motive force-driven ATP synthesis
GO: 0042776	proton motive force-driven mitochondrial ATP synthesis
GO: 0043536	positive regulation of blood vessel endothelial cell migration
GO: 0045471	response to ethanol
GO: 0071549	cellular response to dexamethasone stimulus
GO: 0071732	cellular response to nitric oxide
GO: 1902600	proton transmembrane transport

Molecular Function (MF)

GO ID	GO term
GO: 0002020	protease binding
GO: 0003723	RNA binding
GO: 0005515	protein binding
GO: 0005524	ATP binding
GO: 0016887	ATP hydrolysis activity
GO: 0042288	MHC class I protein binding
GO: 0043531	ADP binding
GO: 0043532	angiostatin binding
GO: 0046933	proton-transporting ATP synthase activity, rotational mechanism

Cellular Component (CC)

GO ID	GO term
GO: 0005737	cytoplasm
GO: 0005739	mitochondrion
GO: 0005743	mitochondrial inner membrane
GO: 0005759	mitochondrial matrix
GO: 0005886	plasma membrane
GO: 0009986	cell surface
GO: 0016020	membrane
GO: 0016469	proton-transporting two-sector ATPase complex
GO: 0045121	membrane raft
GO: 0045259	proton-transporting ATP synthase complex
GO: 0045261	obsolete proton-transporting ATP synthase complex, catalytic core F(1)
GO: 0070062	extracellular exosome
GO: 1902495	transmembrane transporter complex

GO enrichment analysis is a method used to extract GO terms that are significantly overrepresented in a list of genes or gene products (e.g., proteins, RNA) compared to the entire genome (**Figure 3.2**). For example, if a specific Biological Process (BP) is enriched in a list of genes whose expression levels change in a particular disease, that BP is likely to be associated with the disease. Enriched GO terms are often grouped into clusters based on measures of semantic similarity or overlapping annotations, allowing for a more concise understanding of trends in functionally related terms or broader biological themes. Thus, GO analysis makes it easier to extract larger biological meaning or features with a given gene set. In this study, GO analysis of lipid-binding proteins was conducted to understand the biological context of lipid-protein interactions for each lipid.

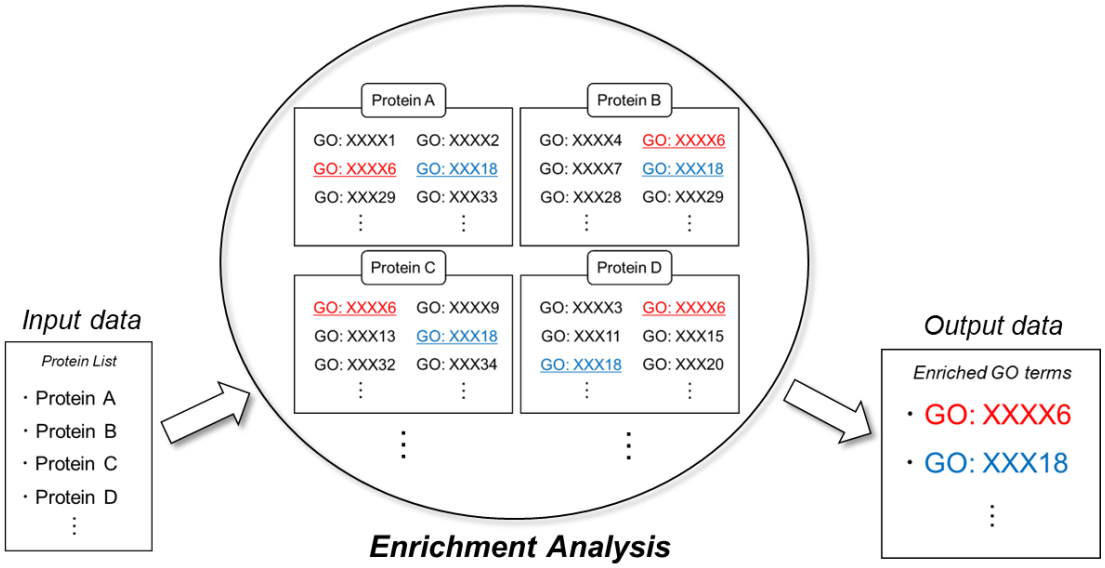

Figure 3.2. Overview of enrichment analysis: First, a list of genes or gene products is provided as input; in this study, a protein list was used. Then, enriched GO terms, which are significantly overrepresented among the GO terms assigned to each protein in the list, are output.

3.3 Experimental Section

3.3.1 Materials and Methods

General

AminoSM (**5**) and AminoCer (**7**) were synthesized as described in **Chapter 2**. NHS-activated FG beads were purchased from Tamagawa Seiki Co., Ltd. (Nagano, Japan). Trifluoroacetic acid (TFA) was purchased from Thermo Fisher Scientific (Waltham, MA, USA); Trypsin/Lys-C mix were from Promega (Madison, WI, USA); Iodoacetamide (IAA) and acetone were from Merck (Darmstadt, Germany); LC/MS-grade formic acid (FA), QTofMS-grade water, and QTofMS-grade acetonitrile were form Fujifilm Wako Pure Chemical (Osaka, Japan). All other reagents were all purchased from FUJIFILM Wako Pure Chemical Corp. (Osaka, Japan), Tokyo Chemical Inc. (Tokyo, Japan), Nacalai Tesque Inc. (Kyoto, Japan), or Sigma-Aldrich (St. Louis, MO, USA).

Synthesis of aminated lipids

The synthesis details of compounds **8**–**15** are given in Supporting Information.

Preparation of the lipid-immobilized beads

The synthesized aminated lipids were immobilized as described in **Chapter 2**. NHS-activated beads (2.0 mg) were washed three times with 400 μL of DMF and incubated with 10 mM triethylamine and 1 mM aminated lipids in 400 μL of DMF overnight at room temperature. The beads were washed three times with 400 μL of DMF and the unreacted NHS ester groups were masked with 1.0 M ethanolamine in DMF. After washing three times with 50% MeOH, the beads were resuspended in 100 μL of 50% MeOH and stored at 4°C. Negative control beads were prepared through a reaction of 1

mM dodecylamine in DMF instead of the aminated lipids.

Nakanori pulldown using lipid-immobilized beads

SM, Chol, SM/Chol, and control beads (0.25 mg) were incubated with Nakanori (100 μg mL^{-1}, 50 μL). After incubation at 4°C for 4 h, the supernatant was removed via magnetic separation. The beads were washed twice with 200 μL of lysis buffer (50 mM Tris [pH 8.0], 150 mM NaCl, and 1% Nonidet P-40), boiled in SDS sample buffer (240 mM Tris-HCl [pH 6.8]), 8% SDS, 40% glycerol, 0.1% bromophenol blue, and 20% 2-mercaptoethanol). The supernatant was applied to a 4%–20% SDS-PAGE gel, followed by silver staining.

Pulldown using lipid-immobilized beads

Each type of the beads (0.5 mg) was washed with 200 μL of lysis buffer followed by dispersion in Neuro2a cell lysate (1 mg mL^{-1}, 50 μL), which was prepared as described in **Chapter 2**. After incubation at 4°C for 4 h, the supernatant was removed via magnetic separation. The beads were washed twice with 200 μL of lysis buffer and boiled in SDS sample buffer. Three samples were prepared for each type of the beads.

Proteomic analysis

Shotgun proteomic analysis was performed as described previously,[7] with modifications. To prepare the samples for proteomic analysis, 10 μL of the above sample was dispensed into a tube, to which 2 μL of 240 mM iodoacetamide (Merck) was added, and the mixture was incubated at room temperature for 30 min. Then, 36 μL of acetone pre-cooled to −30°C was added, and the mixture was stored at −30°C for 2 h. After centrifugation, the

supernatant was discarded. The sample was washed with 100 μL of 90% acetone pre-cooled to −30°C and then centrifuged to remove supernatant. This washing step was repeated once more under the same conditions. The sample was then air-dried, dissolved in 4 μL of 125 ng/μL trypsin/Lys-C Mix (Promega), and sonicated for 90 s using a sonicator UIP400MTP (Hielscher Ultrasonics GmbH, Teltow, Germany), followed by a centrifugation. The sample was then incubated at 37°C for 30 min using a Thermomixer comfort (Eppendorf, Hamburg, Germany) at 300 rpm, and 1 μL of 1.25% trifluoroacetic acid (TFA) containing internal standard peptides was added. A quantitative peptide assay (Pierce™ Quantitative Fluorometric Peptide Assay, Thermo Fisher Scientific) was then performed. For SM, SM/Chol, and Input samples, 100 ng of peptide was used for proteomic analysis. For the other samples, 1 μL was used for analysis, as peptide levels were below the quantitation limit of the assay.

The nano-LC/MS/MS system was composed of a Dionex Ultimate 3000 nano-RSLC system and a Orbitrap Exploris 480, a high-performance benchtop quadrupole Orbitrap mass spectrometer (Thermo Fisher Scientific) equipped with a Dream spray electrospray ionization source (AMR Inc., Tokyo, Japan). An Acclaim™ PepMap™ C18 column (Thermo Fisher Scientific) with dimensions of 300 μm i.d. × 5 mm and a particle size of 5 μm was used as the pre-column for sample trapping. The loading pump was run at 1 μL/min with water/acetonitrile/TFA (98/2/0.1, v/v/v) and trypsin-digested sample was injected. After loading, the sample was switched online to the packed nano-LC column of 2 μm particle-size L-column2 ODS (CERI, Saitama, Japan) with dimensions of 50 μm i.d. × 200 mm. The nano-LC conditions were as follows: mobile phase, water/formic acid (FA) (100/0.1, v/v) (solvent A) and water/acetonitrile/FA (80/20/0.1, v/v/v) (solvent B); flow rate, 200 nL/min; and column temperature, 40°C. The gradient

conditions were as follows: 5% B, 0–5 min; 5–35% B, 5–95 min; 35–80% B, 95–96 min; 80% B, 96–101 min; 80–5% B, 101–102 min; and 5% B, 102–120 min. The MS analysis conditions were as follows: polarity, positive ionization; spray voltage, 1.8 kV; capillary temperature, 275°C; S-lens level, 50; mass resolution, 30,000; automatic gain control (AGC) target, 3,000,000; maximum injection time (IT), 50 ms; and MS scan range, 400–900 (*m/z*). The MS/MS spectra were acquired using DIA mode with higher-energy collision dissociation. The DIA conditions were as follows: mass resolution, 30,000; AGC target, 1,000,000; maximum IT, 41 ms; loop count, 60; isolation window, 4 (Da) from 430 to 670 (*m/z*); fixed first mass, 200 (*m/z*); and normalized collision energy (NCE), 25 eV.

Raw files from DIA were analyzed in DIA-NN 1.8[8] using an in silico DIA-NN predicted spectral library. The parameters of the mouse reference spectral library generated from the SwissProt database (2023.03.18-21.42.04.29) are as follows: enzyme used, trypsin; peptide length range, 7−50; allowed number of maximum missed cleavages, 1; modifications, methionine oxidation, carbamidomethylation of cysteine, and *N*-terminal acetylation; and false discovery rate (FDR), less than 1%.

Calculation of the fold-changes and selection of lipid-binding proteins

The fold-change values, representing the ratio of protein amounts between the lipid-immobilized beads and control beads or the input, were calculated. The protein amounts were determined by summing the peak height values of the top six product ions (MS/MS) with the highest intensity for each sequence-specific peptide. Three measurements were made for each bead and the mean protein amount was used. The protein quantities were normalized to the total amount of binding protein for each bead. For lipid-binding proteins

not identified in the inputs or controls, the fold-change was calculated using the lowest value (7.6×10^2) in the measurement instead of the input and/or control. Proteins were selected in which the fold-change values were in the top 15% for inputs and/or controls and those that had a fold-change greater than two times that of the other beads were extracted to remove duplicates. The resulting proteins identified from the six bead types, excluding SM/Chol beads, were further filtered to remove duplicates within the set. In contrast, the SM/Chol-binding protein candidates were selected to exclude duplicates from the remaining six bead types.

Enrichment and clustering analysis using DAVID

Enrichment analysis was performed using the Database for Annotation, Visualization, and Integrated Discovery (DAVID) Bioinformatics Resource.[9, 10] Significantly enriched GO terms were defined if their *p*-values were < 0.05. The enrichment score for each cluster was defined as the geometric mean (−log scale) of the member's *p*-values in the corresponding annotation cluster. Clusters with enrichment scores greater than $-\log_{10}(0.05)$ were considered significant. For the GO term enrichment and clustering analyses, GO_FAT categories were used.

3.4 Result

3.4.1. Preparation of lipid-immobilized beads

In addition to SM and Cer beads, DHSM, DHCer, Chol, PC, and SM/Chol beads were prepared. These lipids were selected based on their association with lipid rafts. DHSM and DHCer, which feature a single bond replacing the double bond at the C4–C5

position in the sphingosine base, form domains more efficiently than their normal counterparts, SM and Cer, respectively;[5, 6] however, their specific physiological functions remain unclear. The author synthesized amino derivatives of these lipids (**Figure 3.1b**), which were covalently immobilized onto the beads.

An aminated derivative of DHSM **8** was synthesized by the hydrogenation of azidosphingomyelin **7** (**Scheme 3.1**), which was prepared as previously described.[11] The synthesis of amino-DHCer **11** commenced with the deacylation of C18 DHCer in $CHCl_3$/MeOH with HCl to yield dihydrosphingosine **9** (**Scheme 3.1**). The subsequent introduction of the azido acyl chain to dihydrosphingosine, followed by reduction of the azido group through the Staudinger reaction, yielded the desired product **11**. AminoChol **13** was synthesized by introducing the amino group to 3β-hydroxy-Δ5-cholenic acid. After activating the carboxy group of 3β-hydroxy-Δ5-cholenic acid, treatment with an excess amount of ethylenediamine yielded aminoChol **13** (**Scheme 3.2 top**). AminoPC **15** was also synthesized using lysoPC as the substrate according to a scheme similar to that used for aminoDHCer (**Scheme 3.2 bottom**). Following the condensation of lysoPC with the azido acyl chain, the azido group was reduced to obtain aminoPC **15**.

These aminated lipids were immobilized on the FG beads, in the same manner as in **Chapter 2**. These lipids were incubated with NHS beads, in which the carboxyl groups of the FG beads were activated as *N*-hydroxysuccinimide (NHS) esters, and unreacted NHS ester groups were subsequently blocked with aminoethanol, resulting in the preparation of six lipid-immobilized beads (SM, Cer, DHSM, DHCer, Chol, and PC beads). To mimic lipid rafts, SM/Chol beads were also prepared by conjugating equimolar amounts of aminoSM and aminoChol with NHS beads. In addition, dodecylamine was immobilized as a negative control alongside these lipid-immobilized beads.

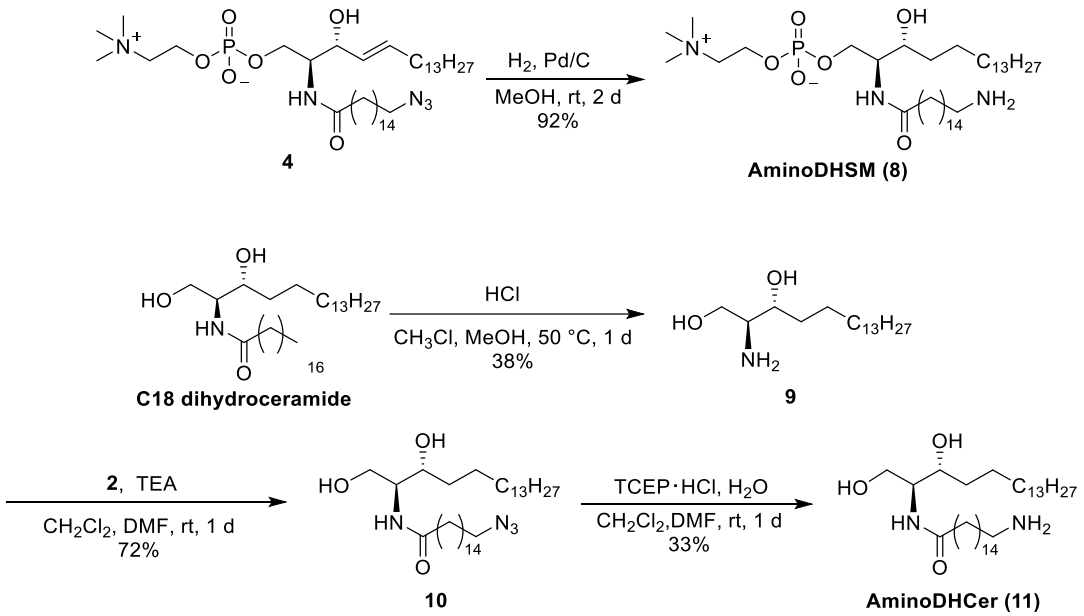

Scheme 3.1. Synthesis of aminoDHSM and aminoDHCer

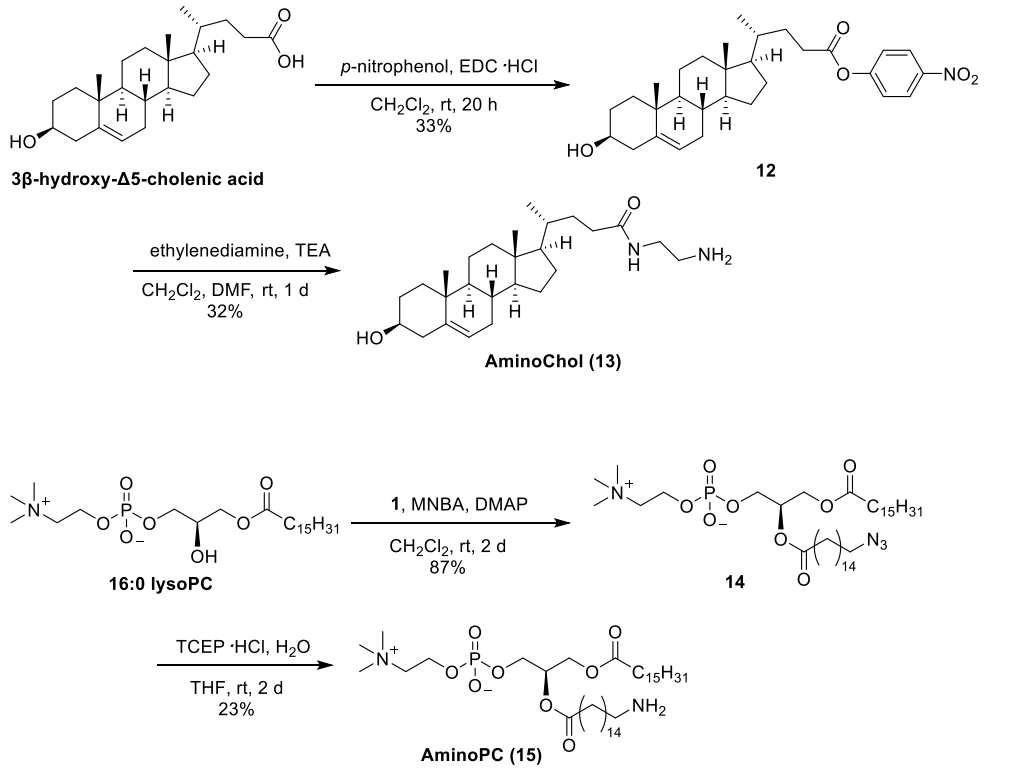

Scheme 3.2. Synthesis of aminoChol and aminoPC

3.4.2. Nakanori selectively bound to SM/Chol beads

Nakanori is a protein isolated from extracts of the edible mushroom *Grifola frondosa*. It specifically recognizes and binds to a complex of SM and Chol, but not to other lipids or proteins.[12] To evaluate the performance of SM/Chol beads, a pulldown assay was conducted using this protein. Nakanori was incubated with SM/Chol, SM, Chol, and control beads overnight at 4°C. After washing, the protein was recovered from each bead type and subjected to electrophoresis and silver staining. The results indicated that Nakanori was detected only with SM/Chol beads, whereas beads immobilized with either SM or Chol alone failed to co-precipitate the protein (**Figure 3.3**). These results are consistent with the fact that Nakanori is specific to SM/Chol raft domains in membranes.[12] More importantly, this experiment clearly demonstrates that the raft domains were successfully reproduced on SM/Chol beads, confirming their effectiveness in identifying raft-associated proteins.

Figure 3.3. Pulldown assay of Nakanori with SM, Chol, SM/Chol, and control beads. Nakanori specifically binds to SM/Chol beads, but not to SM or Chol beads.

3.4.3 Identification of lipid-binding proteins from Neuro 2a cell lysates

Seven different beads were used to screen for lipid-binding proteins from Neuro2a cell lysates. The beads were incubated with the cell lysates, washed, and subjected to heat treatment to elute the bound proteins. The recovered proteins were

enzymatically digested and analyzed by a highly sensitive DIA-based nano-LC-MS/MS system using a nano-spray integrated nano-LC column with a fused silica capillary of 50 μm inner diameter (i.d.) and 2 μm ODS particles.[13] This approach identified over 7,000 proteins along with their fold-change values, which represent the ratios of protein abundance between lipid-immobilized beads and the control beads or the input (**Table S3.1.1**). The putative lipid-binding proteins were refined through a two-step selection process. First, proteins with fold-change values in the top 15% relative to either the input or control were selected. Second, to minimize redundancy among the beads, the proteins were filtered so that the fold-change value for a particular type of the beads was at least twice as large as those for the other beads (**Table 3.2**). For the six bead types, excluding SM/Chol beads, the candidates were filtered within the group. For SM/Chol beads, candidates were selected to exclude duplicates with the other six bead types. The top five proteins based on fold-change values for each type of the beads are listed in **Table 3.3**. The resulting candidates included several known lipid-binding proteins, such as annexin A1 (Anxa1)[14] and ceramide transfer protein (Cert1)[15], which were associated with Cer, interferon-induced transmembrane protein 3 (Ifitm3)[16], which was associated with Chol, and TPD54 (Tpd52l2)[11], which was associated with SM. The results validate this procedure for identifying lipid-binding proteins and suggest that the dataset may include novel candidate proteins. This method effectively identifies proteins that distinguish not only differences in hydrophilic head groups and the presence of double bonds, but also mixed lipid components, offering a robust approach for characterizing lipid-MP interactions.

Table 3.2. Number of lipid-binding proteins after deduplication.

Lipid	*Number of lipid-binding proteins*
Cer	49
SM	177
DHCer	356
DHSM	35
Chol	464
PC	17
SM/Chol	34

Table 3.3. Representative lipid-binding protein candidates after deduplication.

Lipid	*Gene*	*Name*	*Fold-change versus input*	*Gene*	*Name*	*Fold-change versus control*
Cer	Serpinb10	Serpin B10	4997.8	Hand1	Heart- and neural crest derivatives-expressed protein 1	1709.8
	Adh7	All-trans-retinol dehydrogenase [NAD (+)] ADH7	2676.4	Stx1b	Syntaxin-1B	718.6
	Hck	Tyrosine-protein kinase HCK	1914.1	Tm2d2	TM2 domain-containing protein 2	699.9
	Ttc23l	Tetratricopeptide repeat protein 23-like	1602.0	Znf277	Zinc finger protein 277	196.9
	Pmel	Melanocyte protein PMEL	1578.0	Wdcp	WD repeat and coiled-coil-containing protein	24.9
SM	Dact3	Dapper homolog 3	88.6	Dnm1	Dynamin-1	4165.9
	Ipp	Actin-binding protein IPP	77.7	Rab3gap2	Rab3 GTPase-activating protein non-catalytic subunit	3813.7
	Elk3	ETS domain-containing protein Elk-3	74.7	Arhgap17	Rho GTPase-activating protein 17	3443.8
	Dlx1	Homeobox protein DLX-1	71.3	Vwa8	von Willebrand factor A domain-containing protein 8	3235.9
	Ccdc38	Coiled-coil domain-containing protein 38	70.9	Mettl16	RNA N6-adenosine-methyltransferase METTL16	3222.1
DHCer	Tmem19	Transmembrane protein 19	4513.2	Vps52	Vacuolar protein sorting-associated protein 52 homolog	28881.0
	Cmtm7	CKLF-like MARVEL	3191.3	Arl6ip5	PRA1 family protein 3	27579.2

		transmembrane domain-containing protein 7				
	Lyset	Lysosomal enzyme trafficking factor	2160.4	Clcn6	H(+)/Cl(-) exchange transporter 6	25795.4
	Hdac11	Histone deacetylase 11	1604.6	Bst2	Bone marrow stromal antigen 2	22274.2
	Paqr4	Progestin and adipoQ receptor family member 4	1346.9	Ssr3	Translocon-associated protein subunit gamma	19637.9
DHSM	Krt12	Keratin, type I cytoskeletal 12	29822.0	Uqcrh	Cytochrome b-c1 complex subunit 6, mitochondrial	29329.1
	Krt8	Keratin, type II cytoskeletal 8	950.2	Pnpla8	Calcium-independent phospholipase A2-gamma	5394.1
	Nxpe4	NXPE family member 4	212.3	Ccpg1	Cell cycle progression protein 1	1402.1
	Etfrf1	Electron transfer flavoprotein regulatory factor 1	96.5	Hsd17b11	Estradiol 17-beta-dehydrogenase 11	1250.9
	Phb2	Prohibitin-2	79.5	St3gal4	CMP-*N*-acetylneuraminate-beta-galactosamide-alpha-2,3-sialyltransferase 4	1215.4
Chol	Hspb1	Heat shock protein beta-1	3649.1	Scyl1	*N*-terminal kinase-like protein	10913.1
	S100a6	Protein S100-A6	1953.9	Fbxl8	F-box/LRR-repeat protein 8	5075.9
	Insrr	Insulin receptor-related protein	1378.1	Mast2	Microtubule-associated serine/threonine-protein kinase 2	3526.8
	Serpinb5	Serpin B5	1328.3	Slc39a7	Zinc transporter SLC39A7	2899.8
	Saysd1	SAYSvFN domain-containing protein 1	1290.7	Sac3d1	SAC3 domain-containing protein 1	2849.3
PC	Tssk4	Testis-specific serine/threonine-protein kinase 4	174.1	Scd2	Stearoyl-CoA desaturase 2	5007.4
	TCAIM	T-cell activation inhibitor, mitochondrial	150.7	Dennd3	DENN domain-containing protein 3	4299.1
	Abhd18	Protein ABHD18	91.2	Pctp	Phosphatidylcholine transfer protein	1408.3
	Uqcc4	Ubiquinol-cytochrome-c reductase complex assembly factor 4	60.6	Trim23	E3 ubiquitin-protein ligase TRIM23	1056.6
	Znf703	Zinc finger protein 703	20.6	Oxsm	3-oxoacyl-[acyl-carrier-protein] synthase, mitochondrial	749.9
SM/Chol	Nrif1	Neurotrophin receptor-interacting factor 1	324.0	Ap4b1	AP-4 complex subunit beta-1	2377.8
	Sh3tc2†	SH3 domain and tetratricopeptide repeat-containing protein 2†	90.7	Med24	Mediator of RNA polymerase II transcription subunit 24	2368.0
	Dnajc30	DnaJ homolog subfamily C member 30, mitochondrial	42.6	Mtr†	Methionine synthase†	1993.1
	Mettl25b	Methyltransferase-like protein 25B	34.6	Ap4e1	AP-4 complex subunit epsilon-1	1488.2

Ttll7	Tubulin polyglutamylase TTLL7	30.8	Ap5b1	AP-5 complex subunit beta-1	1476.8	

†: Dagger-marked proteins in SM/Chol were also identified in SM beads. For lipid-binding proteins that were not identified from the input or control beads, the fold-change values were calculated using the lowest value (7.6×10^2) in the measurement instead of the input and/or control. The complete lists are presented in **Tables S3.1.2–S.3.1.8** in Supporting Information.

3.4.4 Enrichment analysis of lipid-binding proteins

To examine the BP associated with each lipid, the identified proteins were analyzed for GO terms in the BP category using the Database for Annotation, Visualization, and Integrated Discovery (DAVID) Bioinformatics Resource.[9, 10] This analysis provided enriched GO terms and annotation clusters (**Table 3.4** and **Supporting File 3.2** in Supporting Information). The top five enriched GO terms for each bead type are presented in **Figure 3.4**. The top three significant annotation clusters are illustrated in **Figures 3.5, 3.6, and 3.7**, although the Cer, DHSM, and SM/Chol beads yielded only one or two annotation clusters. For example, GO terms related to lipid biosynthesis and metabolism were shared across several types of the beads, but protein sulfation was uniquely annotated in DHSM-binding proteins and lysosome organization was specifically associated with SM/Chol-binding proteins (**Supporting File 3.2** in Supporting Information). Notably, different proteins were identified and annotated between SM and DHSM beads or between Cer and DHCer beads (**Figures 3.4-3.6**), demonstrating that minor structural differences in lipids, such as the presence or absence of a single double bond, can change the interactions with proteins. In contrast, no significantly enriched pathways or clusters were identified for PC. Similar GO enrichment analyses were conducted for the CC and MF categories (**Supporting Files 3.2 and 3.4** in Supporting Information).

Table 3.4. Number of enriched GO terms and clusters of the BP category.

Lipid	*Number of GO terms**	*Number of clusters***
Cer	24	1
SM	195	18
DHCer	317	34
DHSM	19	1
Chol	268	28
PC	0	0
SM/Chol	27	2

*Enriched GO terms with *p*-values lower than 0.05 were considered significant.
**Clusters with an enrichment score, the geometric mean (in −log scale) of member's *p*-values in a corresponding annotation cluster, that was higher than $-\log_{10}(0.05)$, were considered significant.

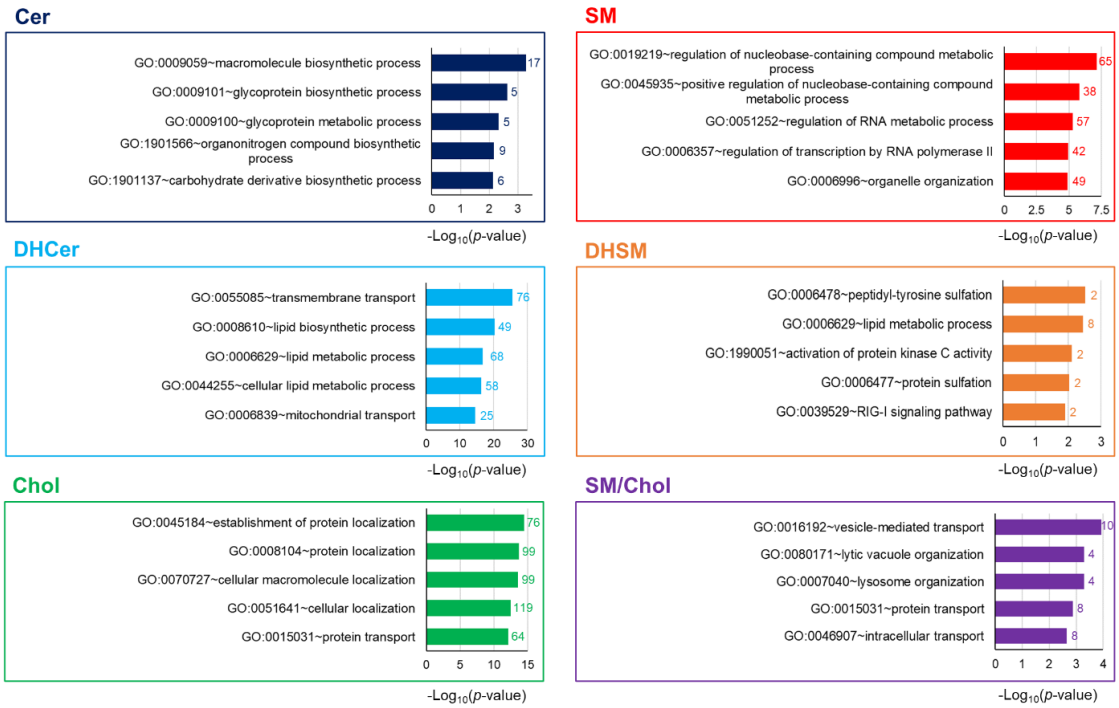

Figure 3.4. The top five enriched GO terms in the BP category, ranked by the lowest *p*-value for each type of lipid-immobilized beads. The corresponding *p*-values (presented by bars) and protein counts (shown next to the bars) for each enriched GO term are shown on the right.

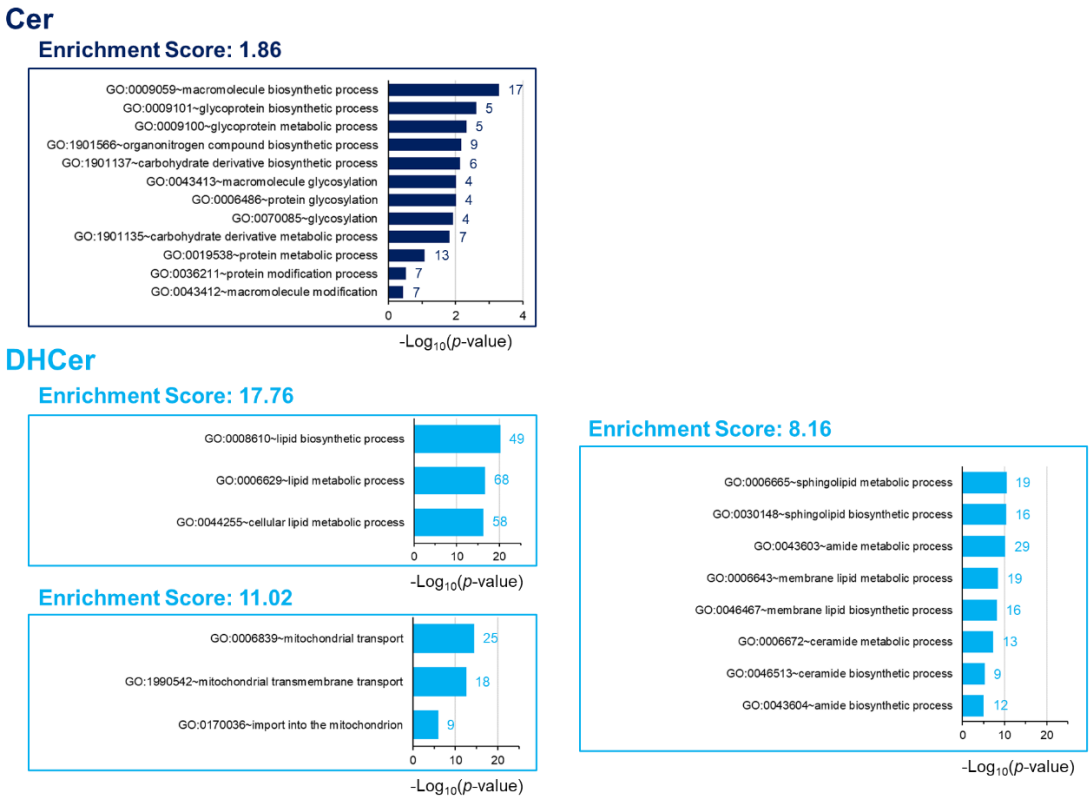

Figure 3.5. The top three significant clusters of the enriched GO terms in the BP category for Cer- and DHCer-binding proteins, although Cer beads yielded only one cluster. The corresponding *p*-values (represented by bars) and protein counts (indicated next to the bars) for each enriched GO term are shown on the right. The clusters with an enrichment score > $-\log_{10}(0.05)$ were considered significant.

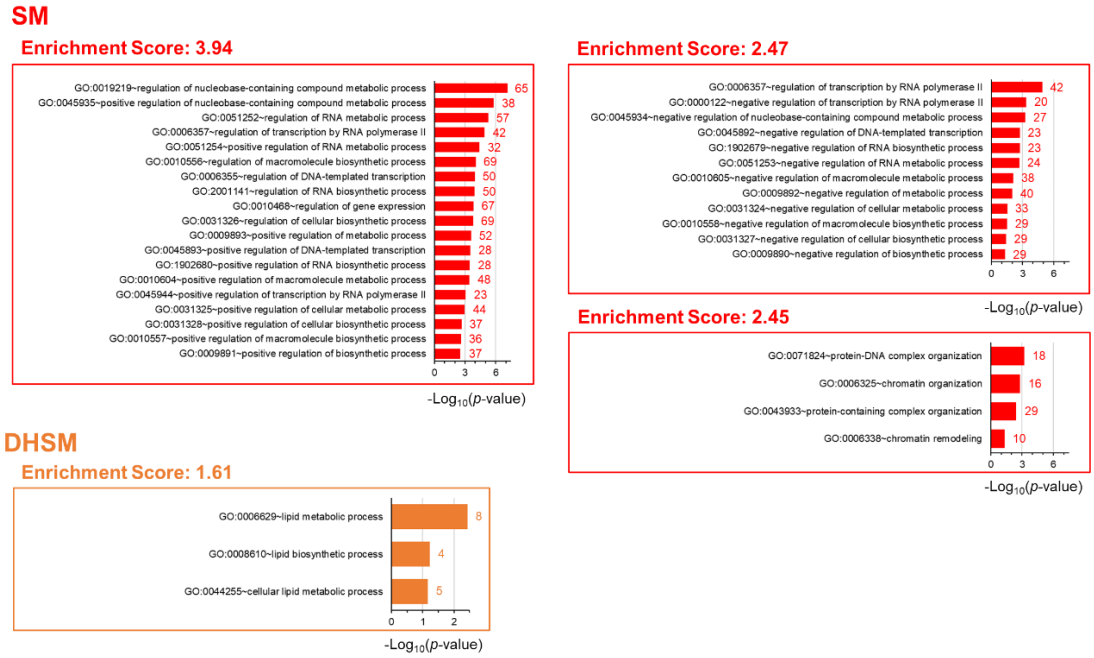

Figure 3.6. The top three significant clusters of the enriched GO terms in the BP category for SM- and DHSM-binding proteins, although DHSM beads yielded only one cluster. The corresponding *p*-values (represented by bars) and protein numbers (indicated next to the bars) for each enriched GO term are shown on the right. The clusters with an enrichment score > $-\log_{10}(0.05)$ were considered significant.

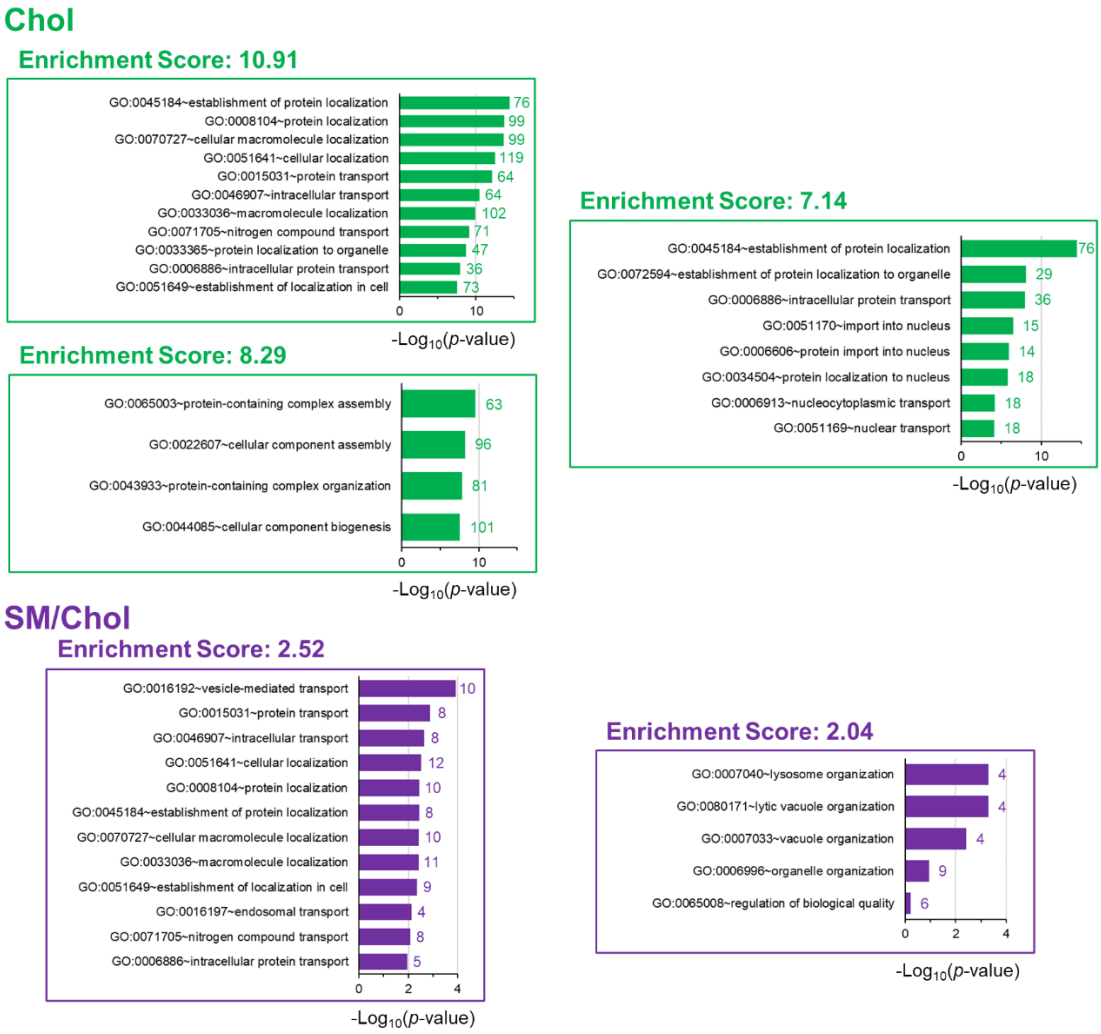

Figure 3.7. The top three significant clusters of the enriched GO terms in the BP category for Chol- and SM/Chol-binding proteins, although SM/Chol beads yielded only two clusters. The corresponding *p*-values (represented by bars) and protein numbers (indicated next to the bars) for each enriched GO term are shown on the right. The clusters with an enrichment score > $-\log_{10}(0.05)$ were considered significant.

3.5 Discussion

In this chapter, the author firstly expands the variety of lipid-immobilized beads. In addition to SM and Cer beads, DHSM and DHCer beads were newly prepared to examine the difference in binding proteins depending on the presence and absence of the

double bond. Along with these sphingolipids, PC, Chol, and heterogeneous SM/Chol beads were prepared. In pull-down assays, nakanori, which specifically recognizes SM/Chol domains such as lipid rafts, bound to SM/Chol beads but did not to either SM or Chol beads (**Figure 3.3**). This result suggests that, despite the covalent immobilization, the surface of SM/Chol beads imitates SM/Chol-rich raft domains in cell membranes. This paves the way for immobilizing more heterogeneous and complicated lipid mixtures to reproduce biological membranes.

Using these prepared beads, the author screened for lipid-binding proteins from cell lysates. Without the use of SDS-PAGE, a high-depth and quantitative comprehensive analysis was conducted with shot-gun proteomics. Owing to this analysis, over 7,000 proteins were comprehensively identified, which were filtered based on fold change values among each type of beads (**Tables 3.2** and **Supporting File 3.1** in Supporting Information). The resultant lipid-binding protein candidates were found to include several known lipid-binding proteins, confirming the efficacy of this method for comprehensive lipid-binding protein analysis.

Subsequently, the identified lipid-binding proteins were annotated using GO enrichment analysis to further understand the biological processes related to each lipid. The analysis suggests that both Cer and DHCer are potentially involved in protein glycosylation, because the GO term "protein glycosylation" was enriched in both Cer- and DHCer-binding proteins (**Figure 4**, **Tables S3.2.1 and S3.2.5** in Supporting Information). However, characteristics of the identified glycosyltransferases are somewhat different between them. Cer-binding glycosyltransferases particularly include acetylgalactosamine transferase (**Table S3.1.2** in Supporting Information), which synthesizes *O*-linked glycans in the Golgi apparatus, while glycosyltransferases identified

from DHCer bead were involved in both *N*-linked and *O*-linked glycan synthesis in the endoplasmic reticulum (ER) and the Golgi apparatus (**Table S3.1.4** in Supporting Information).

DHCer was also involved in lipid biosynthesis and metabolism. Since DHCer is an important biosynthetic precursor of sphingolipids, it is reasonable that the enriched GO terms are related to the biosynthesis and metabolism of sphingolipids (**Figure 3.5**). Interestingly, the GO terms of DHCer were also associated with the biosynthesis and metabolism of glycerolipids, sterols, and fatty acids (**Figure 3.5** and **Table S3.2.6** in Supporting Information), which might suggest that DHCer regulates production and degradation of those lipids. Besides, the GO terms related to transmembrane transport were also significantly enriched in DHCer binding proteins (**Figures 3.4 and 3.5**). Approximately 20% of DHCer-binding proteins were annotated for membrane transport, including the ATP binding cassette (ABC) transporter family, Slc25 family, and Slc35 family (**Table S3.1.4** in Supporting Information). ABC transporters can actively transport molecules by ATP hydrolysis, and their functions are regulated by interactions with lipids.[17] The Slc25 family localizes to mitochondria and maintains mitochondrial function through membrane transport.[18] The Slc35 family transports nucleotide-sugars to the ER and/or the Golgi apparatus, supplying substrates for glycosylation.[19] These results indicate that DHCer interacts with and potentially regulates these transmembrane transporters. However, why and how the minor structural difference between DHCer and Cer results in such distinct protein-binding profiles and BPs requires further investigation.

The enriched GO terms for SM and DHSM were entirely different. In the case of SM-binding proteins, 42% were localized in the nuclear lumen, and most were suggested to be involved in the regulation of nucleic acid biosynthesis and metabolism

(**Figure 3.6**, **Tables S3.2.11, S3.2.12 and S3.3.9** in Supporting Information). Interestingly, SM is reported to be present in the nucleus and regulate DNA synthesis.[20, 21] This consistency suggests that the regulation of DNA synthesis by SM is likely mediated by SM-binding proteins.

In contrast, DHSM-specific proteins enriched the GO term "protein sulfation," which includes tyrosine sulfotransferases TPST1 and TPST2 (**Tables S3.1.5 and S3.2.7** in Supporting Information). Tyrosine sulfation is a crucial post-translational modification involved in various biological processes.[22] TPSTs are known to be inhibited by sphingolipids, including SM.[23] The finding in this study indicated that DHSM is also a potential inhibitor of these enzymes. Additionally, DHSM was previously reported to block viral entry such as human immunodeficiency virus (HIV) through its rigid domain formations.[24] However, given that the chemokine receptor CCR5, one of the receptors for HIV, facilitates HIV entry when its *N*-terminal tyrosines are sulfated,[25] DHSM might prevent the viral entry through its inhibition of tyrosine sulfation, rather than physically blocking viral entry.

With regards to Chol-binding and SM/Chol-binding proteins, “protein localization” was enriched in BP category, but the identified proteins exhibited distinct characteristics. In Chol-binding proteins, nine importins, three transportins, and two exportins, were specifically identified (**Table S3.1.3** in Supporting Information). Consistently, the GO terms related to protein transport to the nucleus were also significantly clustered in MF category (**Table S3.4.4** in Supporting Information). This suggests a potential involvement of Chol in nucleocytoplasmic transport of proteins,[26] although the direct interaction of these proteins with Chol is not known.

In contrast, in SM/Chol-binding proteins, protein localization and vesicle-

mediated transport were clustered together (**Figure 3.7**). In this group, three adaptor protein (AP)-4 subunits and one AP-5 subunit were identified (**Table S3.1.8** in Supporting Information), and both AP-4 and AP-5 are known to mediate clathrin-independent vesicle transport. [27] Considering the possible binding of these proteins to SM/Chol-rich lipid rafts, AP-4 and AP-5 may be involved in raft-mediated transports.

Given that PC is widely distributed in biological membranes, it is not surprising that no significantly enriched annotation was found. Overall, although further analysis is needed to elucidate these latent interactions between proteins and lipids, this method enables a comprehensive understanding of the physiological functions of various lipids, including heterogeneous lipid systems.

3.6 Conclusion

In this chapter, a comprehensive analysis of lipid-specific binding proteins was achieved through a high-depth proteomic analysis and the expansion of lipid species based on lipid-immobilized bead technology. Enrichment-based cluster analyses of proteins identified from the seven types of lipid-immobilized beads suggest that lipid molecules potentially play multiple roles in biological processes. DHCer-binding proteins were enriched in processes related to glycosylation, lipid biosynthesis, and transmembrane transport. DHSM-binding proteins were associated with tyrosine sulfation, a key post-translational modification. SM/Chol-binding proteins are associated with protein localization and vesicle-mediated transport. These findings, although requiring further verification, highlight the functional significance of lipid-MP interactions in cellular processes.

Surprisingly, different proteins were identified and annotated between the SM and DHSM beads as well as between the Cer and DHCer beads (**Figures 3.3–3.5**), which differed only in the presence or absence of a single double bond. This highlights the remarkable selectivity and specificity of the bead technology for characterizing lipid-MP interactions. This technology can be applied to a broader range of lipid species, including polyunsaturated fatty acids, glycolipids, ergosterol, and more complex and heterogeneous lipid mixtures, to reveal the physiological roles of lipid diversity. In this context, this platform facilitates comprehensive and integrated studies of previously unexplored lipid-MP interactions, significantly advancing our understanding of lipid-mediated regulation of MPs.

Reference

(1) Pike, L. J. The challenge of lipid rafts. *J. Lipid Res.* **2009**, *50 Suppl* (Suppl), S323-328. DOI: 10.1194/jlr.R800040-JLR200.
(2) Lingwood, D.; Simons, K. Lipid rafts as a membrane-organizing principle. *Science* **2010**, *327* (5961), 46-50. DOI: 10.1126/science.1174621.
(3) Levental, I.; Levental, K. R.; Heberle, F. A. Lipid Rafts: Controversies Resolved, Mysteries Remain. *Trends Cell Biol.* **2020**, *30* (5), 341-353. DOI: 10.1016/j.tcb.2020.01.009.
(4) Sezgin, E.; Levental, I.; Mayor, S.; Eggeling, C. The mystery of membrane organization: composition, regulation and roles of lipid rafts. *Nat. Rev. Mol. Cell Biol.* **2017**, *18* (6), 361-374. DOI: 10.1038/nrm.2017.16.
(5) Kinoshita, M.; Kyo, T.; Matsumori, N. Assembly formation of minor dihydrosphingomyelin in sphingomyelin-rich ordered membrane domains. *Sci. Rep.* **2020**, *10* (1), 11794. DOI: 10.1038/s41598-020-68688-7.
(6) Hernandez-Tiedra, S.; Fabrias, G.; Davila, D.; Salanueva, I. J.; Casas, J.; Montes, L. R.; Anton, Z.; Garcia-Taboada, E.; Salazar-Roa, M.; Lorente, M.; Nylandsted, J.; Armstrong, J.; Lopez-Valero, I.; McKee, C. S.; Serrano-Puebla, A.; Garcia-Lopez, R.; Gonzalez-Martinez, J.; Abad, J. L.; Hanada, K.; Boya, P.; Goni, F.; Guzman, M.; Lovat, P.; Jaattela, M.; Alonso, A.; Velasco, G. Dihydroceramide accumulation mediates cytotoxic autophagy of cancer cells via autolysosome destabilization. *Autophagy* **2016**, *12* (11), 2213-2229. DOI: 10.1080/15548627.2016.1213927.
(7) Hata, K.; Izumi, Y.; Hara, T.; Matsumoto, M.; Bamba, T. In-Line Sample Processing System with an Immobilized Trypsin-Packed Fused-Silica Capillary Tube for the Proteomic Analysis of a Small Number of Mammalian Cells. *Anal. Chem.* **2020**, *92* (4), 2997-3005. DOI: 10.1021/acs.analchem.9b03993.
(8) Demichev, V.; Messner, C. B.; Vernardis, S. I.; Lilley, K. S.; Ralser, M. DIA-NN: neural networks and interference correction enable deep proteome coverage in high throughput. *Nature Methods* **2020**, *17* (1), 41-44. DOI: 10.1038/s41592-019-0638-x.
(9) Huang da, W.; Sherman, B. T.; Lempicki, R. A. Systematic and integrative analysis of large gene lists using DAVID bioinformatics resources. *Nat. Protoc.* **2009**, *4* (1), 44-57. DOI: 10.1038/nprot.2008.211.
(10) Huang da, W.; Sherman, B. T.; Lempicki, R. A. Bioinformatics enrichment tools: paths toward the comprehensive functional analysis of large gene lists. *Nucleic Acids Res.* **2009**, *37* (1), 1-13. DOI: 10.1093/nar/gkn923.
(11) Morito, M.; Yasuda, H.; Matsufuji, T.; Kinoshita, M.; Matsumori, N. Identification of lipid-specific proteins with high-density lipid-immobilized beads. *Analyst* **2024**, *149*, 3747-3755. DOI: 10.1039/d4an00579a.
(12) Makino, A.; Abe, M.; Ishitsuka, R.; Murate, M.; Kishimoto, T.; Sakai, S.; Hullin-Matsuda, F.; Shimada, Y.; Inaba, T.; Miyatake, H.; Tanaka, H.; Kurahashi, A.; Pack, C. G.; Kasai, R. S.; Kubo, S.; Schieber, N. L.; Dohmae, N.; Tochio, N.; Hagiwara, K.; Sasaki, Y.; Aida, Y.; Fujimori, F.; Kigawa, T.; Nishibori, K.; Parton, R. G.; Kusumi, A.; Sako, Y.; Anderluh, G.; Yamashita, M.; Kobayashi, T.; Greimel, P.; Kobayashi, T. A novel

sphingomyelin/cholesterol domain-specific probe reveals the dynamics of the membrane domains during virus release and in Niemann-Pick type C. *FASEB J.* **2017**, *31* (4), 1301-1322. DOI: 10.1096/fj.201500075R.
(13) Kokubu, M.; Ishihama, Y.; Sato, T.; Nagasu, T.; Oda, Y. Specificity of Immobilized Metal Affinity-Based IMAC/C18 Tip Enrichment of Phosphopeptides for Protein Phosphorylation Analysis. *Anal. Chem.* **2005**, *77* (16), 5144-5154. DOI: 10.1021/ac050404f.
(14) Babiychuk, E. B.; Monastyrskaya, K.; Draeger, A. Fluorescent annexin A1 reveals dynamics of ceramide platforms in living cells. *Traffic* **2008**, *9* (10), 1757-1775. DOI: 10.1111/j.1600-0854.2008.00800.x.
(15) Hanada, K.; Kumagai, K.; Tomishige, N.; Yamaji, T. CERT-mediated trafficking of ceramide. *Biochim. Biophys. Acta* **2009**, *1791* (7), 684-691. DOI: 10.1016/j.bbalip.2009.01.006.
(16) Rahman, K.; Datta, S. A. K.; Beaven, A. H.; Jolley, A. A.; Sodt, A. J.; Compton, A. A. Cholesterol Binds the Amphipathic Helix of IFITM3 and Regulates Antiviral Activity. *J. Mol. Biol.* **2022**, *434* (19), 167759. DOI: https://doi.org/10.1016/j.jmb.2022.167759.
(17) Klappe, K.; Hummel, I.; Hoekstra, D.; Kok, J. W. Lipid dependence of ABC transporter localization and function. *Chem. Phys. Lipids* **2009**, *161* (2), 57-64. DOI: 10.1016/j.chemphyslip.2009.07.004.
(18) Ruprecht, J. J.; Kunji, E. R. S. The SLC25 Mitochondrial Carrier Family: Structure and Mechanism. *Trends Biochem. Sci.* **2020**, *45* (3), 244-258. DOI: 10.1016/j.tibs.2019.11.001.
(19) Hadley, B.; Litfin, T.; Day, C. J.; Haselhorst, T.; Zhou, Y.; Tiralongo, J. Nucleotide Sugar Transporter SLC35 Family Structure and Function. *Comput Struct Biotechnol J* **2019**, *17*, 1123-1134. DOI: 10.1016/j.csbj.2019.08.002.
(20) Ledeen, R. W.; Wu, G. Sphingolipids of the nucleus and their role in nuclear signaling. *Biochimica et Biophysica Acta (BBA) - Molecular and Cell Biology of Lipids* **2006**, *1761* (5), 588-598. DOI: https://doi.org/10.1016/j.bbalip.2006.04.010.
(21) Albi, E.; Cataldi, S.; Rossi, G.; Magni, M. V. A possible role of cholesterol-sphingomyelin/phosphatidylcholine in nuclear matrix during rat liver regeneration. *J. Hepatol.* **2003**, *38* (5), 623-628. DOI: 10.1016/s0168-8278(03)00074-6.
(22) Yang, Y.-S.; Wang, C.-C.; Chen, B.-H.; Hou, Y.-H.; Hung, K.-S.; Mao, Y.-C. Tyrosine Sulfation as a Protein Post-Translational Modification. *Molecules* **2015**, *20* (2), 2138-2164. DOI: 10.3390/molecules20022138.
(23) Kasinathan, C.; Sundaram, P.; Slomiany, B. L.; Slomiany, A. Inhibition of tyrosylprotein sulfotransferase by sphingosine and its reversal by acidic phospholipids. *Biochemistry* **1993**, *32* (4), 1194-1198. DOI: 10.1021/bi00055a026.
(24) Vieira, C. R.; Munoz-Olaya, J. M.; Sot, J.; Jiménez-Baranda, S.; Izquierdo-Useros, N.; Abad, J. L.; Apellániz, B.; Delgado, R.; Martinez-Picado, J.; Alonso, A.; Casas, J.; Nieva, J. L.; Fabriás, G.; Mañes, S.; Goñi, F. M. Dihydrosphingomyelin Impairs HIV-1 Infection by Rigidifying Liquid-Ordered Membrane Domains. *Chem. Biol.* **2010**, *17* (7), 766-775. DOI: 10.1016/j.chembiol.2010.05.023.
(25) Farzan, M.; Mirzabekov, T.; Kolchinsky, P.; Wyatt, R.; Cayabyab, M.; Gerard, N. P.;

Gerard, C.; Sodroski, J.; Choe, H. Tyrosine Sulfation of the Amino Terminus of CCR5 Facilitates HIV-1 Entry. *Cell* **1999**, *96*, 667-676.
(26) Okada, N.; Ishigami, Y.; Suzuki, T.; Kaneko, A.; Yasui, K.; Fukutomi, R.; Isemura, M. Importins and exportins in cellular differentiation. *J. Cell. Mol. Med.* **2008**, *12* (5b), 1863-1871. DOI: 10.1111/j.1582-4934.2008.00437.x.
(27) Guardia, C. M.; De Pace, R.; Mattera, R.; Bonifacino, J. S. Neuronal functions of adaptor complexes involved in protein sorting. *Curr. Opin. Neurobiol.* **2018**, *51*, 103-110. DOI: 10.1016/j.conb.2018.02.021.

Chapter 4
Screening of Ceramide-Binding Proteins from Yeast Cells

Abstract

A comprehensive analysis of lipid-binding proteins has revealed various lipid-protein interactions, but the subsequent interaction analysis and functional analysis are still challenging. In this chapter, a screening of ceramide-binding proteins from *Saccharomyces cerevisiae*, a model organism suitable for biochemical and genetic studies, was performed along with subsequent interaction analysis and functional analyses to gain a functional understanding of lipid-protein interactions. Using phytoceramide (PHCer) and dihydroceramide (DHCer)-immobilized beads, ceramide-binding proteins were identified through proteomics analysis. The main candidates identified were EXO70, a component of the exocyst complex involved in vesicular transport, and SRP-independent targeting protein 3 (SND3), involved in ER protein targeting. Since V-type proton ATPase (V-ATPase) was also identified as DHCer-binding proteins, intermolecular fluorescence resonance energy transfer was measured using fluorescent DHCer and GFP-tagged V-ATPase in vacuolar membranes. This experiment confirmed the specific interaction between DHCer and V-ATPase, further suggesting a regulatory role for ceramide in V-ATPase activity. This study demonstrated that yeast is a useful model in studying lipid-protein interaction and provides a robust platform for further biochemical and genetic analyses. In this context, the current approach established a foundation for exploring the physiological relevance of lipid-protein interactions and a broader lipid-mediated regulatory mechanism.

4.1 Introduction

Budding yeast *Saccharomyces cerevisiae* has been used as a valuable microorganism for alcohol fermentation and other processes for a long time. *S. cerevisiae* is a eukaryote like humans, and has excellent features for molecular biology research, such as being inexpensive, quick, and easy to culture, as well as allowing easy genome modification. For these reasons, the yeast has been extensively studied as a eukaryotic model organism, and various fundamental properties of eukaryotic cells have been uncovered with the yeast.

Sphingolipids are essential components in the eukaryotic cell membranes and play crucial roles in various physiological functions.[1-3] Yeast cells also contain sphingolipids, but their structures differ from those found in mammalian cells in three portions (**Figure 4.1**). (1) Sphingosine portions of mammalian sphingolipids have a trans double bond (sphingosine) or a saturated single bond at the C4-C5 (dihydrosphingosine), whereas yeast sphingosines are composed of phytosphingosine, which has a hydroxy group at the C4 position, and dihydrosphingsine.[4] (2) Yeast sphingolipids typically contain a slightly longer acyl chain, primarily C26[4] (3) Mammalian glycosphingolipids feature glucose or galactose, whereas yeast complex sphingolipids contain an inositol phosphate.[4]

In the previous chapters, a comprehensive analysis of lipid-binding proteins was developed to reveal various lipid-membrane protein interactions; however, the subsequent interaction and functional analyses using the identified proteins have not yet been performed. This is partly due to the challenge in expression and biochemical manipulation of the identified proteins in mammalian cell systems. On the contrary, by using yeast cells, which facilitate genetic and biochemical approaches, investigation on

the physiological roles of the identified lipid-protein interactions would be much easier.

In this chapter, the author focused on ceramide species among yeast sphingolipids for the following reasons: yeast lacks sphingomyelin, a major sphingolipid in mammalian cells; ceramides and glycosphingolipids have strong physiological activity in yeast as signaling lipids, influencing processes such as differentiation, proliferation, and apoptosis,[5-9] but the detailed mechanisms of these processes remain insufficiently understood; and modification of glycosphingolipids for immobilization is more challenging than ceramide modification. As yeast ceramides, dihydroceramide (DHCer) as well as phytoceramide (PHCer) having a 4-OH group (**Figure 4.1**) were immobilized onto beads. Then, the author performed a screening for ceramide-binding proteins from yeast lysates and identified ceramide-binding proteins. The identified V-type proton ATPase (V-ATPase) was further analyzed for interactions with ceramides by fluorescence resonance energy transfer (FRET) between green fluorescent protein (GFP)-tagged V-ATPase and fluorescent lipids.

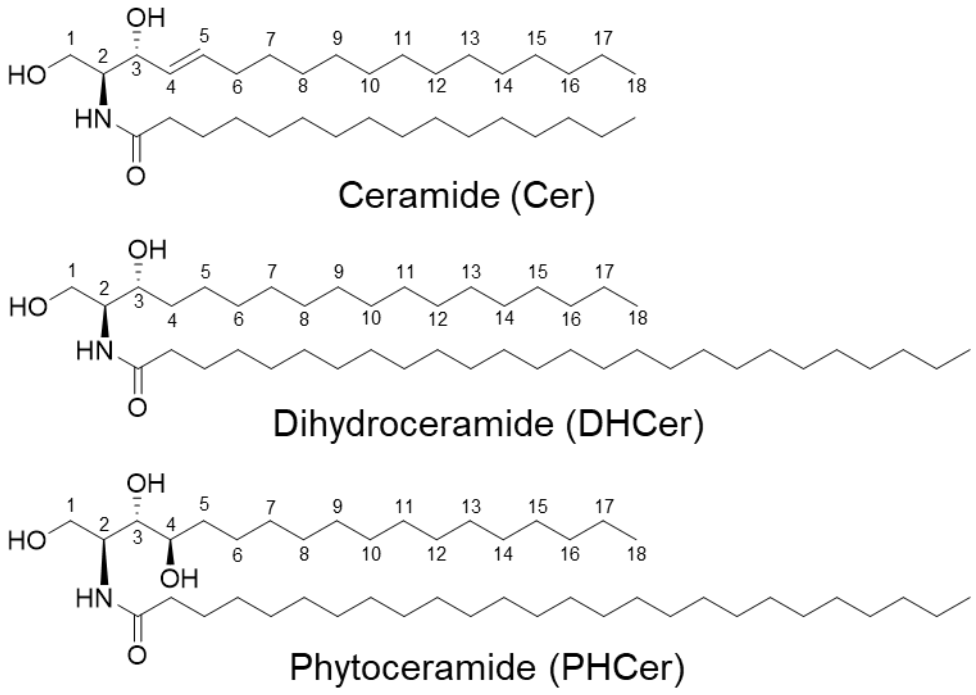

Figure 4.1. Structures of Cer, DHCer and PHCer.

4.2 Experimental Section

4.2.1 Materials and Methods

General

Compounds **11** were synthesized as described in **Chapter 3**. NHS-activated FG beads were purchased from Tamagawa Seiki Co., Ltd. (Nagano, Japan). All other reagents were all purchased from FUJIFILM Wako Pure Chemical Corp. (Osaka, Japan), Tokyo Chemical Inc. (Tokyo, Japan), Nacalai Tesque Inc. (Kyoto, Japan), or Sigma-Aldrich (St. Louis, MO, USA).

Synthesis of aminated PHCer

The details are given in Supporting Information.

Preparation of ceramide-immobilized beads

Ceramide-immobilized beads were prepared as described in **Chapter 2**. NHS-activated beads (1.0 mg) were washed three times with 200 μL of DMF and incubated with 10 mM triethylamine and 1 mM aminated lipids in 200 μL of DMF overnight at room temperature. The beads were washed three times with 200 μL of DMF, and unreacted NHS ester groups were masked with 1.0 M ethanolamine in DMF. After washing three times with 50% MeOH, these beads were resuspended in 50 μL of 50% MeOH, and stored at 4°C. Negative control beads were prepared by reacting with 1 mM dodecylamine in DMF, instead of aminated lipids.

Preparation of yeast lysate

Yeast cells were cultured in YPD (1 % yeast extract, 2 % peptone, and 2 % glucose). Cells were suspended in lysis buffer (50 mM Tris [pH 8.0], 150 mM NaCl, and 1% Nonidet P-40) containing protease inhibitor cocktail (Nacalai Tesque Inc., Kyoto, Japan), incubated on ice for 1 h, and centrifuged at 1,5000 rpm, for 20 min at 4°C. The supernatant was collected to prepare the lysate. The protein content in the lysate was quantified with BCA Protein Assay Kit (Takara Bio Inc., Shiga, Japan), and the lysate was diluted to a concentration of 1 mg mL^{-1}.

Pulldown of ceramide-binding proteins using lipid-immobilized beads

Each type of bead (0.5 mg) was washed with 200 μL of lysis buffer before use, followed by dispersion in 50 μL of protein solution. After incubation at 4°C for 4 h, the supernatant was removed through magnetic separation. The beads were washed twice with 200 μL of lysis buffer and then boiled in SDS sample buffer (240 mM Tris-HCl [pH6.8], 8% SDS,

40% glycerol, 0.1% bromophenol blue, and 20% 2-mercaptoethanol). The eluted proteins were applied to 4%–20% SDS-PAGE. Proteins were detected by silver staining.

Proteomic analysis

Proteomic analysis was conducted as described in **Chapter 2**. Each selected band was cut into pieces and subjected to LC-MS/MS analysis. The gel fragments were destained and digested with mass spectrometry-grade trypsin (PROMEGA, Madison, WI, USA) in 25 mM ammonium bicarbonate. nLC-MS/MS analysis was conducted using Advance UHPLC (Bruker, Billerica, MA, USA) and Orbitrap Velos Pro (Thermo Fisher Scientific, Waltham, MA, USA). Trypsin-digested samples were separated by SilicaTip (0.100 mm i.d. × 15 cm, Nikkyo Technos, Japan) packed with a 3-μm C18 L-column (Chemical Evaluation and Research Institute, Japan) using a linear gradient (30 min, acetonitrile/0.1% formic acid) at a flow rate of 320 nL min^{-1}. The resulting MS and MS/MS data were searched against the Swiss-Prot database using the Mascot search engine software (ver. 2.8.0.1, Matrix Science, Boston, MA, USA). Significance threshold was set to $p < 0.05$. The proteins with at least two peptide matches were listed. Nonspecific proteins identified in control samples were excluded from the list of identified proteins.

Isolation of vacuoles in yeast cells

The mutant strains of *S. cerevisiae* were prepared to express GFP-tagged proteins: Vma5, Vma8, Vma13, and Vph1, which corresponded to V-ATPase subunit C, D, H and a, respectively. These mutants were cultured in TPD. Yeast cells equivalent to 20 OD_{600} were pelleted (3,000 × *g*), resuspended in 1 mL of D-buffer (0.1 M Tris [pH 9.4], 10 mM

DTT), and incubated for 10 min at 30°C. The cells were washed once with 1 mL of spheroplast buffer (1.2 M sorbitol, 10 mM potassium phosphate [pH 7.4]) and resuspended in 1 mL of spheroplast buffer containing 1 mg mL^{-1} Zymolyase for 1 h at 30°C. The spheroplasts were pelleted (3,000 × *g*) for 5 min at room temperature and resuspended in 50 µL of buffer A (0.2 M sorbitol, 10 mM potassium phosphate, pH 7.4) to induce gentle lysis of the spheroplasts without disrupting the vacuoles. The resuspended solution was mixed with 8% polysucrose to obtain a final concentration of 4%, then centrifuged (20,000 × *g*). Finally, 50 µL of the supernatant was collected to obtain the vacuoles.

Fluorescence resonance energy transfer analysis

Dried fluorescent lipids (ATTO594-neg-DHCer and -DPPC) were dissolved into the 4% polysucrose at the concentration of 4 µg mL^{-1}, and sonicated. Isolated vacuole solution was mixed with the lipid solution, and incubated for 30 min at 30°C. The vacuoles were observed by fluorescence using a confocal microscope (LSM880, Carl Zeiss Co., Ltd., Oberkochen, Germany), and the images were analyzed by ImageJ.

4.3 Result

4.3.1 Preparation of Ceramide-Immobilized Beads

In this chapter, DHCer, which is also an endogenous lipid of mammalian cells, and PHCer were selected as yeast ceramides, and their amino derivatives were synthesized for covalent immobilization on beads. AminoDHCer (**11**) was synthesized as described in **Chapter 3**.

An aminated derivative of PHCer was synthesized by the introduction of the azido acyl chain to phytosphingosine, followed by reduction of the azido group through the Staudinger reaction, yielded the desired product **17** (**Scheme 4.1**). Aminated PHCer and DHCer were immobilized on the FG beads, as descried in previous chapters. These lipids were incubated with NHS beads, in which the carboxy groups of the FG beads were activated as NHS esters, and unreacted NHS ester groups were subsequently blocked with aminoethanol. In addition, dodecylamine was immobilized as a negative control (**Figure 4.2**).

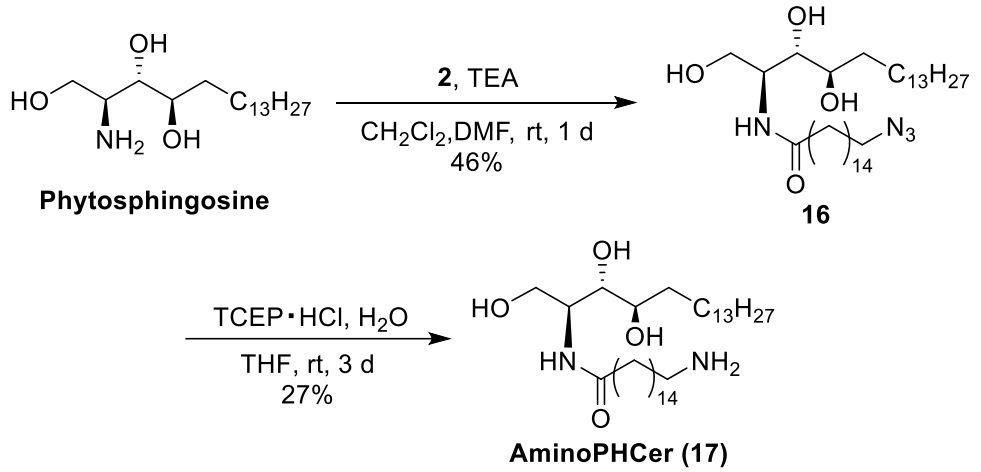

Scheme 4.1. Synthesis of aminoPHCer

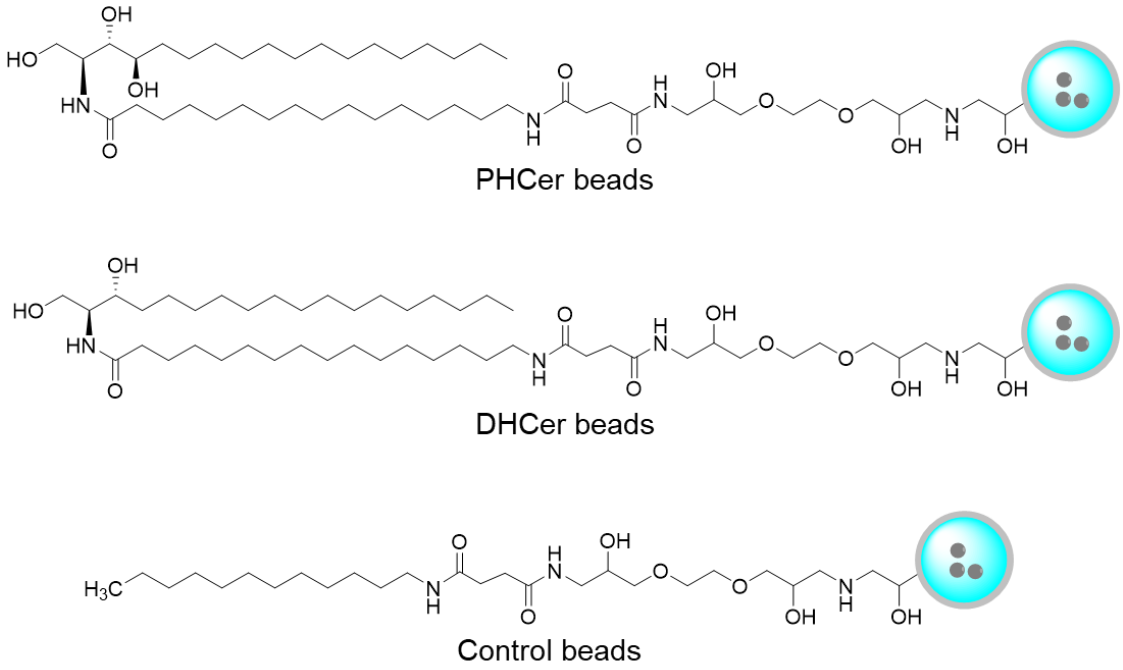

Figure 4.2. Structures of ceramide-immobilized beads used in this chapter.

4.3.2 Screening of ceramide-binding proteins from yeast cells

Next, screening of ceramide binding proteins from the yeast cell lysates was performed using these beads. Each bead was incubated with the lysate, followed by collection of the beads through magnetic separation. After washing the beads, the binding proteins were subjected to SDS-PAGE separation. Several distinct bands were excised (**Figure 4.3**), and the proteins contained in these bands were identified by proteomic analysis (**Table S4.1**). For each band, proteins with top three Mascot scores are presented in **Table 4.1**, and proteins from control beads were excluded as nonspecific bindings.

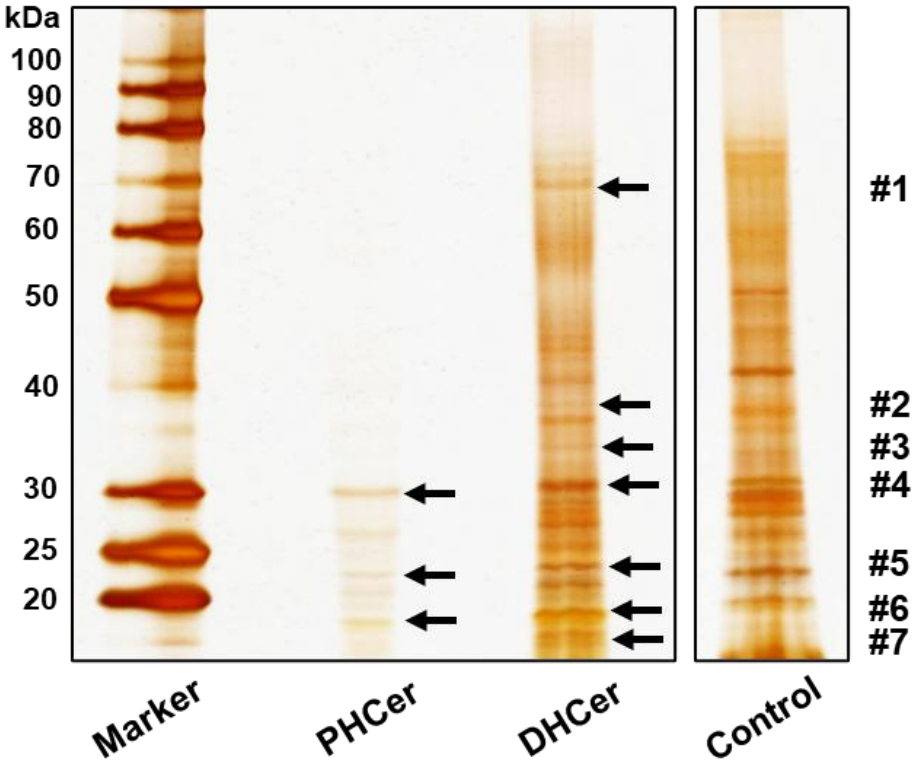

Figure 4.3. SDS-PAGE separation of ceramide-binding proteins obtained from yeast cell lysate; proteins were visualized with silver staining; numbered bands were excised and subjected to LC-MS/MS analyses; lanes not involved in this experiment have been removed. Bands **#4**, **#5**, and **#6** were analyzed for both PHCer and DHCer, while the other bands were analyzed only for DHCer.

Table 4.1. Ceramide-binding protein candidates from each band

Band	*Lipid*	*Protein name*	*Mascot score*	*Mass*	*Number of peptides*
#1	DHCer	Fumarate reductase 2	98	55202	5
		Exocyst complex component EXO70	83	71534	3
		Sphingosine-1-phosphate lyase	49	66037	2
#2	DHCer	Eukaryotic translation initiation factor 3 subunit A	198	110333	9
		Aspartate aminotransferase, mitochondrial	151	52219	7
		Cruciform cutting endonuclease 1, mitochondrial	140	41430	5
#3	DHCer	Glucose-6-phosphate 1-epimerase	269	34048	12
		NADH-cytochrome b5 reductase 2	185	34174	11

		Regulator of Ty1 transposition protein 103	134	46517	3
#4	PHCer	Regulator of Ty1 transposition protein 103	96	46517	4
		Pyruvate dehydrogenase E1 component subunit alpha, mitochondrial	82	46712	3
	DHCer	Regulator of Ty1 transposition protein 103	231	46517	9
		Transcription initiation factor IIB	167	38746	4
		54S ribosomal protein L3, mitochondrial	143	44257	5
#5	PHCer	Transcription initiation factor IIB	93	38746	2
		SRP-independent targeting protein 3	61	21180	2
		Ribonucleoside-diphosphate reductase large chain 1	61	100296	2
	DHCer	Glyceraldehyde-3-phosphate dehydrogenase 1	194	35842	9
		Transcription initiation factor IIB	115	38746	3
		SRP-independent targeting protein 3	106	21180	4
#6	PHCer	SRP-independent targeting protein 3	190	21180	6
		Mitochondrial phosphate carrier protein	118	32962	4
		Elongation factor 1-gamma 2	74	46605	2
	DHCer	SRP-independent targeting protein 3	249	21180	9
		Mitochondrial phosphate carrier protein	171	32962	6
		Pyruvate dehydrogenase E1 component subunit alpha, mitochondrial	146	46712	8
#7	DHCer	eIF-2-alpha kinase activator GCN1	150	297995	4
		Regulator of Ty1 transposition protein 103	135	46517	3
		SRP-independent targeting protein 3	121	21180	5

4.3.3 Interaction Analysis with Fluorescence Resonance Energy Transfer

Using ceramide-immobilized beads, a variety of DHCer- and PHCer-binding proteins were identified from yeast lysates. Among the identified proteins, the author focused on V-ATPase because three subunits (subunit C, D and H) were specifically identified as DHCer-binding proteins (**Table S4.1**). Notably, ceramide expression levels have been reported to influence the activity of V-ATPase,[10] further supporting the

interaction between V-ATPase and DHCer. To assess this interaction, intermolecular FRET was measured between fluorescent DHCer and GFP-tagged V-ATPase.

V-ATPase is a multisubunit complex that is localized in the membranes of acidic organelles such as vacuoles and lysosomes (**Figure 4.4**).[11, 12] In this study, four subunits of V-ATPase: subunit C, D, H and a, were individually tagged with GFP. However, when observing vacuolar membranes isolated from yeast, fluorescence from V-ATPase was significantly weak for all the subunits except when the GFP-tagged subunit a was expressed, probably because the V_1 domain detached from the vacuolar membrane. Therefore, the interaction analysis was conducted using V-ATPase composed of the GFP-tagged subunit a. In parallel, fluorescent DHCer and DPPC, labeled with ATTO594, were prepared according to the previous reports (**Figure 4.5**).[13, 14] To measure intermolecular FRET, the fluorescent lipid probes were introduced to the vacuolar membranes isolated from yeast cells, and the decrease in fluorescence intensity of GFP-tagged V-ATPase was observed with a fluorescence microscope. As a result, GFP fluorescence intensity was significantly decreased in the presence of fluorescent DHCer (**Figure 4.6** and **Table S4.2**), compared to fluorescent DPPC and the control sample, where the fluorescent lipids were not introduced.

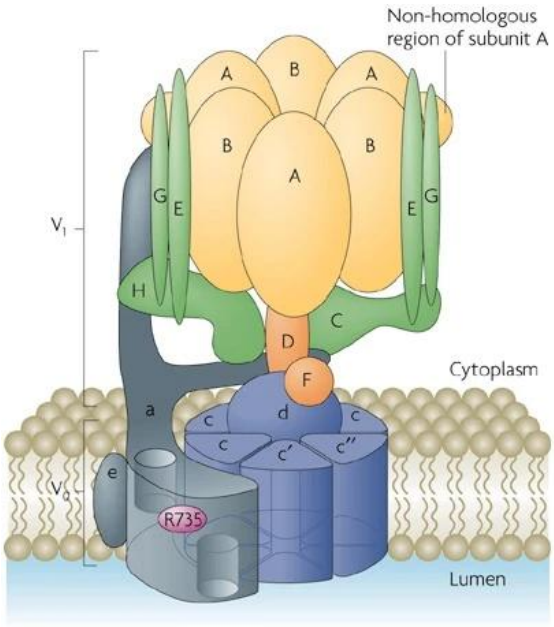

Figure 4.4. Structure of V-ATPase.[11] The V-ATPase complex is composed of a peripheral domain (V_1, shown in yellow and orange), which is responsible for ATP hydrolysis, and an integral domain (V_0, shown in blue and grey), which is involved in proton translocation across the membrane. This figure is cited from ref 11 with permission conveyed through Copyright Clearance Center, Inc.

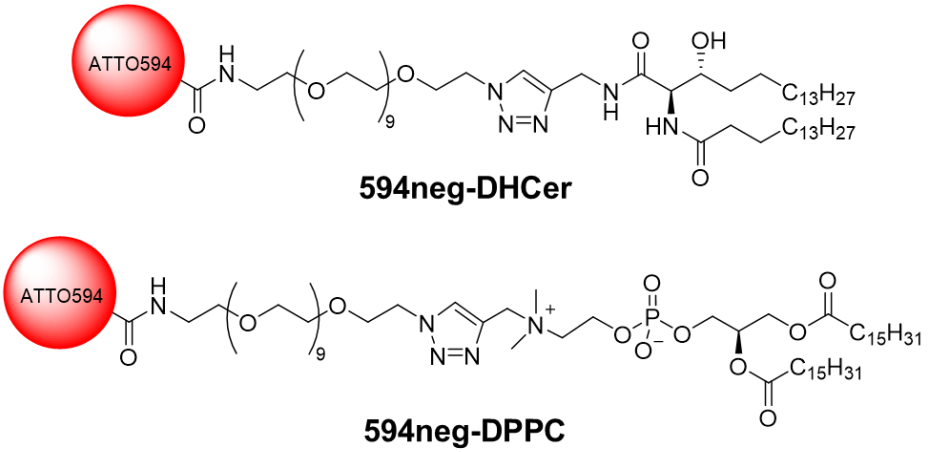

Figure 4.5. Structure of fluorescent lipid probes used in the FRET analysis.

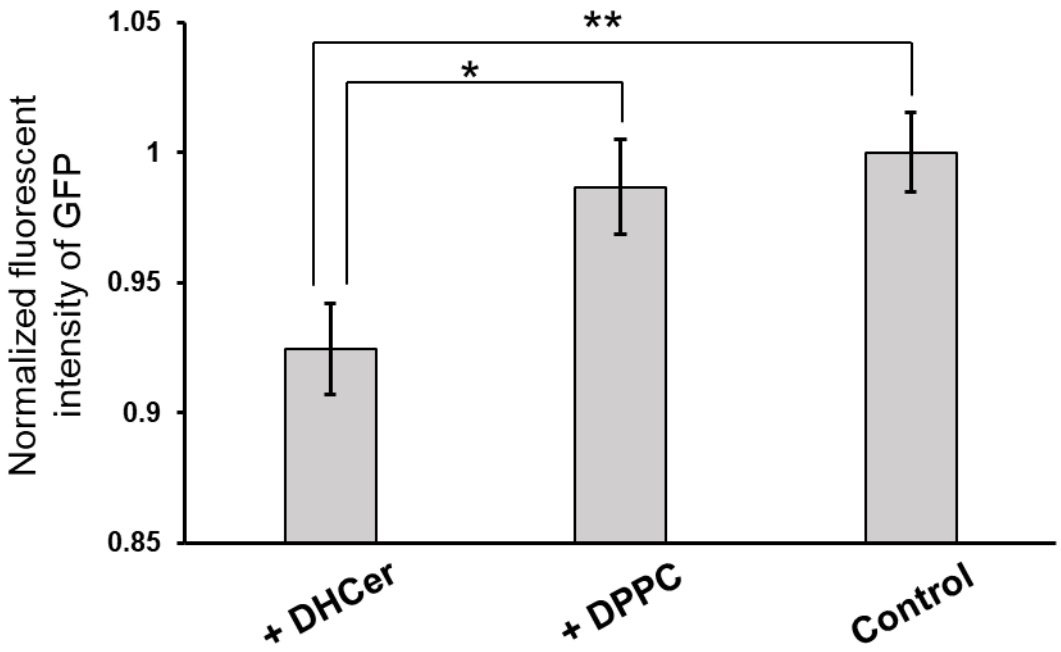

Figure 4.6. Normalized GFP fluorescence intensity in extracted yeast vacuoles. Each fluorescence intensity was normalized to the control sample. $N > 100$ vacuoles were measured for each sample. The error bars are *SE*. *: $p < 0.05$, **: $p < 0.01$.

4.4 Discussion

In this chapter, a screening of ceramide-binding proteins from yeast cells was conducted. This study demonstrates that use of yeast cells as the protein source facilitates biochemical and genetic analyses, enabling detailed investigations of the interactions between the identified proteins and lipids. For the screening, PHCer, an endogenous ceramide in yeast cells, was newly immobilized onto beads, along with DHCer beads prepared in **Chapter 3**. As a result, various ceramide-binding proteins, including membrane proteins, were identified. Bands **#4**, **#5**, and **#6** were analyzed for both PHCer and DHCer, and the proteins binding to PHCer and DHCer were nearly identical.

In Band **#1,** exocyst complex component (EXO70) was identified, which plays

a role in linking secretory vesicles to the plasma membrane.[15] It has been reported that inhibition of ceramide biosynthesis disrupts the localization of EXO70 at plasma membrane buds.[16] The current study suggests that EXO70 localizes to ceramide domains on the plasma membrane through its interaction with ceramide. SRP-independent targeting protein 3 (SND3) was identified at bands **#5**, **#6**, and **#7**. SND3 is predicted to have one transmembrane domain and is localized to the endoplasmic reticulum (ER).[17] SND3 targets proteins to the ER via a signal recognition particle (SRP)-independent pathway, in cooperation with other SND family proteins.[18] The current result suggests that SND3 is inserted into ceramide domains in the ER membrane and contribute to SRP-independent transport in the ER.

In the subsequent FRET-based interaction analysis, V-ATPase was selected because three of its subunits had been identified as DHCer binding proteins, and it was reported that ceramide levels are involved in V-ATPase activity.[10] Vacuoles were extracted from yeast cells expressing GFP-tagged V-ATPase, and fluorescent lipid probes, 594negDHCer and 594negDPPC, were introduced. Compared to the control sample without lipid introduction, the fluorescent intensity from GFP significantly decreased in the presence of DHCer, indicating that intermolecular FRET occurred between GFP-tagged V-ATPase and 594negDHCer. No significant decrease was observed when 594negDPPC was introduced. These results suggested that GFP-tagged V-ATPase and 594negDHCer were localized in close and that V-ATPase interacted specifically with DHCer in yeast vacuolar membranes. On the other hand, while ceramide is necessary for V-ATPase activity,[10] ceramide synthase CERS2 functions as a negative regulator of V-ATPase.[19] It is necessary to quantitatively determine whether this interaction enhances or suppresses V-ATPase activity in future studies.

4.5 Conclusion

A comprehensive analysis of lipid-binding proteins has revealed various lipid-protein interactions, but the subsequent interaction analysis and functional analysis are still challenging. In this chapter, yeast cells, which are well-suited for biochemical and genetic analyses, were employed to demonstrate the identification of ceramide-binding proteins and the subsequent interaction analysis by FRET. Future studies will involve genetic and biochemical assays, such as enzyme activity measurements, to further elucidate the physiological roles of lipid-protein interactions. By integrating multi-faceted approaches for lipid-protein interaction analysis, a comprehensive analytical platform is expected to be established, facilitating the identification of lipid-binding proteins, and understanding the physiological significance of lipid-protein interactions.

Reference

(1) Dickson, R. C. Thematic review series: sphingolipids. New insights into sphingolipid metabolism and function in budding yeast. *J. Lipid Res.* **2008**, *49* (5), 909-921. DOI: 10.1194/jlr.R800003-JLR200.
(2) Hannun, Y. A.; Obeid, L. M. Sphingolipids and their metabolism in physiology and disease. *Nature Reviews Molecular Cell Biology* **2018**, *19* (3), 175-191. DOI: 10.1038/nrm.2017.107.
(3) Quinville, B. M.; Deschenes, N. M.; Ryckman, A. E.; Walia, J. S. A Comprehensive Review: Sphingolipid Metabolism and Implications of Disruption in Sphingolipid Homeostasis. *Int. J. Mol. Sci.* **2021**, *22* (11). DOI: 10.3390/ijms22115793.
(4) Dickson, R. C.; Sumanasekera, C.; Lester, R. L. Functions and metabolism of sphingolipids in Saccharomyces cerevisiae. *Prog. Lipid Res.* **2006**, *45* (6), 447-465. DOI: https://doi.org/10.1016/j.plipres.2006.03.004.
(5) Hannun, Y. A. Functions of ceramide in coordinating cellular responses to stress. *Science* **1996**, *274* (5294), 1855-1859. DOI: 10.1126/science.274.5294.1855.
(6) Geilen, C. C.; Wieder, T.; Orfanos, C. E. Ceramide signalling: regulatory role in cell proliferation, differentiation and apoptosis in human epidermis. *Arch. Dermatol. Res.* **1997**, *289* (10), 559-566. DOI: 10.1007/s004030050240.
(7) Ruvolo, P. P. Intracellular signal transduction pathways activated by ceramide and its metabolites. *Pharmacol. Res.* **2003**, *47* (5), 383-392. DOI: 10.1016/s1043-6618(03)00050-1.
(8) Senkal, C. E.; Ponnusamy, S.; Bielawski, J.; Hannun, Y. A.; Ogretmen, B. Antiapoptotic roles of ceramide-synthase-6-generated C16-ceramide via selective regulation of the ATF6/CHOP arm of ER-stress-response pathways. *FASEB J.* **2010**, *24* (1), 296-308. DOI: 10.1096/fj.09-135087.
(9) Uchida, Y. Ceramide signaling in mammalian epidermis. *Biochimica et Biophysica Acta (BBA) - Molecular and Cell Biology of Lipids* **2014**, *1841* (3), 453-462. DOI: https://doi.org/10.1016/j.bbalip.2013.09.003.
(10) Chung, J. H.; Lester, R. L.; Dickson, R. C. Sphingolipid requirement for generation of a functional v1 component of the vacuolar ATPase. *J. Biol. Chem.* **2003**, *278* (31), 28872-28881. DOI: 10.1074/jbc.M300943200.
(11) Forgac, M. Vacuolar ATPases: rotary proton pumps in physiology and pathophysiology. *Nature Reviews Molecular Cell Biology* **2007**, *8* (11), 917-929. DOI: 10.1038/nrm2272.
(12) Chen, F.; Kang, R.; Liu, J.; Tang, D. The V-ATPases in cancer and cell death. *Cancer Gene Ther.* **2022**, *29* (11), 1529-1541. DOI: 10.1038/s41417-022-00477-y.
(13) Kinoshita, M.; Suzuki, K. G.; Matsumori, N.; Takada, M.; Ano, H.; Morigaki, K.; Abe, M.; Makino, A.; Kobayashi, T.; Hirosawa, K. M.; Fujiwara, T. K.; Kusumi, A.; Murata, M. Raft-based sphingomyelin interactions revealed by new fluorescent sphingomyelin analogs. *J. Cell Biol.* **2017**, *216* (4), 1183-1204. DOI: 10.1083/jcb.201607086.
(14) Matsufuji, T.; Kinoshita, M.; Matsumori, N. Preparation and Membrane Distribution

of Fluorescent Derivatives of Ceramide. *Langmuir* **2019**, *35* (6), 2392-2398. DOI: 10.1021/acs.langmuir.8b03176.
(15) Guo, W.; Sacher, M.; Barrowman, J.; Ferro-Novick, S.; Novick, P. Protein complexes in transport vesicle targeting. *Trends Cell Biol.* **2000**, *10* (6), 251-255. DOI: 10.1016/S0962-8924(00)01754-2.
(16) Guo, Q.; Zhang, T.; Meng, N.; Duan, Y.; Meng, Y.; Sun, D.; Liu, Y.; Luo, G. Sphingolipids are required for exocyst polarity and exocytic secretion in Saccharomyces cerevisiae. *Cell Biosci.* **2020**, *10* (1), 53. DOI: 10.1186/s13578-020-00406-2.
(17) Huh, W. K.; Falvo, J. V.; Gerke, L. C.; Carroll, A. S.; Howson, R. W.; Weissman, J. S.; O'Shea, E. K. Global analysis of protein localization in budding yeast. *Nature* **2003**, *425* (6959), 686-691. DOI: 10.1038/nature02026.
(18) Aviram, N.; Ast, T.; Costa, E. A.; Arakel, E. C.; Chuartzman, S. G.; Jan, C. H.; Haßdenteufel, S.; Dudek, J.; Jung, M.; Schorr, S.; Zimmermann, R.; Schwappach, B.; Weissman, J. S.; Schuldiner, M. The SND proteins constitute an alternative targeting route to the endoplasmic reticulum. *Nature* **2016**, *540* (7631), 134-138. DOI: 10.1038/nature20169.
(19) Mei, F.; You, J.; Liu, B.; Zhang, M.; Liu, J.; Zhang, B.; Pei, F. LASS2/TMSG1 inhibits growth and invasion of breast cancer cell in vitro through regulation of vacuolar ATPase activity. *Tumour Biol.* **2015**, *36* (4), 2831-2844. DOI: 10.1007/s13277-014-2910-0.

Chapter 5
A Quantitative Analysis of the Interaction between KcsA and Anionic Lipids with SPR-based Method

Abstract

To understand the precise molecular mechanisms by which lipids modulate MP structure and function, reliable and efficient approaches for the quantitative analysis of lipid-MP interactions are essential. In this chapter, the surface plasmon resonance (SPR)-based SAMPLIA method was improved by the introduction of single-cycle kinetics (SCK) analysis, enabling precise evaluation of binding and dissociation rates for lipids with slow dissociation. To demonstrate that this method efficiently evaluates lipid-membrane protein (MP) interactions, the author performed quantitative analyses of the interactions between the potassium channel KcsA and various lipids. Since the KcsA channel opening requires both acidic conditions and the presence of anionic lipids, phosphatidylglycerol (PG), cardiolipins (CL) and phosphatidic acids (PA) were tested for the interaction with KcsA. The analysis revealed that CL exhibits the strongest binding affinity to KcsA, even in the absence of the *N*-terminal M0 helix, a putative lipid binding site, indicating the presence of additional binding sites. In contrast, PA and PG primarily interact with the M0 helix. Mutation experiments suggested that the additional CL binding site was located around two arginine residues in the transmembrane domain. Therefore, it was suggested that the interaction of CL with KcsA stabilizes its open state through long-range allosteric coupling. These results highlight CL's specific role in modulating KcsA gating and provide a platform for the quantitative analysis of lipid-MP interactions.

5.1 Introduction

A comprehensive analysis of lipid-binding proteins has uncovered various lipid-membrane protein (MP) interactions in previous chapters. However, the precise molecular mechanisms by which lipids modulate MP structure and function remain poorly understood, primarily due to the absence of quantitative data on lipid-MP interactions. To advance our comprehension of lipid roles, the reliable and efficient approaches for the quantitative analysis of lipid-MP interactions is essential.

Recently, a surface plasmon resonance (SPR)-based method for quantitative analysis of the interactions between MPs and lipids was developed in this laboratory, referred to as self-assembled monolayer-assisted MP-lipid interaction analysis (SAMPLIA, **Figure 5.1**).[1] SPR is an optical technique that employs a sensor chip coated with a thin gold layer (~50 nm). A *p*-polarized laser directed at the chip causes total internal reflection, generating an evanescent electric field that interacts with the medium's dielectric properties. This field excites surface plasmons (SPs), transferring energy from the incident light and decreasing its intensity when the SPs resonate with the light. The SPR signal is measured at the angle where this intensity is minimized, and changes in the signal allow for the analysis of binding kinetics and affinity. The SAMPLIA method is characteristic of the surface modification of the SPR sensor chip with a self-assembled monolayer (SAM), on which MP is covalently immobilized. SAM allows for more efficient immobilization of MPs and provides a partial membranous environment to these immobilized MPs. To the MP immobilized on SAM-coated sensor chip, lipids solubilized with surfactant are added for interaction analysis.

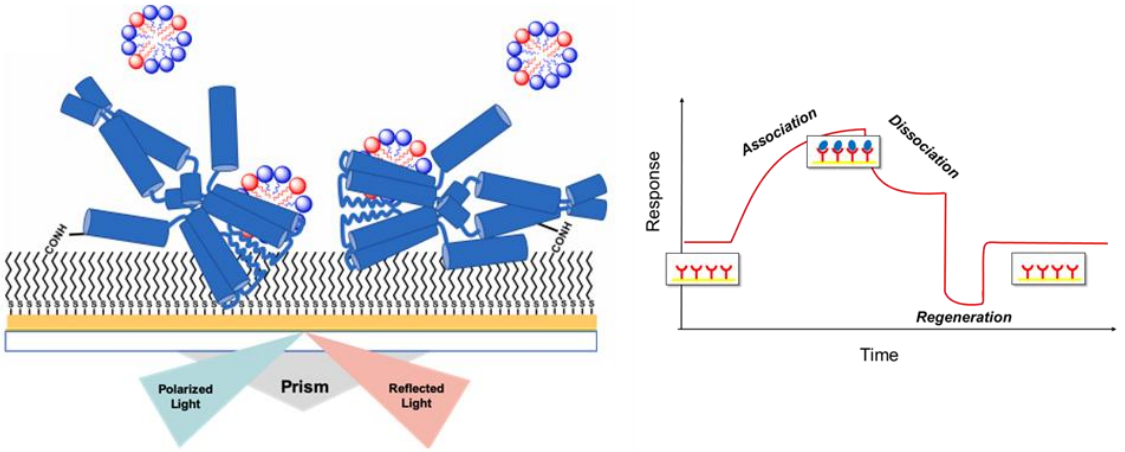

Figure 5.1. SAMPLIA method for lipid-MP interactions.[1] Solubilized MPs are covalently immobilized onto the SAM-coated sensor chip. Surfactant-solubilized lipid solution is added to the immobilized MPs, to detect the binding amount of lipids, and its time-course shows the kinetics and affinity of the interaction.

For a quantitative measurement of lipid-MP interactions, the author employed the SAMPLIA method and demonstrated the interaction analysis between anionic lipids and KcsA potassium channels,[2] which is a homo-tetrameric potassium channel from *Streptomyces lividans* and serves as a model for general potassium channels.[3, 4] To fully activate the KcsA channel, not only acidic conditions (**Figure 5.2a**)[5-8] but specific membrane lipids are necessary. While phosphatidylglycerol (PG) can open the KcsA pore,[4, 9] PG is not contained in streptomycete membranes,[10, 11] leaving the role of streptomycete native lipids in channel gating unclear.

In this chapter, the SAMPLIA was applied to quantitatively analyze interactions between KcsA and anionic lipids. Since the streptomycete membrane contains cardiolipins (CL) and phosphatidic acids (PA) as major anionic lipid components,[11] these lipids were selected for the analysis (**Figure 5.2b**). Their interactions were evaluated using both wild-type KcsA (wt-KcsA) and mutants to estimate the binding site of these lipids. In addition to evaluating the interactions between KcsA and anionic lipids, single-

cycle kinetics (SCK) analysis[12] was combined with the SAMPLIA method to improve quantitativeness of lipid-MP interaction analysis.

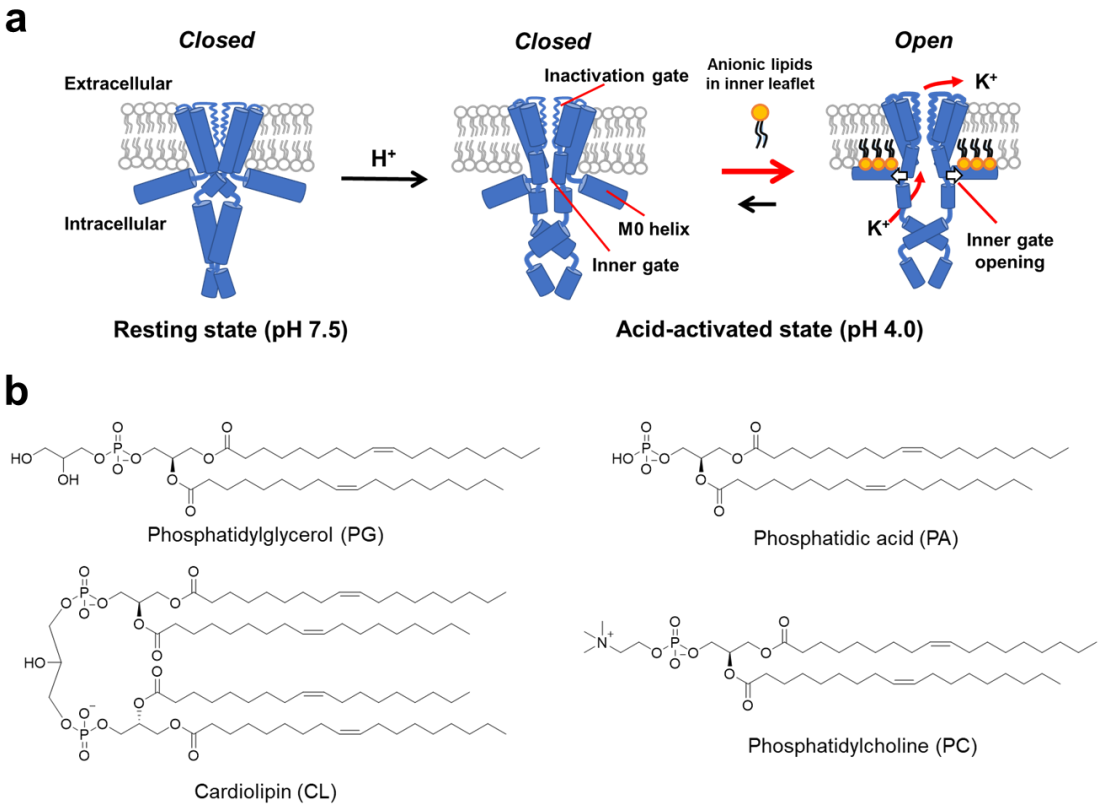

Figure 5.2. (a) Gating states of the KcsA channel. The gate does not open at a neutral pH. At an acidic pH on the intracellular side, the channel becomes acid-activated; the pH sensor in the cytoplasmic domain changes conformation, and the inner gate is ready to open via a global twisting motion. Negatively charged lipids in the inner leaflet make the channel fully open via binding to the *N*-terminal amphipathic M0 helix.[13] (b) Chemical structures of lipids used in this chapter.

5.2 Experimental Section

5.2.1 Materials and Method

Materials

All lipids used in this study were purchased from Avanti Polar Lipids (Alabaster, AL, USA). The sensor chips for the SPR measurements were purchased from Cytiva (Little Chalfont, Buckinghamshire, UK). Any other reagents and materials were all purchased from FUJIFILM Wako Pure Chemical Corp. (Osaka, Japan), Tokyo Chemical Inc. (Tokyo, Japan), or Sigma-Aldrich (St. Louis, MO, USA). M0 mimicking peptide was purchased from custom peptide synthesis service of GenScript (Piscataway, NJ, USA).

Preparation of SPR sensor chip and immobilization of KcsA

The SAM-modified sensor chip was prepared using bare Au sensor chip (SIA Kit Au, Cytiva), which was modified with a mixture of 6-mercaptohexanoic acid and 6-mercaptohexanol (8:2), as previously reported.[1] Wt-KcsA, ΔM0-KcsA or ΔM0-KcsA with mutated Arg residues (R52Q, R64Q, R89Q, and R64Q/R89Q) solubilized with 0.06% *n*-dodecyl-β-D-maltoside (DDM) was immobilized onto SAM-modified sensor chip, according to a standard amino coupling method. HBS-EP buffer (10 mM HEPES [pH 7.4], 150 mM NaCl, 3 mM EDTA, 0.05 % (v/v) Tween 20) was used as the running buffer. Briefly, COOH groups on the surface were activated by injecting a mixture of 390 mM 1-(3-dimethylaminopropyl)-3-ethylcarbodiimide (EDC) and 100 mM *N*-hydrosuccinimide (NHS) for 7 min, followed by the immobilization of KcsA by injecting the solubilized KcsA solution (100 μg mL^{-1}) for 20 min. Unreacted carboxy groups were deactivated by injecting the blocking solution (1 M ethanolamine-HCl, pH 8.5) for 7 min, at a flow rate of 5 μL min^{-1}.

KcsA-lipid interaction analysis

SPR analyses were carried out at 25.0°C using Biacore T100 system (GE Healthcare, Chicago, IL, USA). In all protocols, acidic buffer (10 mM succinic acid [pH 4.0], 200 mM KCl, 3 mM EDTA, 0.5% (v/v) Tween 20) and neutral buffer (10 mM HEPES [pH 7.5], 200 mM KCl, 3 mM EDTA, 0.5% (v/v) Tween 20) were used as running buffers. Evaluation of KcsA-lipid interactions was made within 2 days after KcsA immobilization.

In SPR analysis of wt-KcsA and ΔM0-KcsA, both of acidic buffer and neutral buffer were used. Analyte samples were prepared by dissolving dried lipids into the buffer at the concentration of 100 μM, and the samples were sonicated prior to use. All procedures were automated, using repetitive cycles of sample injection and regeneration. The binding assays were performed after three cycles of start-up injections to normalize the two flow cells, and just before the injection of lipid solutions, the buffer alone was injected in the first two cycles in order to obtain baseline value. Afterward, lipid solutions were injected for 180 s at a flow rate of 30 μL min^{-1}, followed by 180 s of dissociation at the same flow rate. The surface of the chip was regenerated by three sequential injection of regeneration solution (10 mM NaOH, 0.5% (v/v) Tween 20) for 30 s at a flow rate of 30 μL min^{-1}.

SPR analysis of ΔM0-KcsA with mutated Arg residues was performed using SCK analysis.[12] CL samples at the concentration of 0.3, 1, 3, 10, 30 μM were prepared by dissolving the lipids in the acidic buffer. After three cycles of start-up injections to normalize the two flow cells, the acidic buffer alone was injected in the first two cycles. Subsequently, each lipid solution was injected for 300 s at a flow rate of 30 μL min^{-1} in increasing order of concentration, followed by 6000 s of single dissociation at the same flow rate. The surface of the chip was regenerated by three sequential injections of the

regeneration solution for 60 s at a flow rate of 30 μL min^{-1}.

Association and dissociation of lipid molecules were monitored as sensorgrams, representing the time-dependent changes. To remove the contribution from non-specific binding between SAM and lipids, a blank channel without KcsA immobilization was used as a reference, and the response of the reference channel (SAM-lipid interactions) was subtracted from that of the sample channel. The evaluation of interactions was performed using BiaEvaluation software (Cytiva). Kinetic parameters were extracted by a local fit of the corrected sensorgrams and by a global fit in SCK, using a 1:2 heterogeneous ligand binding model.[14, 15] For more description on the heterogeneous binding model, see Table S5.1 caption. The correlations of the fitting were evaluated using $\chi 2$ analyses and residual plots.

M0 peptide-membrane interaction analysis

Liposome immobilization on the dodecylamine-modified sensor chip was performed as previously reported.[16] DOPC (5.0 mg, 6.4 μmol) and 0.71 μmol of DOPG, DOPA, or tetraC18:1 CL were mixed in MeOH/$CHCl_3$, dried under N_2 gas flow, and suspended in 1 mL of acidic buffer (10 mM succinic acid [pH 4.0], 200 mM KCl, 3 mM EDTA), to prepare multilamellar vesicles (MLVs). The MLV suspension was extruded through 200 nm, and then 100 nm polycarbonate membranes (LiposoFast Liposome Factory, Sigma-Aldrich, St. Louis, MO, USA) (21 passes for each type of membrane), to prepare 100 nm large unilamellar vesicles (LUVs). The LUV solution was then diluted with the buffer used, to prepare 1 mM LUV solution. The following measurements were performed at 25.0°C on a Biacore T100 system. LUV solution was injected for 40 min over flowcell on the dodecylamine-modified sensor chip at 2 μL min^{-1} to immobilize LUV onto the

chip surface, and washed with 50 mM NaOH solution for 3 times at a flow rate of 20 μL min^{-1} to remove immobilized LUV. The amount of immobilized LUV was recorded after 10 min of signal stabilization. Afterward, the peptide solution (10 μg mL^{-1}) was injected for 300 s at a flow rate of 10 μL min^{-1}, followed by 300 s of dissociation at the same flow rate. The surface of the chip was regenerated by two sequential injections of 0.5% (w/v) SDS for 120 s and 50 mM NaOH/2-propanol (3/2, v/v) at a flow rate of 20 μL min^{-1}. To remove the contribution from non-specific binding of the peptide to the chip surface, a blank channel without liposome was used as a reference, and the response of the reference channel was subtracted from that of the sample channel. The kinetic parameters were extracted by a local fit of the corrected sensorgrams using a 1:1 interaction (Langmuir interaction), performed by BiaEvaluation software (Cytiva).

5.3 Result

5.3.1 CL interacts more strongly than PG and PA with KcsA

KcsA was immobilized on SAM-modified sensor chips at approximately 3000 resonance units, allowing for clear observation of interactions between KcsA and lipid molecules.[1] To validate the SAMPLIA method, the interaction between PG and wt-KcsA was evaluated. Since KcsA adopts an acid-activated state at acidic pH and a resting state at neutral pH, both acidic and neutral buffers were used in the analysis. Sensorgrams were recorded upon initiating lipid perfusion and fitted to a 1:2 heterogeneous ligand binding model,[14, 15] assuming lipid binding to KcsA at two distinct sites. The analysis provides two association constants (K_A) and corresponding two sets of association and dissociation rate constants (k_{on} and k_{off}). The bindings with smaller k_{on} were considered to be non-

specific and hydrophobic, as k_{on} should generally be at least approximately ~10^3 if a protein recognizes and binds to a molecule.[17-19] Therefore, the author focused on the K_A values derived from larger k_{on} values in the subsequent experiments. Further verification of this treatment for the two K_A values is given in the supplementary information.

The SAMPLIA method revealed that PG binds to wt-KcsA more strongly at pH 4.0 than at pH 7.5 (**Figures 5.3**). On the other hand, the interaction between wt-KcsA and PC was not sensitive to the pH change (**Figure 5.3**). This result is consistent with previous studies showing that the KcsA channel opens in the presence of PG at acidic pH,[13, 20, 21] confirming that the SAMPLIA method can effectively evaluate KcsA-lipid interactions.

Subsequently, the author assessed the interaction of wt-KcsA with PA and CL, which are key components of streptomyces membranes. PA exhibited significantly stronger binding to wt-KcsA at pH 4.0 compared to pH 7.5, with a markedly higher affinity for wt-KcsA than PC at pH 4.0 (**Figures 5.3**). In contrast, CL displayed a notable difference in its affinity for KcsA under acidic versus neutral conditions. CL showed an exceptionally high affinity for acid-activated KcsA at pH 4.0. At pH 7.5, CL and other anionic lipids exhibited binding similar to that of PC, suggesting less specific interactions with resting-state KcsA. The remarkably high affinity of CL for KcsA at pH 4.0 indicates the presence of a specific binding site for CL in the acid-activated form of KcsA. This was corroborated by kinetic data (**Table S5.2**), which showed that CL dissociates more slowly from the binding site at pH 4.0 compared to other monoanionic lipids.

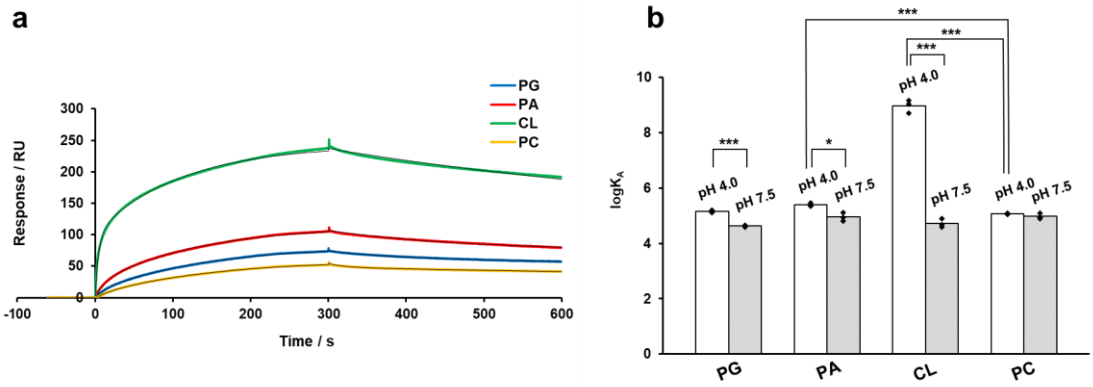

Figure 5.3. (a) SPR sensorgrams showing the interactions of PG, PC, PA, and CL with wt-KcsA immobilized on the C6-SAM modified sensor chip; 100 μM of the lipids dissolved in acidic buffer (pH 4.0) were injected at a flow rate of 30 μL min^{-1}. Colored lines indicate experimentally obtained sensorgrams, while black lines indicate fitted curves. (b) the affinity of PG, PA, CL, and PC toward wt-KcsA in acidic (pH 4.0) and neutral (pH 7.5) buffers, calculated from the sensorgrams by fitting to a 1:2 heterogeneous ligand binding model, as listed in **Table S5.1**. Asterisks denote statistical significance (*$p < 0.05$, **$p < 0.01$, ***$p < 0.001$).

5.2.2 CL binds to an alternative site other than the M0 helix

Previous studies have indicated that the M0 helix plays a key role in sensing monoanionic phospholipids, such as PG, within the membrane and facilitates the transition to the open conformation of KcsA.[13] To examine the contribution of the M0 helix to the high-affinity binding of dianionic CL, an M0 helix-deleted mutant of KcsA, ΔM0-KcsA (**Figure 5.4a**), was analyzed for the interaction with the lipids. Consequently, CL bound tightly to ΔM0-KcsA, with the K_A value comparable to that of wt-KcsA (**Figures 5.4b and 5.4c**). In contrast, binding of PA and PG to ΔM0-KcsA was significantly weaker than that to wt-KcsA ($p < 0.001$) (**Figures 5.4b and 5.4c**). These findings suggest that CL binds to an additional site apart from the M0 helix, while the M0 helix is primarily responsible for binding PA and PG. On the other hand, no significant difference was observed in PC binding between wt-KcsA and ΔM0-KcsA (**Figures 5.4b and 5.4c**), indicating that PC binds less specifically to KcsA without interacting with the

M0 helix.

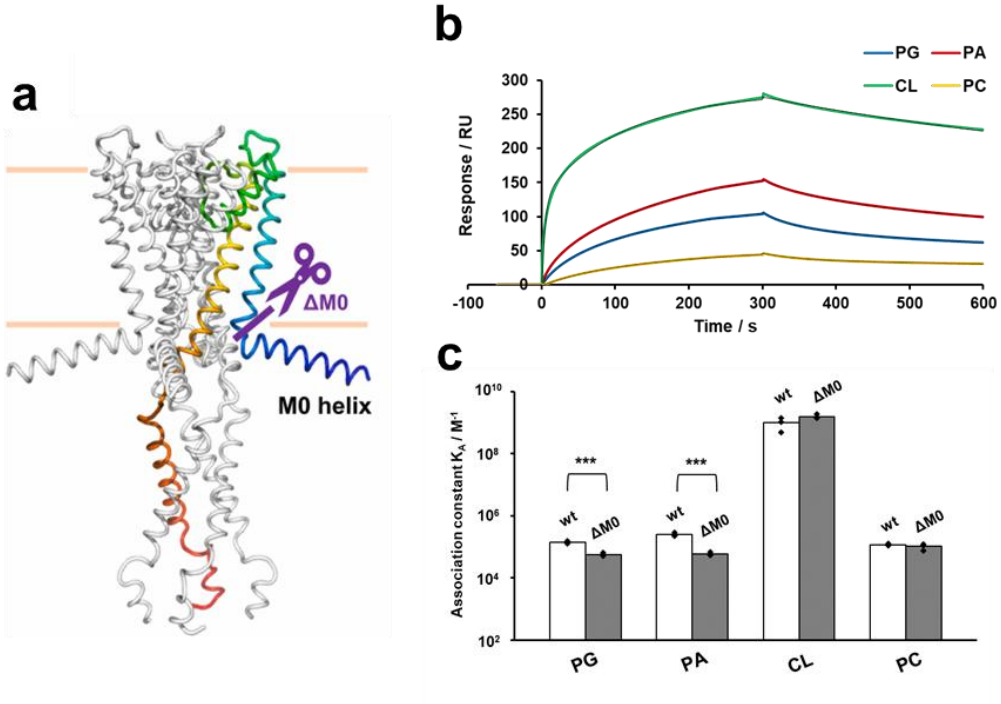

Figure 5.4. (a) Location of deletion on KcsA. ΔM0-KcsA is the mutant in which the *N*-terminal M0-helix domain was truncated (purple line). (b) SPR sensorgrams showing the interactions of PG, PA, CL, and PC with ΔM0-KcsA immobilized on the C6-SAM modified sensor chip; 100 μM of the lipids dissolved in acidic buffer (pH 4.0) were injected at a flow rate of 30 μL min^{-1}. Colored lines indicate experimentally obtained sensorgrams, while black lines indicate fitted curves. (c) Affinity of PG, PA, CL, and PC toward wt-KcsA and ΔM0-KcsA in acidic buffer (pH 4.0). Each affinity was calculated from the sensorgrams by fitting to a 1:2 heterogeneous ligand binding model, as listed in **Table S5.3**. Asterisks denote statistical significance (***$p < 0.001$).

Then, the involvement of the M0 helix in CL binding was investigated using an M0 helix-mimicking peptide (**Figure 5.5a**). In this experiment, liposomes containing anionic lipids were immobilized on an SPR sensor chip modified with an alkyl chain (**Figure 5.5b**),[16] and their interaction with the peptide was assessed. Although various methods for immobilizing lipid molecules on sensor chips, such as biotin-tagged lipids, exist, liposome immobilization was chosen for this study as a more appropriate method, because the M0 domain likely interacts with lipid molecules within the bilayer, as shown

in **Figure 5.2a**. **Figure 5.5c** presents the resulting sensorgrams, which, strangely enough, began to decrease during the association phase (up to 300 s), making it impossible to fit the data to theoretical curves. This is likely because the M0 peptide affected the immobilized liposomes, causing them to detach from the sensor chip surface. Nonetheless, the data confirmed that the M0 peptide strongly bound to CL, to a similar extent as monoanionic lipids PG and PA (**Figure 5.5c**). These results clearly demonstrate that CL interacts with acid-activated KcsA at multiple sites, including the M0 helix, while PA and PG primarily bind to the M0 helix.

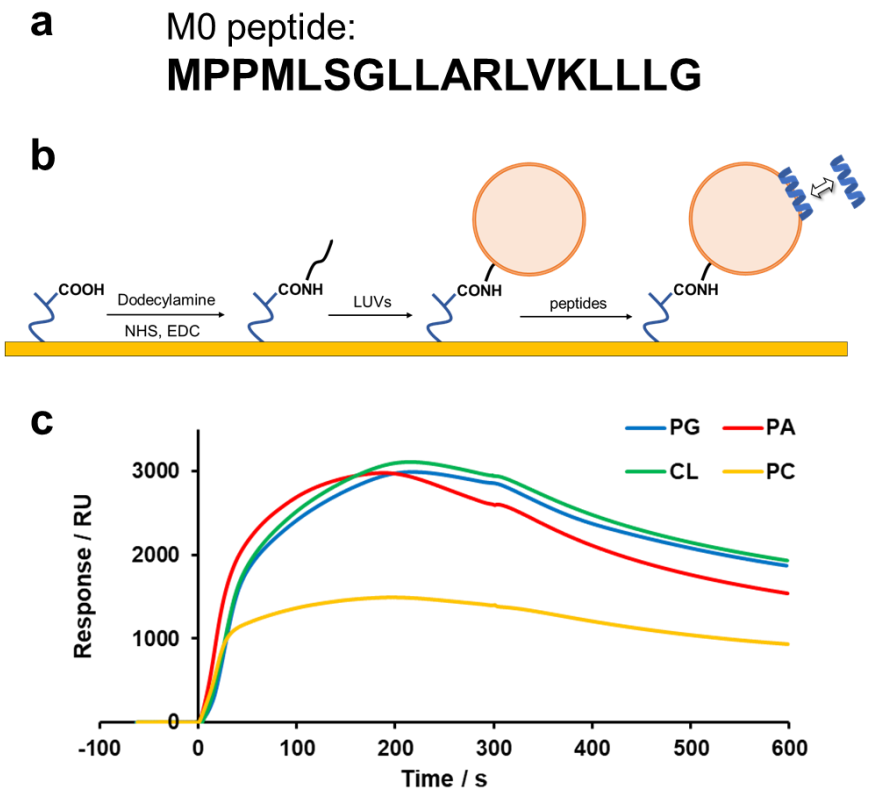

Figure 5.5. (a) Amino acid sequence of wild type M0 peptide. (b) Procedure for analyzing the interaction.[16] Dodecylamine was coupled with COOH group on the CM5 sensor chip via a conventional amine coupling method. Next, 100 nm LUV solution was injected to be immobilized onto the chip surface. Then the peptide aqueous solution was added to the immobilized liposomes and their interactions were analyzed. (c) Sensorgrams indicating the interaction of M0 peptide to pure PC, PG/PC (1:9), PA/PC (1:9), and CL/PC (1:9) membranes in acidic buffer (pH 4.0).

5.3.3 CL binds to Arg residues in the extracellular surface of KcsA

SPR experiments demonstrated that CL binds not only to the M0 helix but also to multiple sites on KcsA. CL is a divalent anion with two phosphate groups, located near the membrane interface (**Figure 5.2b**). Consequently, the author focused on two positively charged residues (Arg64 and Arg89) located at the outer membrane interface of the transmembrane domain (TMD) and facing the inter-subunit space (**Figure 5.6**). These residues were previously reported to interact with PA,[22] and it was hypothesized in this study that they also serve as counterparts for specific CL binding. To prove this, SAMPLIA analysis was performed on R52Q, R64Q, and R89Q mutants with CL. These mutations were introduced into ΔM0-KcsA to eliminate the effect of the interaction between CL and the M0 helix.

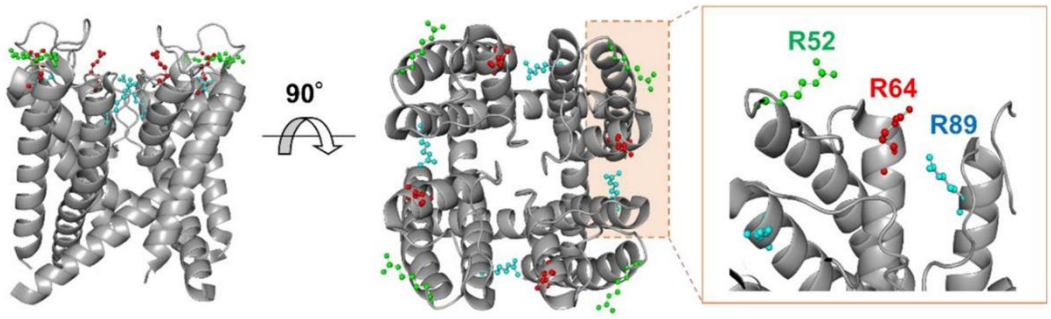

Figure 5.6. The positions of Arg52 (green), Arg64 (red) and Arg89 (blue) in KcsA (Protein Data Bank ID 6by3). All of the three residues are located at the outer membrane interface (extracellular side) of the TMD, while Arg64 and Arg89 also face the inter-subunit space.

To achieve a more detailed quantitative analysis of lipid-protein interactions, the author introduced SCK analysis, which is a continuous measurement of binding and dissociation at multiple concentrations in a single cycle without the need for sensor chip regeneration.[12] SCK analysis is advantageous for samples with slow dissociation rates and challenging regeneration, making it suitable for evaluating the CL-KcsA interaction.

The SCK-combined SAMPLIA analysis was applied with five concentrations of CL (0.3–30 μM) and ΔM0-KcsA with mutated Arg residues. To reliably assess slow dissociation, a long dissociation time of 6000 s was set. The result showed that mutations at Arg64 and/or Arg89 significantly reduced the affinity for CL (**Figure 5.7** and **TableS5.4**). In contrast, mutation at Arg52, located at the outer membrane interface of the TMD (**Figure 5.6**), slightly increased the binding affinity for CL (**Figure 5.7b**). These results suggest that CL selectively interacts with Arg64 and Arg89 and may open the inner gate located in the intracellular half of the TMD via long-range allosteric coupling.

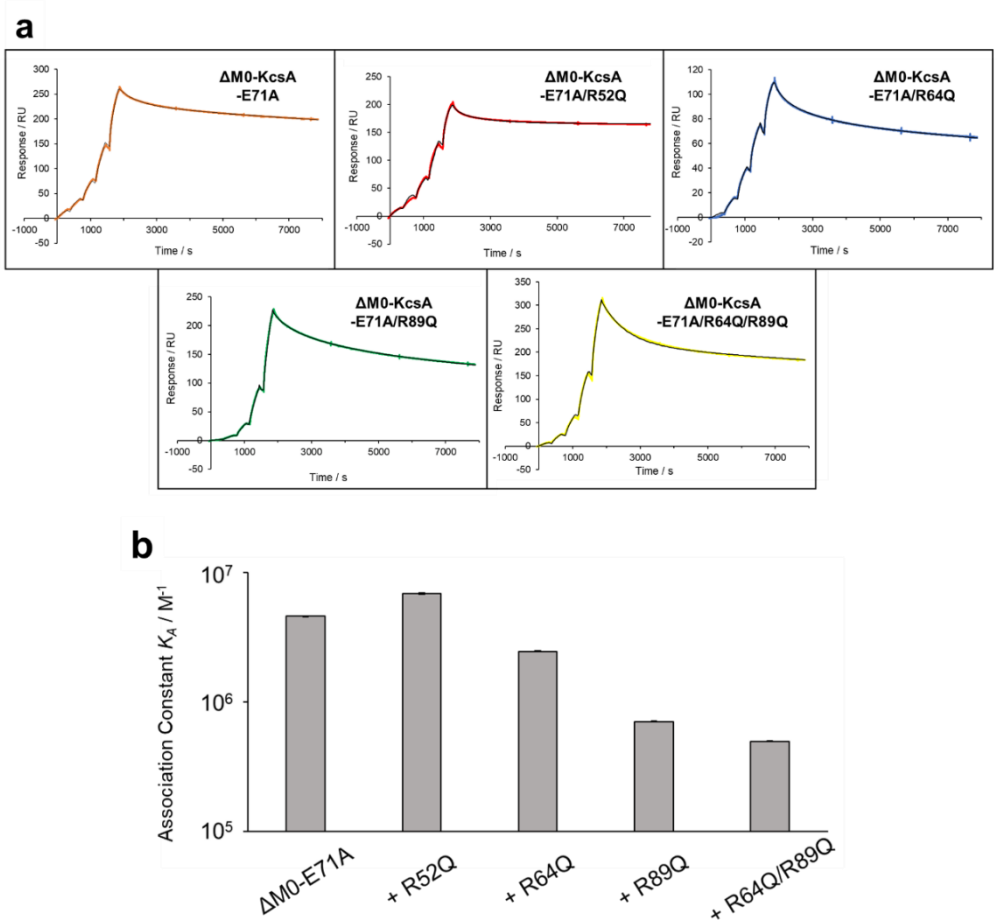

Figure 5.7. (a) SPR sensorgrams showing the interactions of CL with KcsA mutants in SCK analysis.[12] The CL solutions with the concentration of 0.3, 1, 3, 10, 30 μM were injected for 300 s at a flow rate of 30 μL min^{-1} in increasing order of concentration. Colored lines indicate

experimentally obtained sensorgrams, while black lines indicate fitted curves. (b) Affinity of CL toward KcsA mutants in acidic buffer (pH 4.0). Each affinity was calculated from the sensorgrams by fitting to a 1:2 heterogeneous ligand binding model, as listed in **Table S5.4**. *SE* was calculated by χ^2 analyses and residual plots.

5.4 Discussion

In this chapter, the quantitative analysis of the interactions between KcsA and anionic lipids was demonstrated using the SAMPLIA method. Regarding the direct effects of anionic lipids on KcsA, two modes of interaction have been proposed: one involves electrostatic interactions between anionic lipids and the *N*-terminal M0 helix,[13] while the other involves interactions between anionic lipids and the inter-subunit groove on the extracellular surface of KcsA.[23-29]

Due to the inherent disorder of the M0 helix, either its conformation or its specific binding to lipids has not been revealed.[3, 26] This study demonstrates that the M0 helix serves as the primary binding site for anionic lipids (**Figure 5.8**), with PG and PA preferentially binding to it (**Figure 5.4**). However, crystal structures and NMR show that PG and PA also bind to the extracellular inter-subunit groove of KcsA.[4, 9, 22] The K_A values for PA and PG to ΔM0-KcsA, around 10^5, (**Figure 5.4**) indicate that while these lipids can bind to the groove, the interaction is significantly weaker. These findings show that, although PG and PA may bind to the groove in a less specific manner, as observed in NMR and crystal structures, their primary binding site is the M0 helix, and their action on KcsA is mediated through this binding. This is consistent with previous findings showing that PG in the outer membrane does not affect channel function.[13]

In contrast, CL bound to KcsA with significantly stronger affinity compared to monoanionic lipids, and this strong binding was also maintained in the ΔM0-KcsA mutant

(**Figure 5.4**), suggesting that the groove within the TMD could serve as an alternative binding site for CL (**Figure 5.8**). Subsequent analysis of ΔM0-KcsA with Arg mutation suggested that CL binds more readily to Arg64 and Arg89 at the outer membrane interface of the TMD in the open conformation (**Figure 5.7**), shifting the equilibrium toward the open state and exerting its allosteric effect. This conformation-dependent binding of CL is partly supported by the finding that CL binds more selectively to acid-activated KcsA (pH 4.0) compared to resting-state KcsA (pH 7.5), while the selectivity of PA and PG for the acid-activated state is less pronounced (**Figure 5.3**).

Here, the author refers to the SAMPLIA method, which is characterized by the use of SAM.[1] The hydrophobic nature of the SAM-modified sensor chip allows for the efficient immobilization of KcsA and is expected to provide a partially membranous environment for the immobilized KcsA molecules. The combination with SCK analysis enables the interaction analysis of samples with slow dissociation and difficult regeneration, such as the CL-KcsA interaction, effectively eliminating non-specific interactions and providing reliable quantitative data. This approach can address a variety of lipid-MP interactions and contribute to a deeper understanding of the interactions identified in previous chapters.

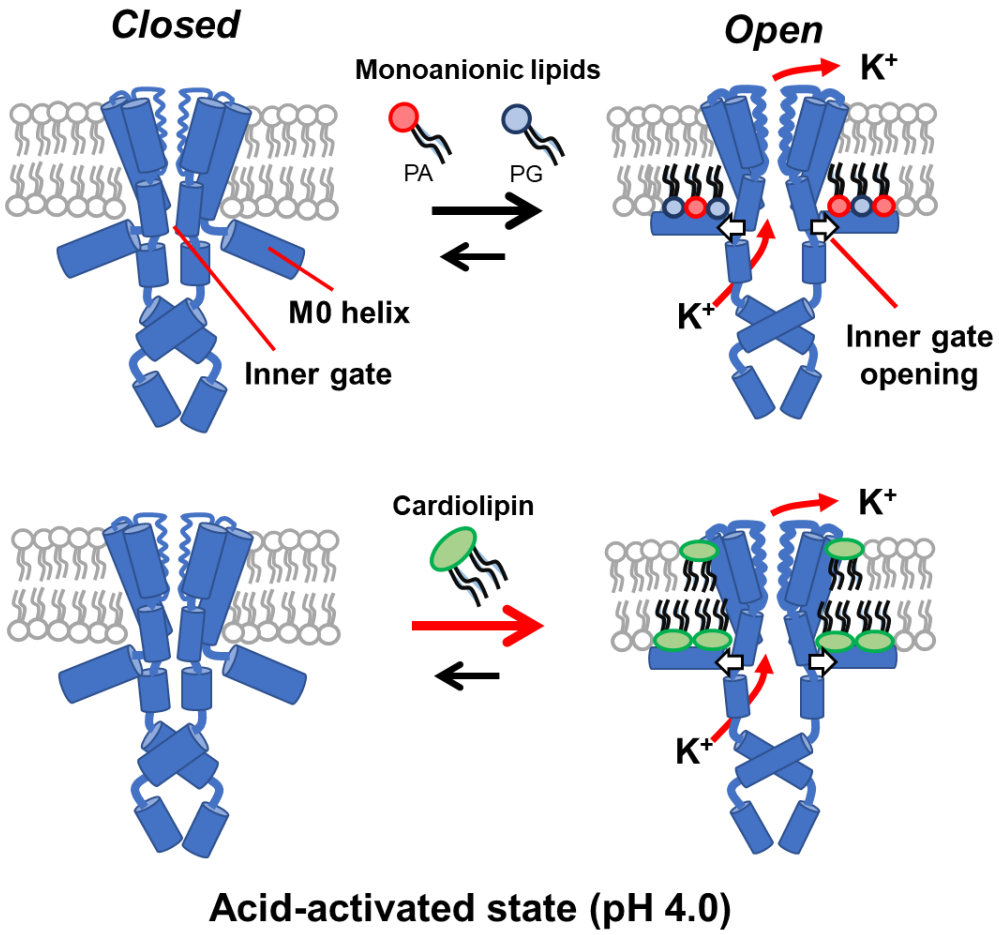

Figure 5.8. The interactions of mono- and dianionic lipids with KcsA stabilize its open state. Monoanionic lipids, including PA and PG, primarily bind to the M0 helix and open the inner gate (**top**). CL interacts with acid-activated KcsA not only at the M0 helix but also at the outer membrane interface of the TMD (**bottom**). The latter interaction of CL may open the inner gate located in the intracellular half of the TMD through long-range allosteric coupling.

5.5 Conclusion

The conclusion of this chapter is that the high-affinity binding of CL to ΔM0-KcsA suggests the presence of an additional binding site for CL, selectively recognizing dianions. This site is likely located in the groove, where dianionic CL interacts with multiple arginine residues (Arg64 and Arg89) in adjacent subunits. In contrast, the M0 helix serves as a binding site for both mono- and dianionic lipids via simple electrostatic interactions. These mechanistic views will be examined in future. Furthermore, the quantitative methodology developed in this study, which combines SAMPLIA and SCK analysis followed by physiological evaluation, provides a solid foundation for investigating the biological roles of various membrane lipids on MPs.

Reference

(1) Inada, M.; Kinoshita, M.; Sumino, A.; Oiki, S.; Matsumori, N. A concise method for quantitative analysis of interactions between lipids and membrane proteins. *Anal. Chim. Acta* **2019**, *1059*, 103-112. DOI: 10.1016/j.aca.2019.01.042.
(2) Heginbotham, L.; Odessey, E.; Miller, C. Tetrameric Stoichiometry of a Prokaryotic K+ Channel. *Biochemistry* **1997**, *36* (33), 10335-10342. DOI: 10.1021/bi970988i.
(3) Doyle, D. A.; Morais Cabral, J.; Pfuetzner, R. A.; Kuo, A.; Gulbis, J. M.; Cohen, S. L.; Chait, B. T.; MacKinnon, R. The structure of the potassium channel: molecular basis of K+ conduction and selectivity. *Science* **1998**, *280* (5360), 69-77. DOI: 10.1126/science.280.5360.69.
(4) Zhou, Y.; Morais-Cabral, J. H.; Kaufman, A.; MacKinnon, R. Chemistry of ion coordination and hydration revealed by a K+ channel-Fab complex at 2.0 A resolution. *Nature* **2001**, *414* (6859), 43-48. DOI: 10.1038/35102009.
(5) Perozo, E.; Cortes, D. M.; Cuello, L. G. Structural rearrangements underlying K+-channel activation gating. *Science* **1999**, *285* (5424), 73-78. DOI: 10.1126/science.285.5424.73.
(6) Takeuchi, K.; Takahashi, H.; Kawano, S.; Shimada, I. Identification and characterization of the slowly exchanging pH-dependent conformational rearrangement in KcsA. *J. Biol. Chem.* **2007**, *282* (20), 15179-15186. DOI: 10.1074/jbc.M608264200.
(7) Chill, J. H.; Louis, J. M.; Delaglio, F.; Bax, A. Local and global structure of the monomeric subunit of the potassium channel KcsA probed by NMR. *Biochim. Biophys. Acta* **2007**, *1768* (12), 3260-3270. DOI: 10.1016/j.bbamem.2007.08.006.
(8) Thompson, A. N.; Posson, D. J.; Parsa, P. V.; Nimigean, C. M. Molecular mechanism of pH sensing in KcsA potassium channels. *Proc. Natl. Acad. Sci. U. S. A.* **2008**, *105* (19), 6900-6905. DOI: 10.1073/pnas.0800873105.
(9) Valiyaveetil, F. I.; Zhou, Y.; MacKinnon, R. Lipids in the structure, folding, and function of the KcsA K+ channel. *Biochemistry* **2002**, *41* (35), 10771-10777. DOI: 10.1021/bi026215y.
(10) Hoischen, C.; Gura, K.; Luge, C.; Gumpert, J. Lipid and fatty acid composition of cytoplasmic membranes from Streptomyces hygroscopicus and its stable protoplast-type L form. *J. Bacteriol.* **1997**, *179* (11), 3430-3436. DOI: 10.1128/jb.179.11.3430-3436.1997.
(11) Sandoval-Calderón, M.; Guan, Z.; Sohlenkamp, C. Knowns and unknowns of membrane lipid synthesis in streptomycetes. *Biochimie* **2017**, *141*, 21-29. DOI: 10.1016/j.biochi.2017.05.008.
(12) Palau, W.; Di Primo, C. Simulated single-cycle kinetics improves the design of surface plasmon resonance assays. *Talanta* **2013**, *114*, 211-216. DOI: https://doi.org/10.1016/j.talanta.2013.04.022.
(13) Iwamoto, M.; Oiki, S. Amphipathic antenna of an inward rectifier K+ channel responds to changes in the inner membrane leaflet. *Proc. Natl. Acad. Sci. U. S. A.* **2013**, *110* (2), 749-754. DOI: 10.1073/pnas.1217323110.
(14) Morton, T. A.; Myszka, D. G.; Chaiken, I. M. Interpreting complex binding kinetics

from optical biosensors: a comparison of analysis by linearization, the integrated rate equation, and numerical integration. *Anal. Biochem.* **1995**, *227* (1), 176-185. DOI: 10.1006/abio.1995.1268.
(15) Khalifa, M. B.; Choulier, L.; Lortat-Jacob, H.; Altschuh, D.; Vernet, T. BIACORE data processing: an evaluation of the global fitting procedure. *Anal. Biochem.* **2001**, *293* (2), 194-203. DOI: 10.1006/abio.2001.5119.
(16) Mouri, R.; Konoki, K.; Matsumori, N.; Oishi, T.; Murata, M. Complex formation of amphotericin B in sterol-containing membranes as evidenced by surface plasmon resonance. *Biochemistry* **2008**, *47* (30), 7807-7815. DOI: 10.1021/bi800334p.
(17) Nakajima, H.; Kiyokawa, N.; Katagiri, Y. U.; Taguchi, T.; Suzuki, T.; Sekino, T.; Mimori, K.; Ebata, T.; Saito, M.; Nakao, H.; Takeda, T.; Fujimoto, J. Kinetic analysis of binding between Shiga toxin and receptor glycolipid Gb3Cer by surface plasmon resonance. *J. Biol. Chem.* **2001**, *276* (46), 42915-42922. DOI: 10.1074/jbc.M106015200.
(18) Sykes, D. A.; Parry, C.; Reilly, J.; Wright, P.; Fairhurst, R. A.; Charlton, S. J. Observed drug-receptor association rates are governed by membrane affinity: the importance of establishing "micro-pharmacokinetic/pharmacodynamic relationships" at the β2-adrenoceptor. *Mol. Pharmacol.* **2014**, *85* (4), 608-617. DOI: 10.1124/mol.113.090209.
(19) Ijzerman, A. P.; Guo, D. Drug-Target Association Kinetics in Drug Discovery. *Trends Biochem. Sci.* **2019**, *44* (10), 861-871. DOI: 10.1016/j.tibs.2019.04.004.
(20) Deol, S. S.; Domene, C.; Bond, P. J.; Sansom, M. S. Anionic phospholipid interactions with the potassium channel KcsA: simulation studies. *Biophys. J.* **2006**, *90* (3), 822-830. DOI: 10.1529/biophysj.105.071407.
(21) Marius, P.; Alvis, S. J.; East, J. M.; Lee, A. G. The interfacial lipid binding site on the potassium channel KcsA is specific for anionic phospholipids. *Biophys. J.* **2005**, *89* (6), 4081-4089. DOI: 10.1529/biophysj.105.070755.
(22) Poveda, J. A.; Giudici, A. M.; Renart, M. L.; Millet, O.; Morales, A.; González-Ros, J. M.; Oakes, V.; Furini, S.; Domene, C. Modulation of the potassium channel KcsA by anionic phospholipids: Role of arginines at the non-annular lipid binding sites. *Biochim Biophys Acta Biomembr* **2019**, *1861* (10), 183029. DOI: 10.1016/j.bbamem.2019.183029.
(23) Marius, P.; Zagnoni, M.; Sandison, M. E.; East, J. M.; Morgan, H.; Lee, A. G. Binding of anionic lipids to at least three nonannular sites on the potassium channel KcsA is required for channel opening. *Biophys. J.* **2008**, *94* (5), 1689-1698. DOI: 10.1529/biophysj.107.117507.
(24) Raja, M. The potassium channel KcsA: a model protein in studying membrane protein oligomerization and stability of oligomeric assembly? *Arch. Biochem. Biophys.* **2011**, *510* (1), 1-10. DOI: 10.1016/j.abb.2011.03.010.
(25) Weingarth, M.; Prokofyev, A.; van der Cruijsen, E. A.; Nand, D.; Bonvin, A. M.; Pongs, O.; Baldus, M. Structural determinants of specific lipid binding to potassium channels. *J. Am. Chem. Soc.* **2013**, *135* (10), 3983-3988. DOI: 10.1021/ja3119114.
(26) Molina, M. L.; Giudici, A. M.; Poveda, J. A.; Fernández-Ballester, G.; Montoya, E.; Renart, M. L.; Fernández, A. M.; Encinar, J. A.; Riquelme, G.; Morales, A.; González-Ros, J. M. Competing Lipid-Protein and Protein-Protein Interactions Determine

Clustering and Gating Patterns in the Potassium Channel from Streptomyces lividans (KcsA). *J. Biol. Chem.* **2015**, *290* (42), 25745-25755. DOI: 10.1074/jbc.M115.669598.
(27) van der Cruijsen, E. A.; Prokofyev, A. V.; Pongs, O.; Baldus, M. Probing Conformational Changes during the Gating Cycle of a Potassium Channel in Lipid Bilayers. *Biophys. J.* **2017**, *112* (1), 99-108. DOI: 10.1016/j.bpj.2016.12.001.
(28) Poveda, J. A.; Marcela Giudici, A.; Lourdes Renart, M.; Morales, A.; González-Ros, J. M. Towards understanding the molecular basis of ion channel modulation by lipids: Mechanistic models and current paradigms. *Biochim Biophys Acta Biomembr* **2017**, *1859* (9 Pt B), 1507-1516. DOI: 10.1016/j.bbamem.2017.04.003.
(29) Xu, Y.; McDermott, A. E. Inactivation in the potassium channel KcsA. *J Struct Biol X* **2019**, *3*, 100009. DOI: 10.1016/j.yjsbx.2019.100009.

Chapter 6
Conclusion and Perspective

In this doctoral thesis, to elucidate the roles of membrane lipids in regulating the structure and activity of membrane proteins (MPs), the author developed a methodology for the comprehensive analysis of lipid-MP interactions using lipid-immobilized beads.

In **Chapter 1**, the author explained the research background on lipid-membrane protein interactions and the current status of the field.

In **Chapter 2**, the author developed lipid-immobilized beads for the identification of lipid-binding MPs. Sphingolipids: sphingomyelin and ceramide were immobilized to demonstrate the utility of the beads. Following the confirmation of their utility through various experiments, a screening for lipid-binding proteins from cell lysates was performed. As a result, the author succeeded in preparing *detergent-tolerant* and *membrane-mimetic* lipid-immobilized beads.

In **Chapter 3**, the author conducted a more comprehensive identification of lipid-binding MPs. To achieve a comprehensive analysis, the bead-based method was enhanced in three aspects: 1) in-depth proteomics without SDS-PAGE separation, 2) the incorporation of Gene Ontology enrichment analysis, and 3) the extension of lipid-immobilized bead variations. This approach successfully identified over 7000 lipid-binding proteins. Filtering based on fold-change values and subsequent enrichment analysis revealed distinct binding protein profiles for each lipid, highlighting the functional diversity of lipid-MP interactions and their roles in cellular processes.

In **Chapters 4 and 5**, the author tried to extend this approach by the subsequent interaction analysis and functional analysis. In **Chapter 4**, the use of yeast cells, which facilitate genetic and biochemical approaches, enabled easier investigations into the physiological roles of the identified lipid-protein interactions. Yeast-derived ceramide species were immobilized on beads, and a screening for binding proteins was conducted.

As a result, vacuolar-type ATPase (V-ATPase) was identified as one of the dihydroceramide (DHCer)-binding protein candidates. The specific interaction between DHCer and V-ATPase was confirmed by fluorescence resonance energy transfer (FRET), further suggesting a regulatory role for ceramide in V-ATPase activity. In **Chapter 5**, the surface plasmon resonance (SPR)-based SAMPLIA method was improved by the incorporation of single-cycle kinetics analysis. To demonstrate the efficiency of this method in evaluating lipid- MP interactions, the author conducted quantitative analyses of the interactions between the potassium channel KcsA and various lipids, and between KcsA mutants and cardiolipin. As a result, it was suggested that cardiolipin interacts with two Arg resides located at the outer membrane interface of the KcsA transmembrane domain, stabilizing the open state through long-range allosteric effects. This SPR-based method provides a platform for the quantitative analysis of lipid-MP interactions.

Diverse lipids regulate MP function through interactions. However, the details of how lipid-MP interactions regulate MPs remain unknown, and the significance of lipid diversity remains a mystery. To investigate this regulation, lipid-MP interaction analysis is required, but methods are limited, especially for analyzing lipid-binding MPs. In this thesis, the author developed a comprehensive and systematic approach to identify lipid-binding MPs using high-density lipid-immobilized beads. This method facilitates comprehensive and integrated studies of lipid-MP interactions, advancing our understanding of lipid-mediated MP regulation. In the future, applying this methodology to a broader range of lipid species may elucidate the physiological roles of lipid diversity. Furthermore, it is hoped that integrating multi-faceted approaches, such as interaction and functional analyses, will establish a comprehensive and systematic platform that accelerates the understanding of lipid functions and lipid-protein interactions.

Publication List

Original Papers

1. Identification of Lipid-Specific Proteins with High-Density Lipid-Immobilized Beads
   Analyst **2024**, *149*, 3747–3755.
   Masayuki Morito, Hiroki Yasuda, Takaaki Matsufuji, Masanao Kinoshita and Nobuaki Matsumori

2. Comprehensive Identification of Lipid-Membrane Protein Interactions via Advanced Proteomics and Extended Lipid-Immobilized Bead Technology
   Anal. Chem. (submitted)
   Masayuki Morito, Kosuke Hata, Yoshihiro Izumi, Takeshi Bamba, Nobuaki Matsumori

Joint Papers

1. Cardiolipin Binding Enhances KcsA Channel Gating via Both its Specific and Dianion-Monoanion Interchangeable Sites
   iScience **2023**, *26*(12), 108471.
   Masayuki Iwamoto, Masayuki Morito, Shigetoshi Oiki, Yudai Nishitani, Daisuke Yamamoto, Nobuaki Matsumori

2. Truncated Derivatives of Amphidinol 3 Reveal the Functional Role of Polyol Chain in Sterol-Recognition and Pore Formation
   Bioorg. Med. Chem. Lett. **2024**, *98*, 129594.
   Nobuaki Matsumori, Manami Hieda, Masayuki Morito, Yuma Wakamiya, Tohru Oishi

Acknowledgments

This research was conducted under the supervision of Professor Nobuaki Matsumori at the Department of Chemistry, Graduate School of Sciences, Kyushu University.

I would like to express my deepest gratitude to Professor Nobuaki Matsumori for supervising this thesis, providing an excellent research environment, offering valuable discussions, and supporting all my work. I also wish to extend my sincere appreciation to Associate Professor Masanao Kinoshita at the Graduate School of Science and Technology, Gunma University, for his insightful comments, advice, and encouragement. I am also grateful to Associate Professor Takayuki Kawai and Associate Professor Kohei Torikai for their valuable discussions and insightful comments.

I would like to thank Professor Takeshi Bamba, Associate Professor Yoshihiro Izumi, and Assistant Professor Kosuke Hata at the Division of Metabolomics, Medical Research Center for High Depth Omics, Medical Institute of Bioregulation, Kyushu University, for performing the proteomic analysis in Chapter 3 and for their valuable discussions.

I would like to express my gratitude to Professor Motohiro Tani at the Faculty of Applied Biological Sciences, Gifu University, for providing yeast cells expressing GFP-tagged V-ATPase and for our valuable discussions.

I am also grateful to Professor Shigetoshi Oiki at Biomedical Imaging Research

Center, University of Fukui, and Professor Masayuki Iwamoto at the Department of Molecular Neuroscience, Faculty of Medical Sciences, University of Fukui, for providing the KcsA samples and for their valuable discussions.

I would like to thank Professor Junichi Ikenouchi at the Department of Biochemistry, Graduate School of Medical Sciences, Kyushu University, for providing lysenin.

I would also like to thank Associate Professor Keiichi Konoki at the Graduate School of Agricultural Science, Tohoku University, for providing nakanori.

I am deeply thankful to all the members of the Matsumori laboratory for their kind support not only for my research but also for my daily life. Their assistance made my time in the laboratory very meaningful.

Finally, I would like to express my special thanks to my family. They have always been supportive, and no matter what I have done, they have always been there to help me along the way.

Masayuki Morito

March 2025

Supporting Information

S1. Supplementary Methods for Synthesis of Lipid Derivatives

General

EggSM was purchased from Avanti Polar Lipids (Alabaster, AL, USA). Sphingosine was purchased from Toronto Research Chemicals (Toronto, Canada). All other reagents were all purchased from FUJIFILM Wako Pure Chemical Corp. (Osaka, Japan), Tokyo Chemical Inc. (Tokyo, Japan), Nacalai Tesque Inc. (Kyoto, Japan), or Sigma-Aldrich (St. Louis, MO, USA). Thin-layer chromatography was performed on Merck precoated silica gel 60 F-254 plates, which were visualized by UV irradiation (254 nm) or staining with anisaldehyde/sulfuric acid. ^{1}H NMR spectra were obtained on a Bruker Ascend 500 (500 MHz) spectrometer and a JEOL ECA 600 (600 MHz) spectrometer. High-resolution mass spectra (HRMS) of synthetic compounds were acquired on a Bruker micrOTOF II ESI-TOF mass spectrometer.

Synthesis of 16-azidohexadecanoic acid (1)

To a solution of 16-bromohexadecanoic acid (394 mg, 1.18 mmol) in DMF (5 mL) was added NaN_3 (115 mg, 1.76 µmol). The reaction mixture was stirred at room temperature overnight and then extracted with ethyl acetate. The organic layer was dried over anhydrous Na_2SO_4, filtered, and concentrated *in vacuo*. Purification by silica gel column chromatography (hexane/ethyl acetate 3:1 v/v) afforded a colorless solid (310.8 mg, 1.05 mmol, 89%). R_f = 0.22 (3/1 hexane/ethyl acetate, v/v), ^{1}H NMR (600 MHz, $CDCl_3$): δ 3.25 (t, J = 7.2 Hz, 2H), 2.34 (t, J = 7.6 Hz, 2H), 1.65-1.57 (m, 4H), 1.37-1.25 (m, 22H), HRMS (*m*/*z*): $[M + H]^+$ calcd for $C_{16}H_{31}N_3NaO_2^+$, 320.2308; found, 320.2313.

Synthesis of 16-azidohexadecanoic acid 4-nitrophenyl ester (2)

To a solution of the azidoacylacid (**1**) (29.7 mg, 99.8 µmol) in CH_2Cl_2 (2 mL) were added *p*-nitrophenol (20.9 mg, 150 µmol) and EDC·HCl (28.8 mg, 150 µmol). The reaction mixture was stirred at room temperature for 17 h and then extracted with $CHCl_3$. Purification by silica gel column chromatography (hexane/ethyl acetate 10:1 v/v) afforded a colorless solid (23.6 mg, 55.9 µmol, 56%). R_f = 0.39 (10/1 hexane/ethyl acetate, v/v), ^{1}H NMR (600 MHz, $CDCl_3$): δ 8.27 (d, *J* = 12.6 Hz, 2H), 7.27 (d, *J* = 12.6 Hz, 2H), 3.25 (t, *J* = 8.6 Hz, 2H), 2.59 (t, *J* = 9.1 Hz, 2H), 1.78-1.74 (m, 2H), 1.62-1.57 (m, 2H), 1.40-1.26 (m, 22H), HRMS (*m*/*z*): $[M + Na]^+$ calcd for $C_{22}H_{34}N_4NaO_4^+$, 441.2472; found, 441.2483.

Synthesis of lysoSM (3)

A solution of egg sphingomyelin (50.4 mg, 71.7 µmol) in hydrochloric acid methanolic solution (0.5M, 2.5 mL) was stirred at 50°C for 2 days and then the solvent was removed by evaporation. Purification by silica gel column chromatography ($CHCl_3$/MeOH/NH_4OH 4:6:1 v/v) afforded a colorless solid (13.4 mg, 28.8 µmol, 40%). R_f = 0.14 (65/35/8 $CHCl_3$/MeOH/NH_4OH, v/v), ^{1}H NMR (600 MHz, CD_3OD): δ 5.81-5.76 (m, 1H), 5.39 (q, J = 7.3 Hz, 1H), 4.51 (s, 1H), 4.18 (q, J = 6.2 Hz, 3H), 4.06-3.90 (m, 2H), 3.56 (t, J = 4.5 Hz, 2H), 3.13 (s, 9H), 2.01 (q, J = 6.9 Hz, 2H), 1.33-1.19 (m, 24H), 0.80 (t, J = 6.9 Hz, 3H), HRMS (*m*/*z*): $[M + H]^+$ calcd for $C_{23}H_{50}N_2O_5P^+$, 465.3452; found, 465.3479. $[M + Na]^+$ calcd for $C_{23}H_{49}N_2NaO_5P^+$, 487.3271; found, 487.3300.

Synthesis of azidoSM (4)

To a mixture of the lysoSM (**3**) (13.4 mg, 28.8 µmol) dissolved in CH_2Cl_2 (1 ml) and triethylamine (6.0 µL, 43.3 µmol) was added 16-hexadecanoic acid 4-nitrophenyl ester

(**2**) (18.1 mg, 43.3 μmol). The reaction mixture was stirred at room temperature for 1 day and then extracted with $CHCl_3$. Purification by silica gel column chromatography ($CHCl_3$/MeOH/NH_4OH 65:35:3 v/v) afforded a colorless solid (16.2 mg, 21.6 μmol, 75%). R_f = 0.20 (65/35/3 $CHCl_3$/MeOH/NH_4OH, v/v), ^1H NMR (600 MHz, CD_3OD): δ 5.64 (td, J = 14.4, 6.9 Hz, 1H), 5.38 (q, J = 7.6 Hz, 1H), 4.23 (d, J = 27.5 Hz, 2H), 4.05-3.88 (m, 3H), 3.57 (d, J = 2.7 Hz, 2H), 3.15 (s, 9H), 2.19-2.07 (m, 2H), 1.94 (d, J = 34.4 Hz, 2H), 1.51 (q, J = 7.1 Hz, 4H), 1.23-1.22 (m, 48H), 0.83 (t, J = 6.9 Hz, 3H), HRMS (*m*/*z*): $[M + Na]^+$ calcd for $C_{39}H_{78}N_5NaO_6P^+$, 766.5582; found, 766.5567.

Synthesis of aminoSM (5)

To a solution of the azidoSM (**4**) (16.2 mg, 21.8 μmol) in DMF (1 mL) were added triphenyl phosphine (17.1 mg, 65.3 μmol) and water (100 μL). The reaction mixture was stirred at room temperature for 2 days and then extracted with $CHCl_3$. Purification by silica gel column chromatography ($CHCl_3$/MeOH/NH_4OH 1:1:0.2 v/v) afforded a colorless solid (5.2 mg, 7.2 μmol, 33%) as a white solid. R_f = 0.26 (1/1/0.2 $CHCl_3$/MeOH/NH_4OH, v/v), ^1H NMR (600 MHz, CD_3OD): δ 5.70-5.66 (m, 1H), 5.42 (q, J = 7.6 Hz, 1H), 4.35-4.25 (m, 2H), 4.10-3.89 (m, 3H), 3.61 (t, J = 4.5 Hz, 2H), 3.20 (s, 9H), 2.74 (t, J = 7.6 Hz, 2H), 2.20-2.12 (m, 2H), 2.01 (d, J = 5.2 Hz, 2H), 1.57-1.18 (m, 48H), 0.88 (t, J = 7.2 Hz, 3H), HRMS (*m*/*z*): $[M + H]^+$ calcd for $C_{39}H_{81}N_3O_6P^+$, 718.5858; found, 718.5929.

Synthesis of azidoCer (6)

To a solution of *D-erythro*-sphingosine (10 mg, 33.4 μmol) in CH_2Cl_2/DMF (2:1, v/v, 2 mL) were added 16-hexadecanoic acid 4-nitrophenyl ester (**2**) (21.0 mg, 50.0 μmol) and

triethylamine (7.0 µL, 50.0 µmol). The mixture was stirred at room temperature for 1 day and then extracted with $CHCl_3$. Purification by silica gel column chromatography ($CHCl_3$/MeOH 30:1 v/v) afforded a colorless solid (12.6 mg, 13.0 µmol, 39%). R_f = 0.28 (30/1 $CHCl_3$/MeOH, v/v), ^{1}H NMR (600 MHz, $CDCl_3$): δ 6.24 (d, J = 7.6 Hz, 1H), 5.79-5.75 (m, 1H), 5.52 (dd, J = 15.8, 6.2 Hz, 1H), 4.31 (d, J = 4.1 Hz, 1H), 3.96-3.88 (m, 2H), 3.70-3.63 (m, 1H), 3.24 (t, J = 7.2 Hz, 2H), 2.21 (q, J = 7.1 Hz, 2H), 2.06-2.00 (m, 2H), 1.65-1.56 (m, 6H), 1.39-1.24 (m, 44H), 0.86 (t, J = 6.9 Hz, 3H), HRMS (*m*/*z*): $[M + Na]^+$ calcd for $C_{34}H_{66}N_4NaO_3^+$, 601.5027; found, 601.5020.

Synthesis of aminoCer (7)

To a solution of the azidoCer (**6**) (12.6 mg, 21.8 µmol) in THF (1 mL) were added triphenyl phosphine (17.1 mg, 65.3 µmol) and water (20 µL). The reaction mixture was stirred at room temperature for 2 days and then extracted with $CHCl_3$. Purification by silica gel column chromatography ($CHCl_3$/MeOH/NH_4OH 40:20:4 v/v) afforded a colorless solid (5.8 mg, 10.5 µmol, 48%) as a white solid. R_f = 0.39 (40/20/4 $CHCl_3$/MeOH/NH_4OH, v/v), ^{1}H NMR (600 MHz, $CDCl_3$): δ 6.27 (d, J = 6.9 Hz, 1H), 5.79-5.74 (m, 1H), 5.52 (dd, J = 15.5, 6.5 Hz, 1H), 4.29 (s, 1H), 3.95-3.88 (m, 2H), 3.68 (dd, J = 11.7, 3.4 Hz, 1H), 2.66 (t, J = 7.2 Hz, 2H), 2.23-2.16 (m, 2H), 2.06-1.99 (m, 2H), 1.63 (q, J = 7.3 Hz, 4H), 1.42-1.24 (m, 44H), 0.86 (t, J = 6.9 Hz, 3H), HRMS (*m*/*z*): $[M + H]^+$ calcd for $C_{34}H_{69}N_2O_3^+$, 553.5303; found, 553.5353.

Synthesis of aminoDHSM (8)

A solution of azidoSM (**4**) (2.8 mg, 3.8 µmol) in MeOH (1.0 mL) was stirred under hydrogen with Pd/C (1.1 mg) at room temperature for 2 days and then filtered through

Celite. Concentration in vacuo yielded a colorless solid (2.5 mg, 3.5 µmol, 92%). ^{1}H-NMR (600 MHz, CD_3OD) δ 4.30 (d, J = 26.8 Hz, 2H), 4.11-4.11 (m, 1H), 3.96-3.84 (m, 2H), 3.66-3.60 (m, 2H), 3.23 (s, 9H), 2.99-2.85 (m, 2H), 2.27-2.19 (m, 2H), 1.65-1.59 (m, 4H), 1.42-1.28 (m, 48H), 0.89 (t, J = 6.9 Hz, 3H), HRMS (*m/z*): $[M + H]^+$ calcd for $C_{39}H_{83}N_3O_6P^+$, 720.6014; found, 720.5940.

Synthesis of dihydrosphingosine (9)

A solution of C18 dihydroceramide (11.2 mg, 19.7 µmol) in CH_3Cl/MeOH (4/1, v/v, 5.0 mL) and hydrochloric acid (12 M, 0.12 mL) was stirred at 50°C overnight and then the solvent was removed by evaporation. Purification by silica gel column chromatography (CHCl3/MeOH 4:1 v/v) afforded a colorless solid (2.28 mg, 7.5 µmol, 38%). R_f = 0.22 (4/1 $CHCl_3$/MeOH, v/v), ^{1}H-NMR (600 MHz, CD_3OD) δ 3.63 (dd, J = 11.0, 4.1 Hz, 1H), 3.42-3.35 (m, 2H), 2.63-2.60 (m, 1H), 1.48-1.44 (m, 2H), 1.34-1.19 (m, 26H), 0.80 (t, J = 7.2 Hz, 3H), HRMS (m/z): $[M + H]^+$ calcd for $C_{18}H_{40}NO_2^+$, 302.3054; found, 302.3059. $[M + Na]^+$ calcd for $C_{18}H_{39}NNaO_2^+$, 324.2873; found, 324.2879.

Synthesis of azidoDHCer (10)

To a mixture of the dihydrosphingosine (**9**) (2.3 mg, 7.6 µmol) dissolved in CH_2Cl_2/DMF (1:2, v/v, 1.5 mL) and triethylamine (3.2 µL, 22.8 µmol) was added 16-azidohexadecanoic acid 4-nitrophenyl ester (**2**) (4.8 mg, 11.4 µmol). The reaction mixture was stirred at room temperature for 1 day and then extracted with $CHCl_3$. Purification by silica gel column chromatography ($CHCl_3$/MeOH 20:1 v/v) afforded a colorless solid (3.2 mg, 5.5 µmol, 72%). R_f = 0.71 (30/1 EtOAc/MeOH, v/v), ^{1}H-NMR (600 MHz, $CDCl_3$) δ 6.32 (d, J = 6.9 Hz, 1H), 4.14 (qd, J = 5.3, 2.7 Hz, 1H), 3.92 (d, J = 8.9 Hz, 2H), 3.75 (s,

1H), 3.62 (s, 1H), 3.57 (s, 1H), 3.25 (t, J = 7.2 Hz, 2H), 2.23 (t, J = 7.6 Hz, 2H), 1.62 (qd, J = 14.9, 7.7 Hz, 4H), 1.53-1.45 (m, 2H), 1.36-1.25 (m, 48H), 0.88 (t, J = 6.9 Hz, 3H), HRMS (*m*/*z*): $[M + Na]^+$ calcd for $C_{34}H_{68}N_4NaO_3^+$, 603.5184; found, 603.5265.

Synthesis of aminoDHCer (11)

To a solution of the azidoDHCer (**10**) (3.2 mg, 5.5 μmol) in CH_2Cl_2/DMF (1:2, v/v, 1.5 mL) were added tris(2-carboxyethyl)phosphine hydrochloride (4.8 mg, 16.5 μmol) and water (200 μL). The reaction mixture was stirred at room temperature for 1 days and then extracted with ethyl acetate. Purification by silica gel column chromatography ($CHCl_3$/MeOH/NH_4OH 75:25:3 v/v) afforded a colorless solid (1.0 mg, 1.8 μmol, 33%) as a white solid. R_f = 0.15 (10/1 $CHCl_3$/MeOH, v/v), ^{1}H-NMR (600 MHz, $CDCl_3$) δ 3.99 (s, 1H), 3.71-3.57 (m, 2H), 3.47-3.43 (m, 1H), 2.57 (t, J = 7.2 Hz, 2H), 2.12 (t, J = 7.6 Hz, 2H), 1.59-1.37 (m, 6H), 1.21-1.17 (m, 48H), 0.79 (t, J = 6.9 Hz, 3H), HRMS (m/z): $[M + H]^+$ calcd for $C_{34}H_{71}N_2O_3^+$, 555.5459; found, 555.5522.

Synthesis of 3β-hydroxy-Δ5-cholenic acid 4-nitrophenyl ester (12)

To a solution of the 3β-hydroxy-Δ5-cholenic acid (45.7 mg, 122 μmol) in CH_2Cl_2 (0.5 mL) were added *p*-nitrophenol (32.2 mg, 231 μmol) and EDC·HCl (40.2 mg, 210 μmol). The reaction mixture was stirred at room temperature for 20 h and then extracted with ethyl acetate. Purification by silica gel column chromatography ($CHCl_3$/MeOH 10:1 v/v) afforded a colorless solid (20.0 mg, 40.3 μmol, 33%). R_f = 0.28 (10/1 $CHCl_3$/MeOH, v/v), ^{1}H NMR (500 MHz, $CDCl_3$): δ 8.27 (d, J = 9.2 Hz, 2H), 7.27 (d, J = 9.0 Hz, 2H), 5.35 (t, J = 5.2 Hz, 1H), 3.57-3.50 (m, 1H), 2.68-2.62 (m, 1H), 2.55-2.49 (m, 1H), 2.32-2.21 (m, 2H), 2.05-1.83 (m, 6H), 1.64-1.42 (m, 6H), 1.37-0.91 (m, 15H), 0.70 (s, 3H), HRMS

(m/z): $[M + H]^+$ calcd for $C_{30}H_{42}NO_5^+$, 496.3058; found, 496.3054.

Synthesis of aminoChol (13)

To a solution of 3β-hydroxy-Δ5-cholenic acid 4-nitrophenyl ester (**12**) (20.0 mg, 40.3 µmol) in CH_2Cl_2/DMF (2:1, v/v, 0.3 mL) were added ethylenediamine (26.8 µL, 40.3 µmol) and triethylamine (6.0 µL, 50.6 µmol). The mixture was stirred at room temperature for 1 day and then extracted with $CHCl_3$. Purification by silica gel column chromatography ($CHCl_3$/MeOH NH_4OH 8:2:0.5 v/v) afforded a colorless solid (5.4 mg, 12.9 µmol, 32%). R_f = 0.39 (8/2/0.5 $CHCl_3$/MeOH NH_4OH v/v), ^1H NMR (500 MHz, CD_3OD): δ 5.33 (d, J = 5.3 Hz, 1H), 3.43-3.35 (m, 3H), 3.02 (t, J = 6.1 Hz, 2H), 2.32-2.10 (m, 4H), 2.06-1.75 (m, 6H), 1.65-1.40 (m, 6H), 1.36-1.30 (m, 2H), 1.22-0.91 (m, 13H), 0.72 (s, 3H), HRMS (*m/z*): $[M + H]^+$ calcd for $C_{26}H_{45}N_2O_2^+$, 417.3476; found, 417.3481.

Synthesis of azidoPC (14)

To a solution of the 16:0 lysoPC (13.0 mg, 26.2 µmol) in CH_2Cl_2(3.5 mL) were added a solution of 16-azdohexadecanoic acid (**1**) (15.6 mg, 52.4 µmol), 2-methyl-6-nitrobenzoic Anhydride (76.2 mg, 219 µmol) and 4-dimethylaminopyridine (64.0 mg, 437 µmol) in CH_2Cl_2 (1.5 mL). The reaction mixture was stirred at room temperature for 2 days under N_2 atmosphere and then extracted with $CHCl_3$. Purification by silica gel column chromatography ($CHCl_3$/MeOH/NH_4OH 40:20:4 v/v) afforded a colorless solid (17.6 mg, 22.7 µmol, 87%) as a white solid. R_f = 0.39 (70/30/5 $CHCl_3$/MeOH/NH_4OH, v/v), ^1H-NMR (600 MHz, $CDCl_3$) δ 5.17 (d, J = 4.8 Hz, 1H), 4.38-4.30 (m, 3H), 4.10 (dd, J = 11.7, 7.6 Hz, 1H), 3.95-3.87 (m, 2H), 3.35 (s, 9H), 3.23 (t, J = 6.9 Hz, 2H), 2.30-2.24 (m, 4H),

1.57 (td, J = 14.6, 7.3 Hz, 6H), 1.35-1.23 (m, 48H), 0.86 (t, J = 7.2 Hz, 3H), HRMS (*m*/*z*): $[M + Na]^+$ calcd for $C_{40}H_{79}N_4NaO_8P^+$, 797.5528; found,797.5589.

Synthesis of aminoPC (15)

To a solution of the azidoPC (**14**) (8.8 mg, 11.4 µmol) in in CH_2Cl_2/DMF (1:1, v/v, 2 mL) were added tris(2-carboxyethyl)phosphine hydrochloride (12.5 mg, 34.2 µmol) and water (200 µL).The reaction mixture was stirred at room temperature for 2 days and then extracted with $CHCl_3$. Purification by silica gel column chromatography ($CHCl_3$/MeOH/NH_4OH 65:35:4 v/v) afforded a colorless solid (2.0 mg, 2.7 µmol, 23%) as a white solid. R_f = 0.06 (70/30/5 $CHCl_3$/MeOH/NH_4OH, v/v), ^{1}H-NMR (600 MHz, CD_3OD) δ 5.25-5.21 (m, 1H), 4.43 (dd, J = 12.0, 3.1 Hz, 1H), 4.27 (d, J = 2.7 Hz, 2H), 4.17 (q, J = 6.2 Hz, 1H), 4.04-3.89 (m, 2H), 3.22 (s, 9H), 2.91-2.81 (m, 2H), 2.36-2.15 (m, 4H), 1.70-1.58 (m, 6H), 1.37-1.28 (m, 48H), 0.89 (t, J = 6.9 Hz, 3H), HRMS (*m*/*z*): $[M + H]^+$ calcd for $C_{40}H_{82}N_2O_8P^+$, 749.5804; found, 749.5778.

Synthesis of azidoPHCer (16)

To a mixture of the phytosphingosine (9.5 mg, 31.5 µmol) dissolved in CH_2Cl_2/DMF (1:1, v/v, 3.0 mL) and triethylamine (13.2 µL, 94.5 µmol) was added 16-azidohexadecanoic acid 4-nitrophenyl ester (**2**) (22.5 mg, 53.8 µmol). The reaction mixture was stirred at room temperature for 1 day and then extracted with ethyl acetate. Purification by silica gel column chromatography ($CHCl_3$/MeOH 30:1 v/v) afforded a colorless solid (8.4 mg, 14.5 µmol, 46%). R_f = 0.51 (20/1 EtOAc/MeOH, v/v), ^{1}H-NMR (600 MHz, $CDCl_3$) δ 6.30 (d, J = 7.6 Hz, 1H), 4.12 (td, J = 5.2, 2.5 Hz, 1H), 3.91-3.86 (m, 1H), 3.72 (q, J = 5.7 Hz, 1H), 3.60-3.55 (m, 2H), 3.23 (t, J = 7.2 Hz, 2H), 2.21 (t, J = 7.9 Hz, 2H), 1.64-1.58

(m, 4H), 1.47-1.43 (m, 2H), 1.34-1.24 (m, 46H), 0.86 (t, J = 6.9 Hz, 3H), HRMS (*m*/*z*): $[M + Na]^+$ calcd for $C_{34}H_{68}N_4NaO_4^+$, 619.5133; found, 619.5177.

Synthesis of azidoPHCer (17)

To a solution of the azidoPHCer (**16**) (8.4 mg, 14.5 μmol) in THF (3.0 mL) were added tris(2-carboxyethyl)phosphine hydrochloride (12.4 mg, 43.3 μmol) and water (300 μL). The reaction mixture was stirred at room temperature for 3 days and then extracted with $CHCl_3$. Purification by silica gel column chromatography ($CHCl_3$/MeOH/NH_4OH 7:3:0.1 v/v) afforded a colorless solid (2.2 mg, 4.0 μmol, 27%) as a white solid. R_f = 0.64 (7/3/0.1 $CHCl_3$/MeOH/ NH_4OH, v/v), ^{1}H-NMR (600 MHz, CD_3OD) δ 4.06 (d, J = 4.8 Hz, 1H), 3.75-3.67 (m, 2H), 3.60-3.56 (m, 1H), 3.51 (d, J = 8.2 Hz, 1H), 2.83 (t, J = 7.6 Hz, 2H), 2.23-2.15 (m, 2H), 1.61 (t, J = 7.6 Hz, 6H), 1.35-1.24 (m, 46H), 0.89 (t, J = 6.9 Hz, 3H), HRMS (*m*/*z*): $[M + H]^+$ calcd for $C_{34}H_{71}N_2O_4^+$, 551.5408; found, 551.5459.

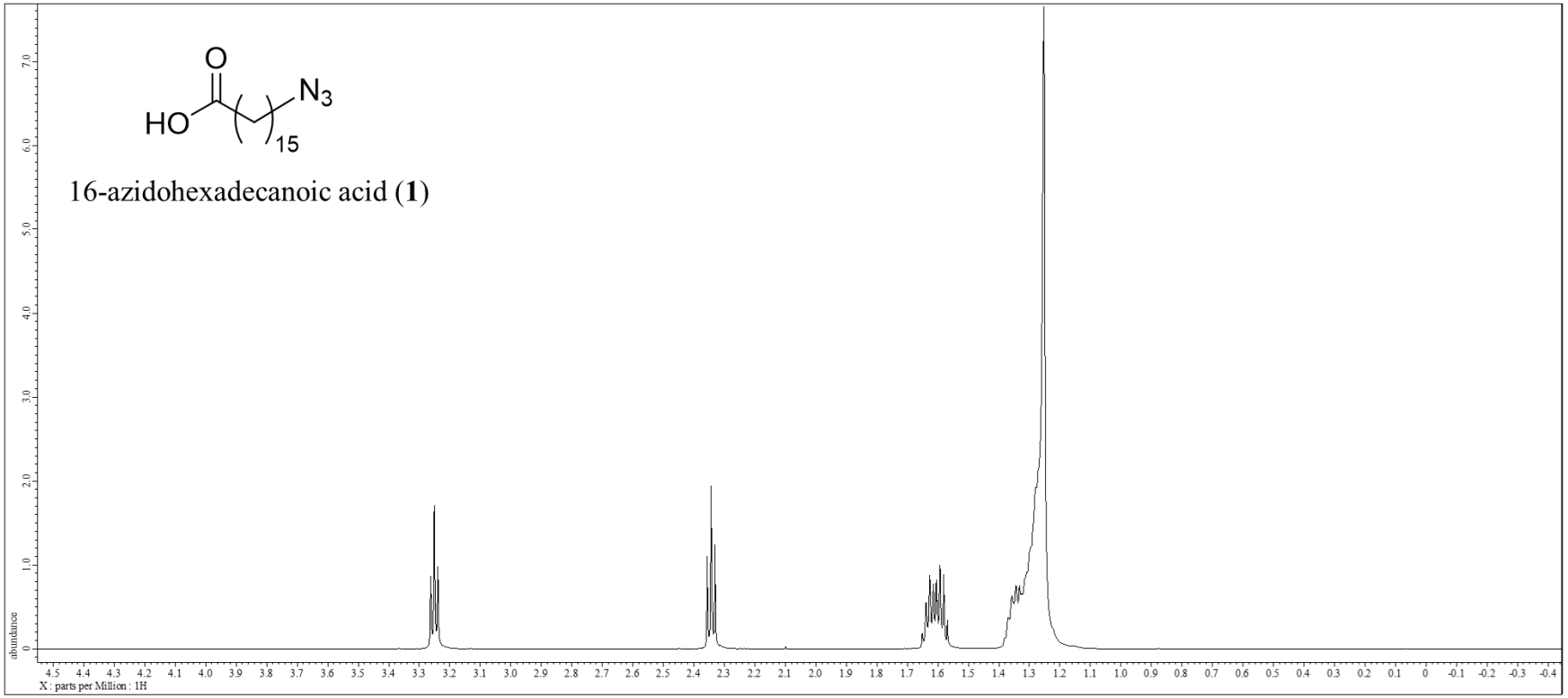

Figure S1.1. 600 MHz ^{1}H NMR spectrum of 16-azidohexadecanoic acid (**1**)

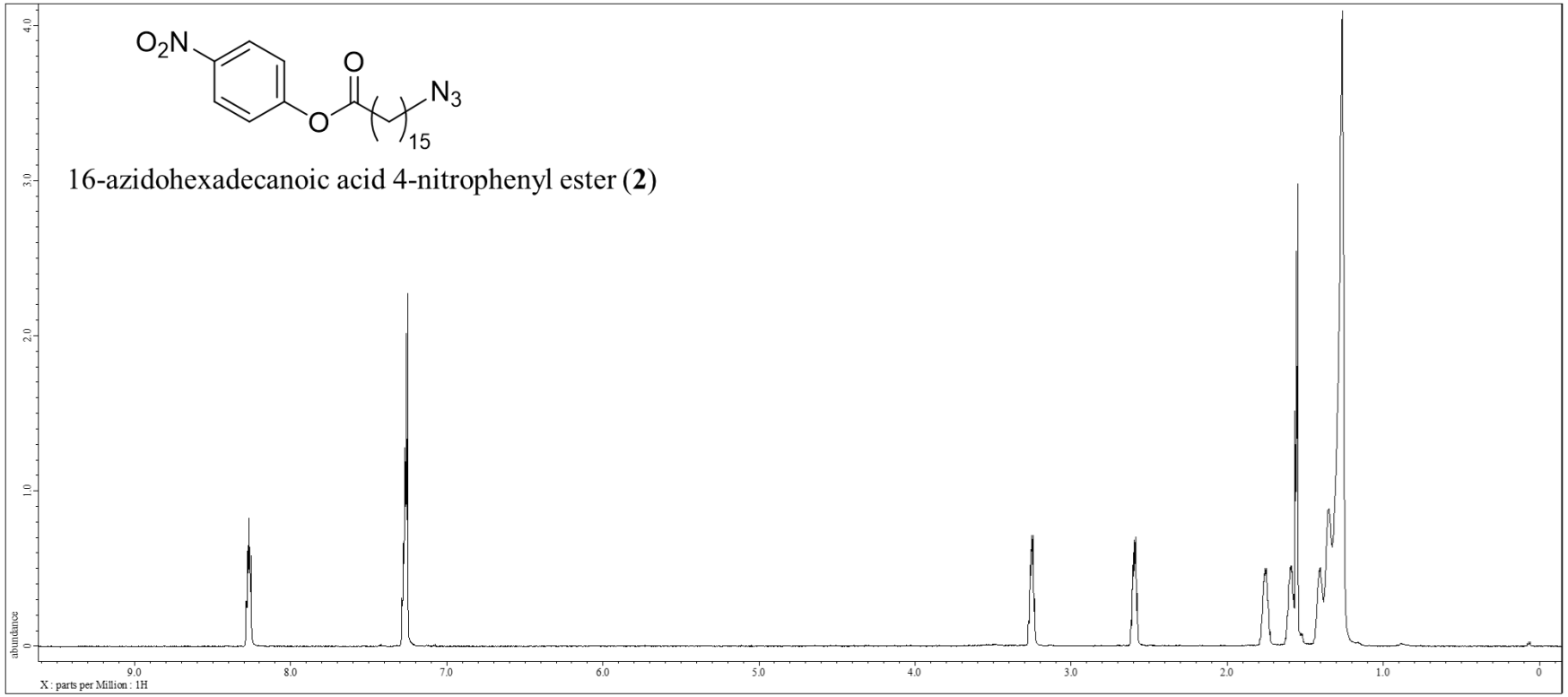

Figure S1.2. 600 MHz ^{1}H NMR spectrum of 16-azidohexadecanoic acid NHS ester (**2**)

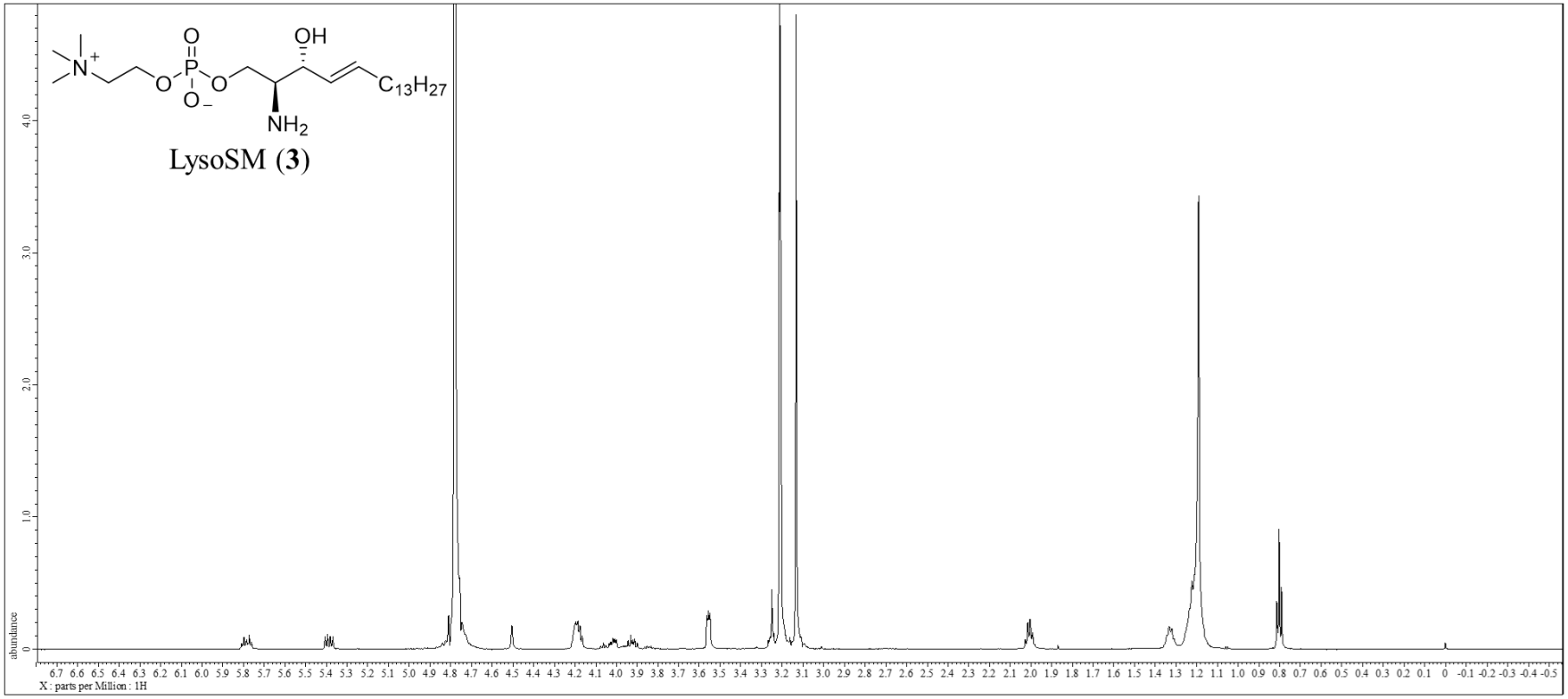

Figure S1.3. 600 MHz ^{1}H NMR spectrum of lysoSM (**3**)

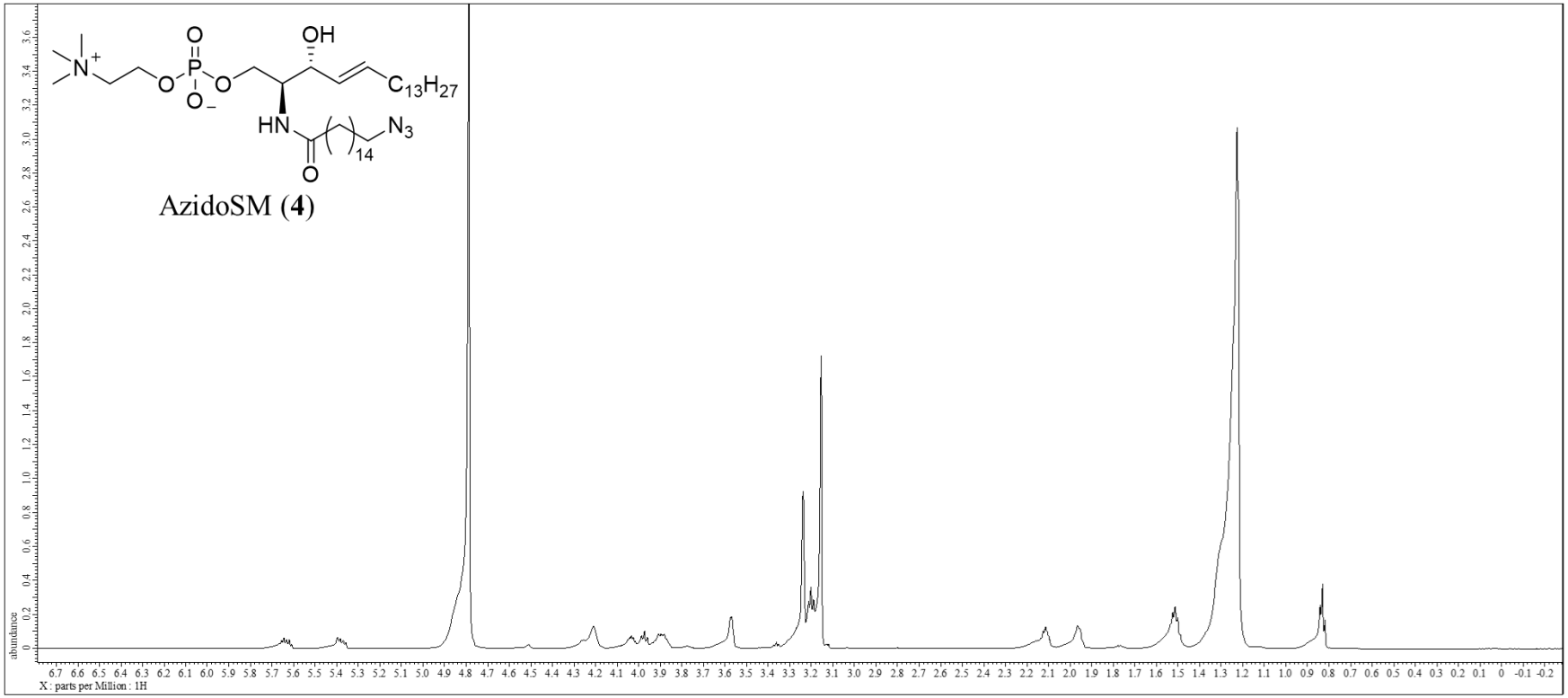

Figure S1.4. 600 MHz 1H NMR spectrum of azidoSM (4)

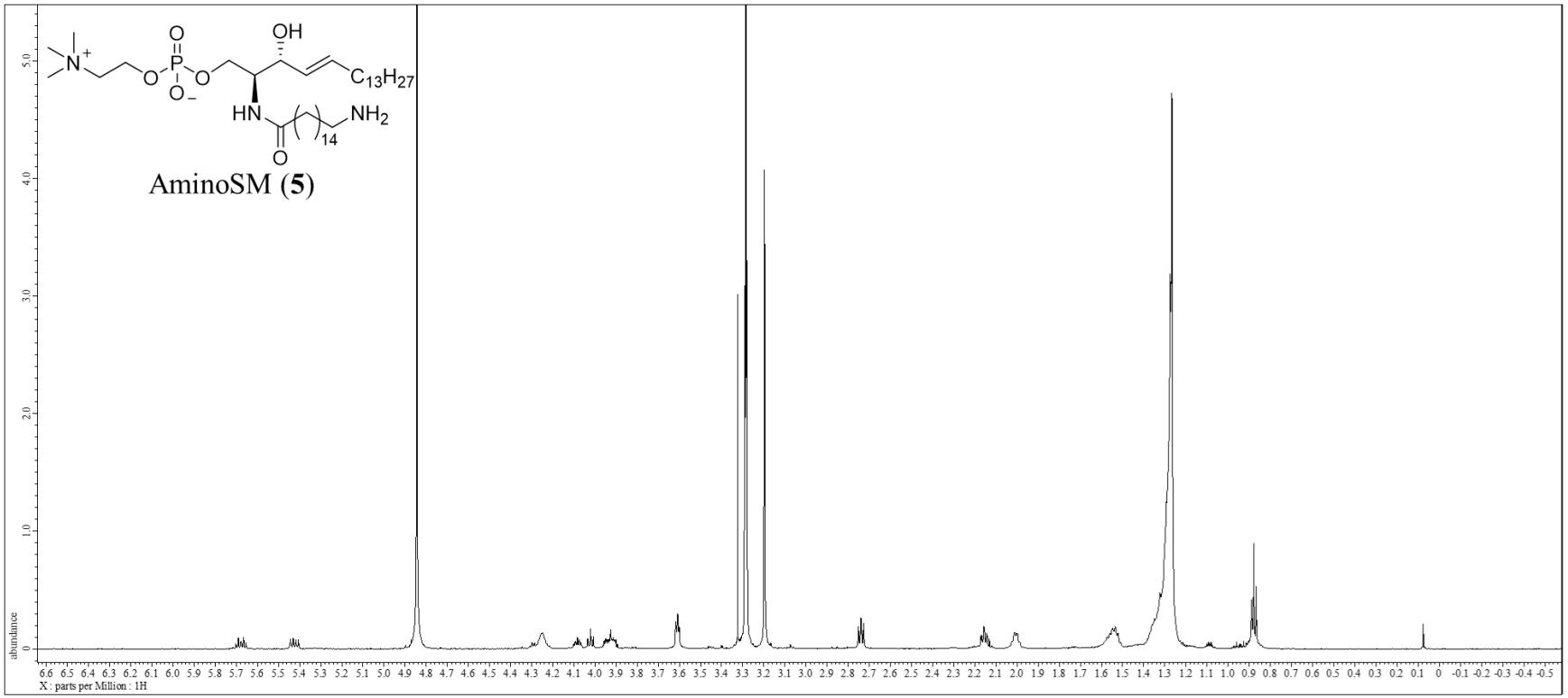

Figure S1.5. 600 MHz ^{1}H NMR spectrum of aminoSM (**5**)

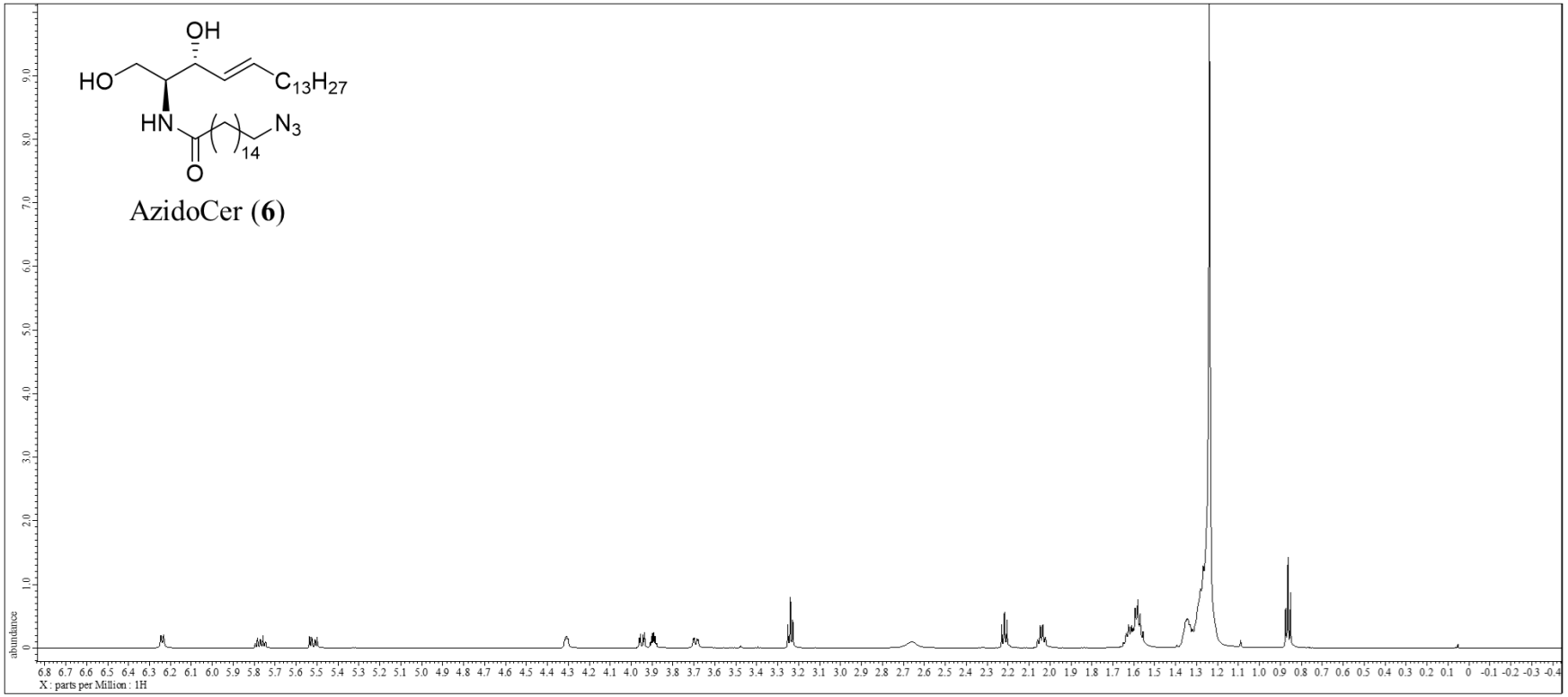

Figure S1.6. 600 MHz ^{1}H NMR spectrum of azidoCer (**6**)

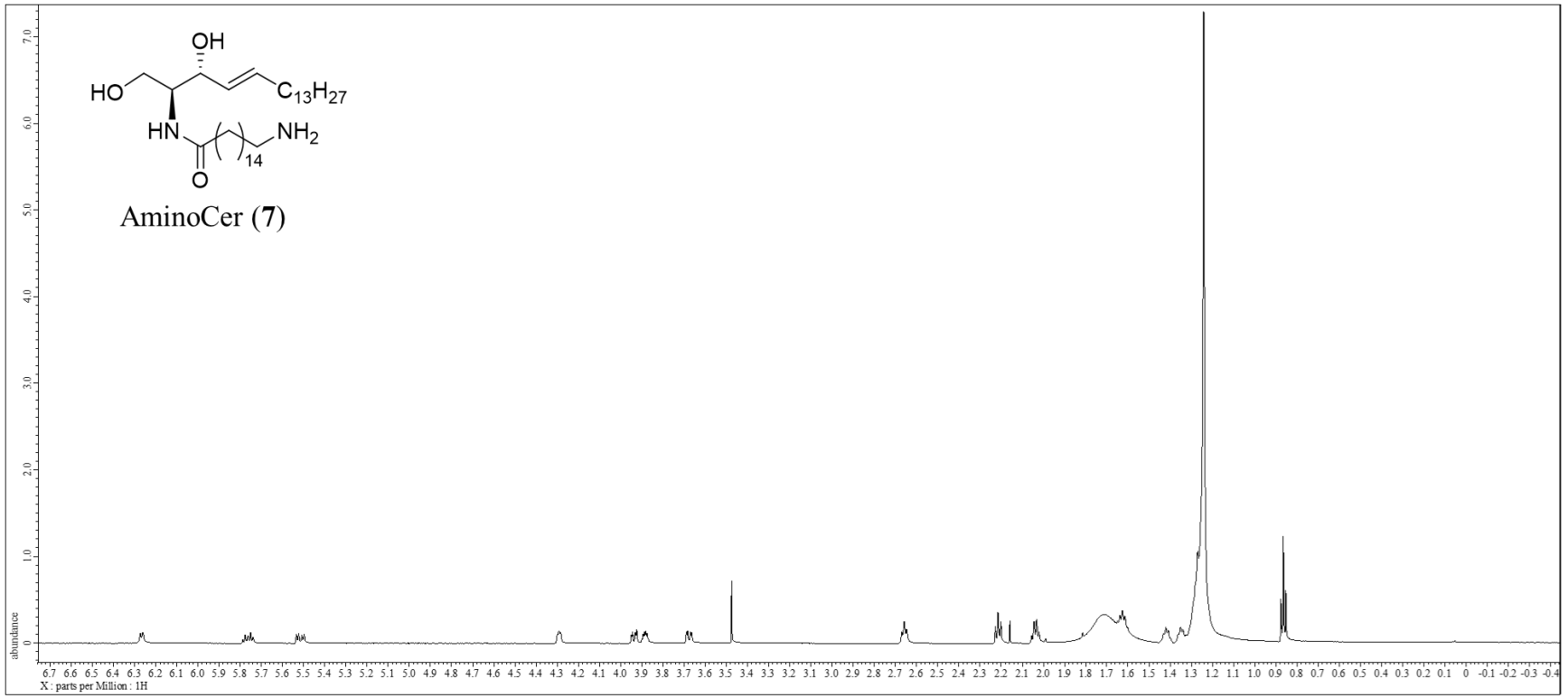

Figure S1.7. 600 MHz ^{1}H NMR spectrum of aminoCer (**7**)

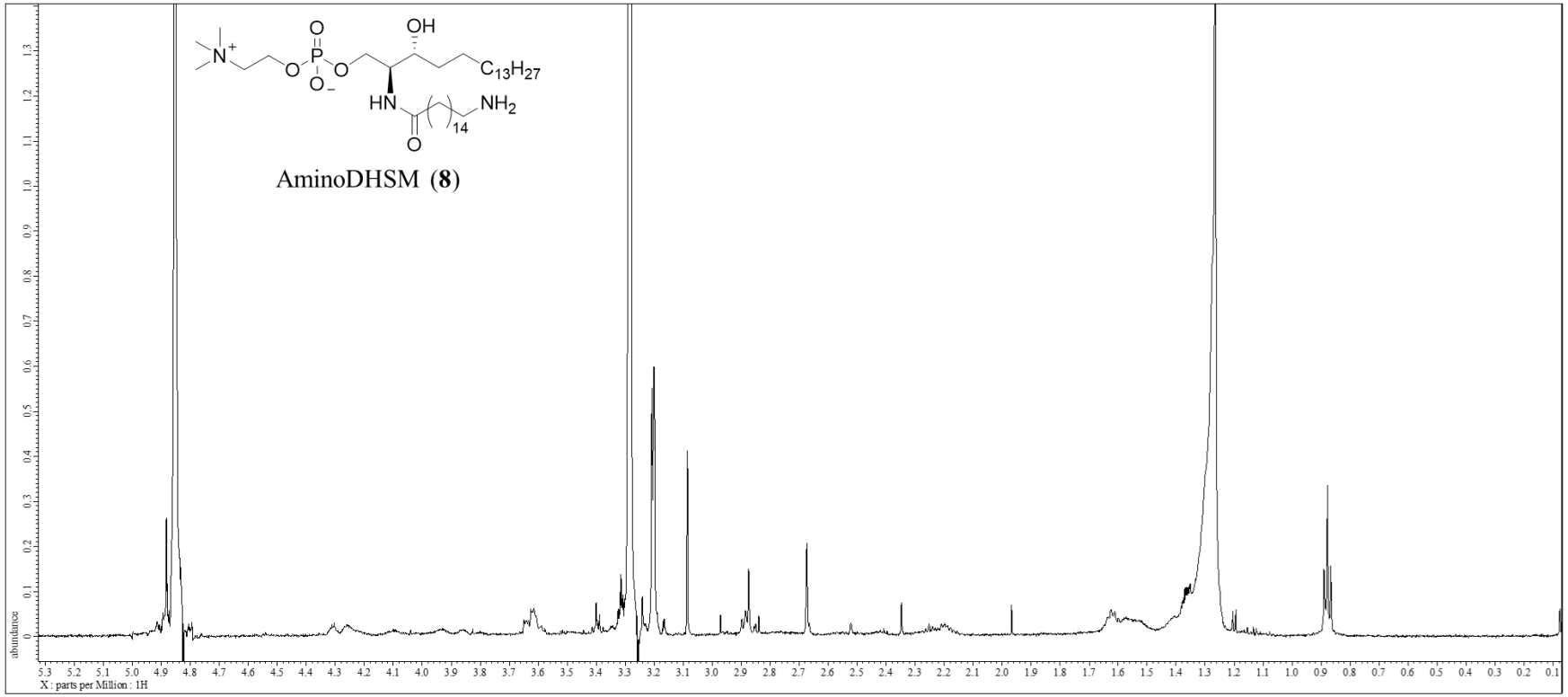

Figure S1.8. 600 MHz ^{1}H NMR spectrum of aminoDHSM (**8**)

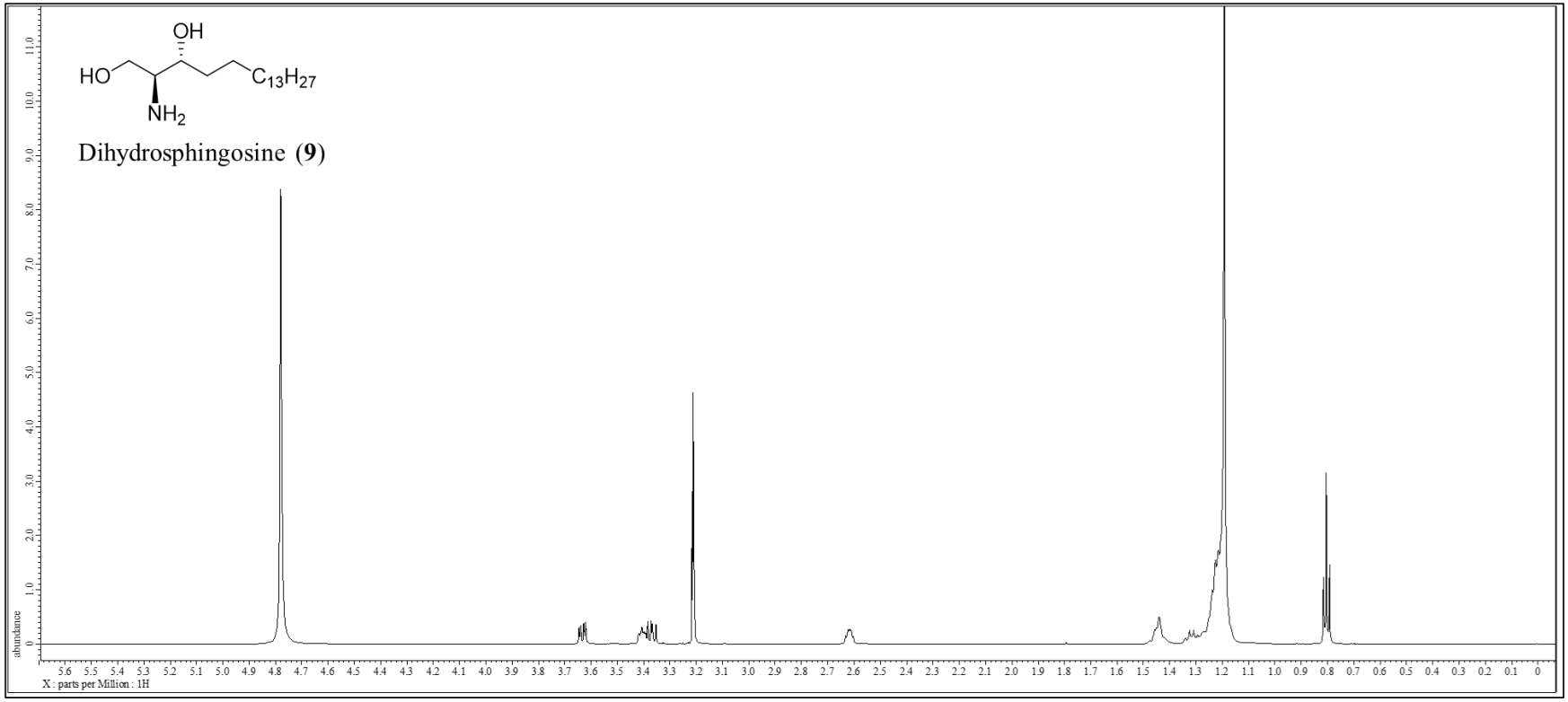

Figure S1.9. 600 MHz ^{1}H NMR spectrum of dihydrosphingosine (**9**)

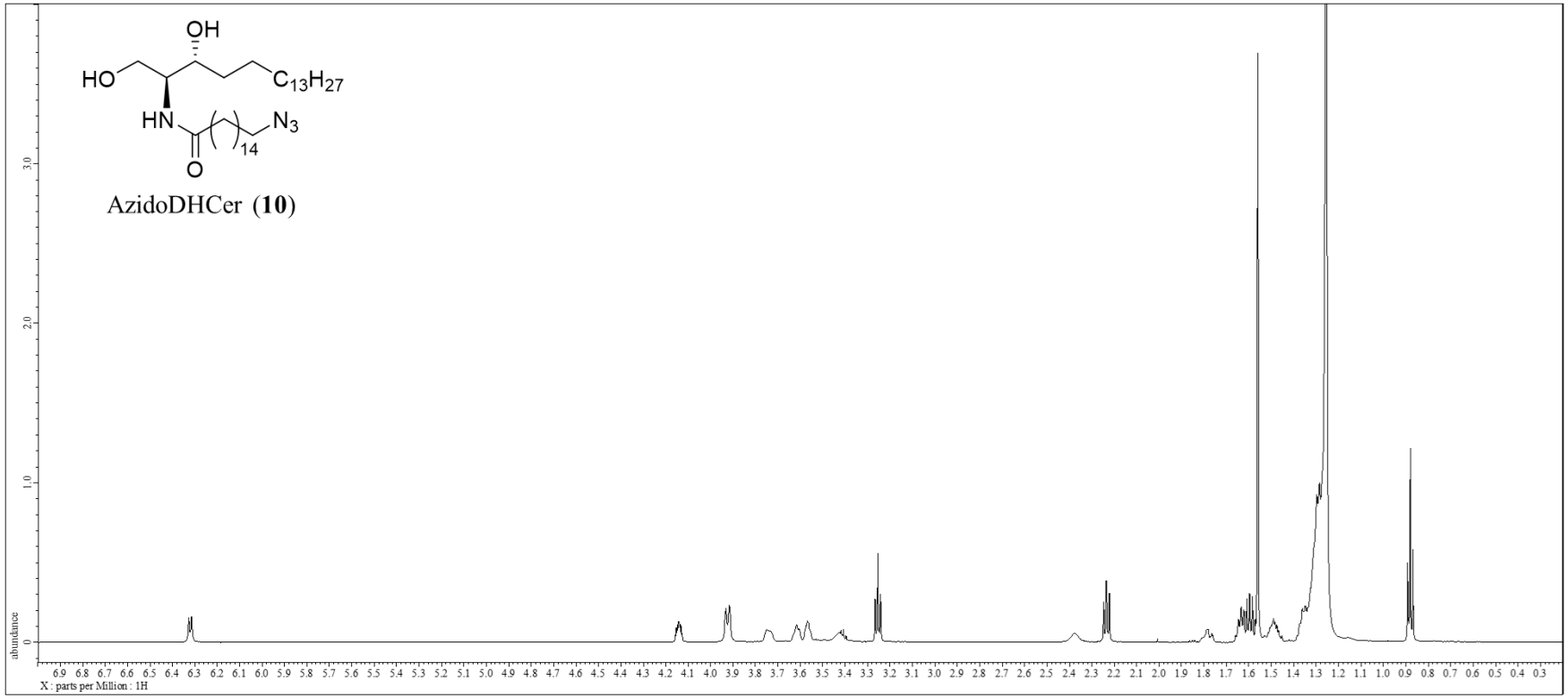

Figure S1.10. 600 MHz ^{1}H NMR spectrum of azidoDHCer (**10**)

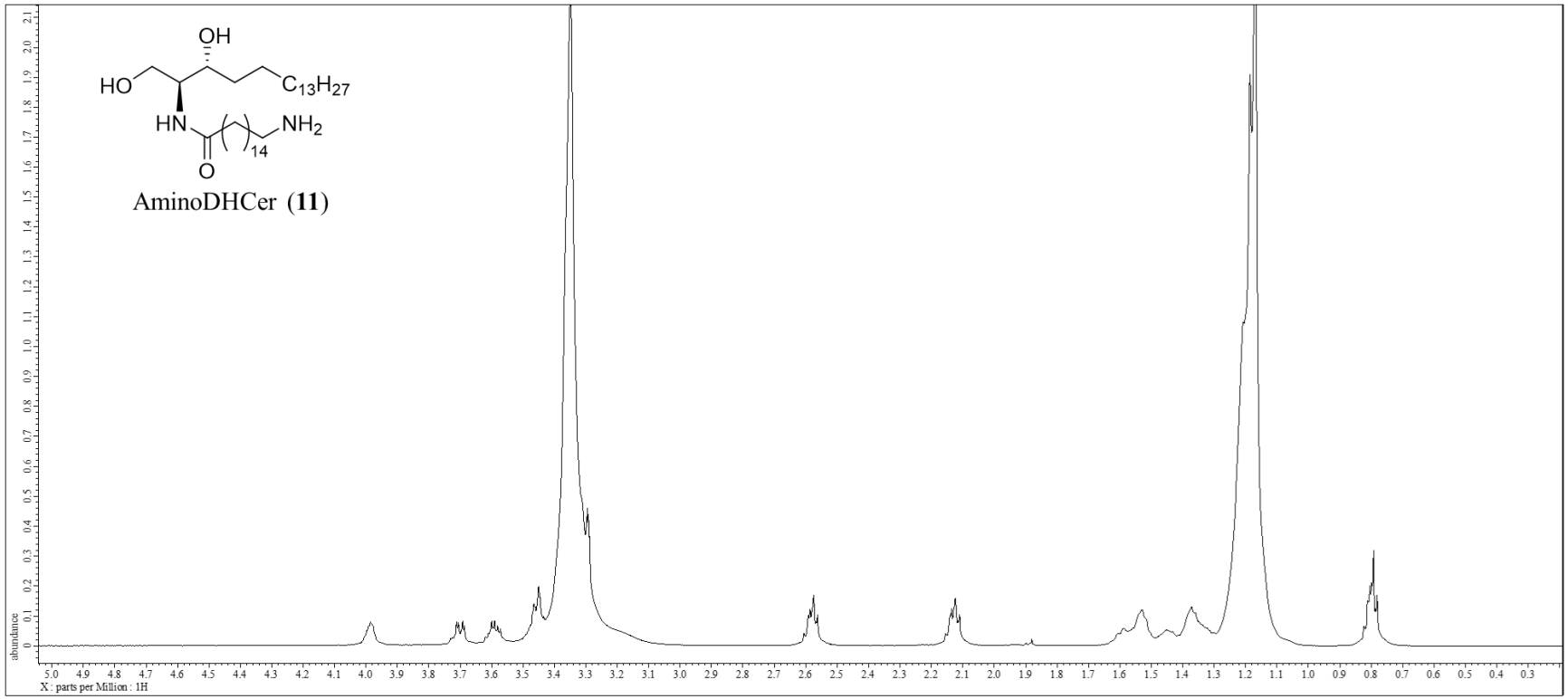

Figure S1.11. 600 MHz ^{1}H NMR spectrum of aminoDHCer (**11**)

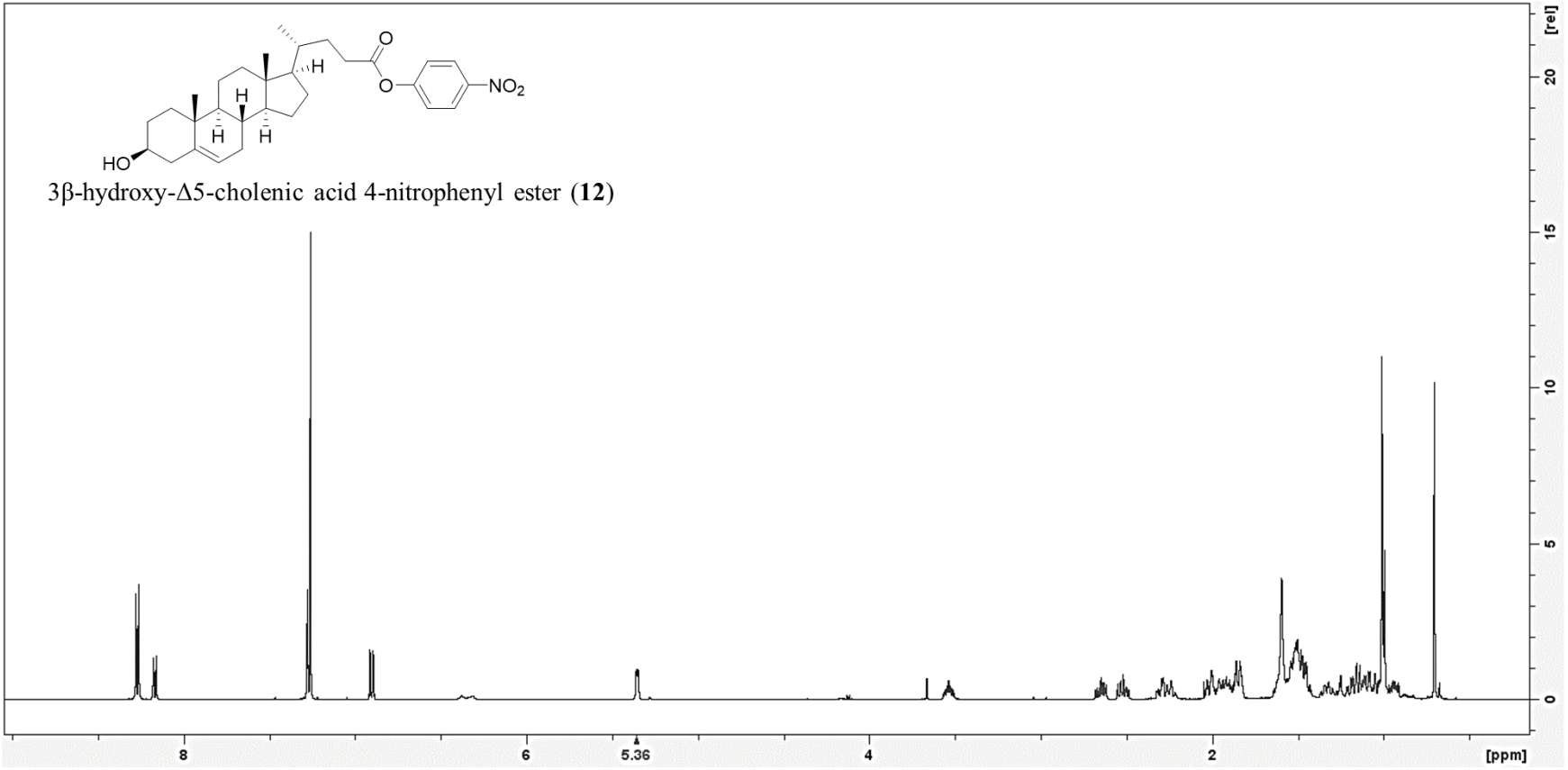

Figure S1.12. 500 MHz ^{1}H NMR spectrum of 3β-hydroxy-Δ5-cholenic acid 4-nitrophenyl ester (**12**)

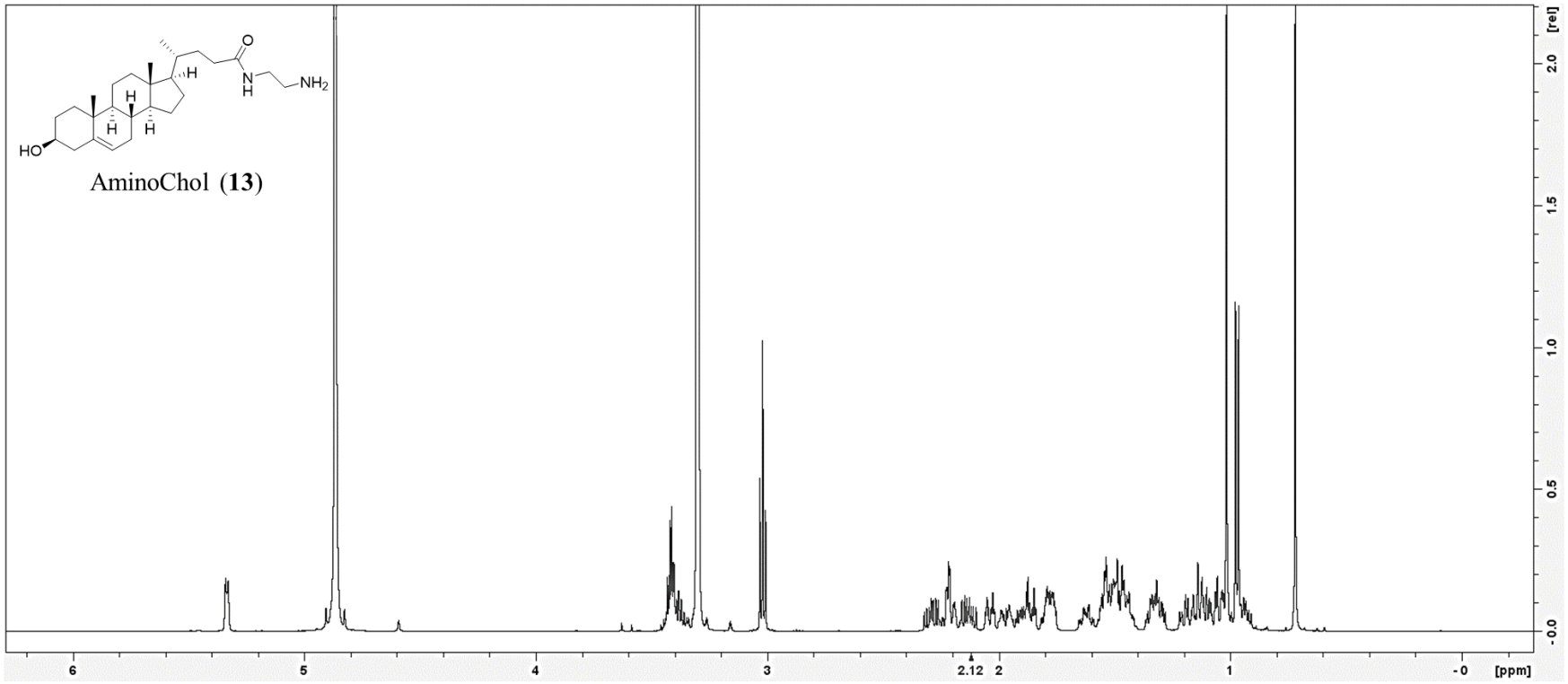

Figure S1.13. 500 MHz ^{1}H NMR spectrum of aminoChol (**13**)

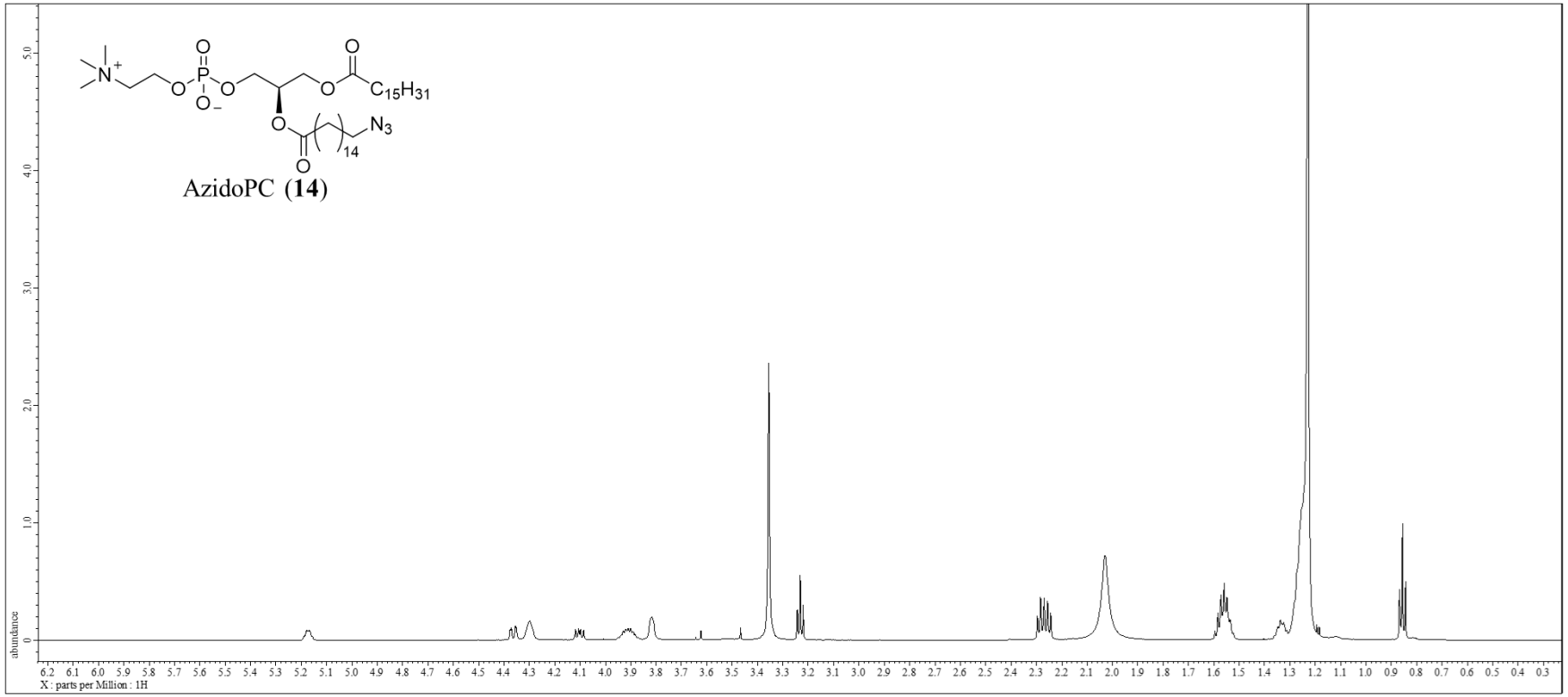

Figure S1.14. 600 MHz ^{1}H NMR spectrum of azidoPC (**14**)

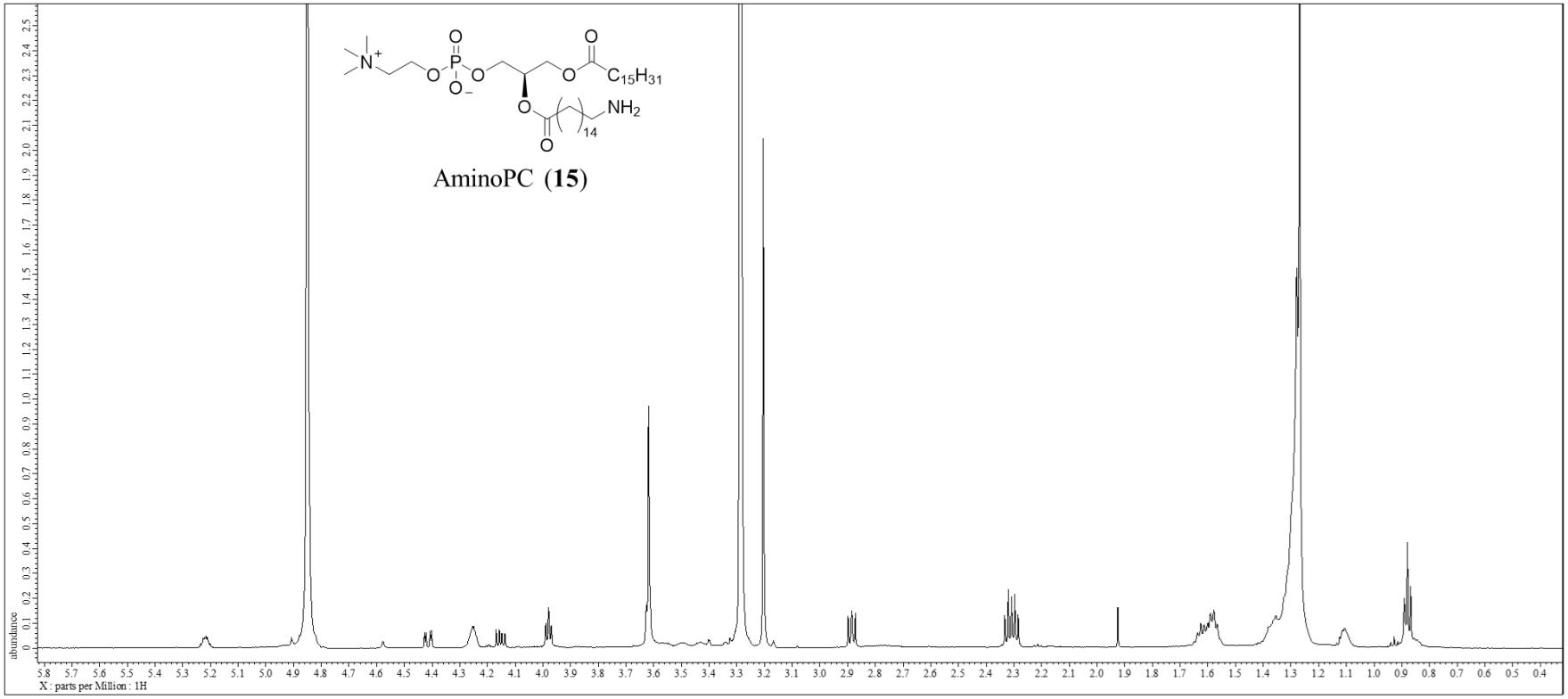

Figure S1.15. 600 MHz ^{1}H NMR spectrum of aminoPC (**15**)

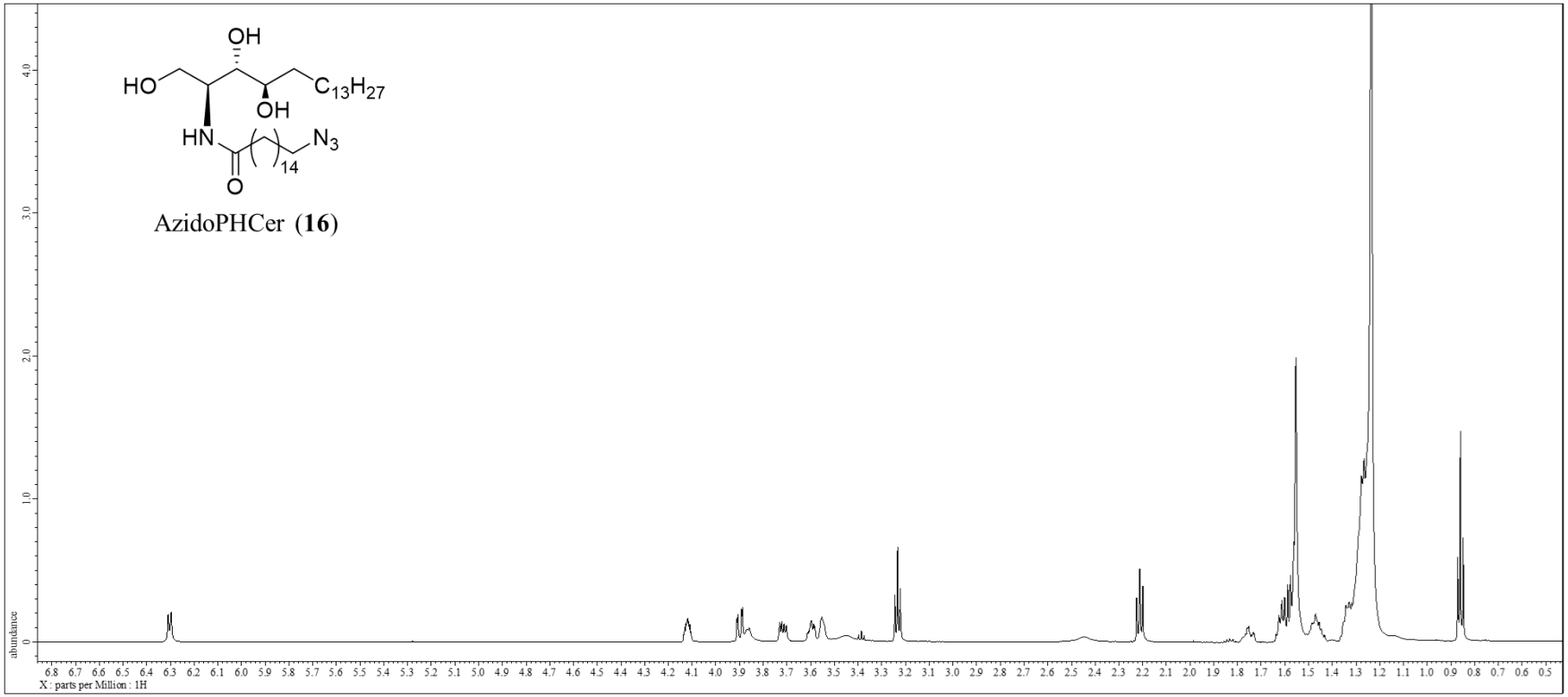

Figure S1.16. 600 MHz ^{1}H NMR spectrum of azidoPHCer (**16**)

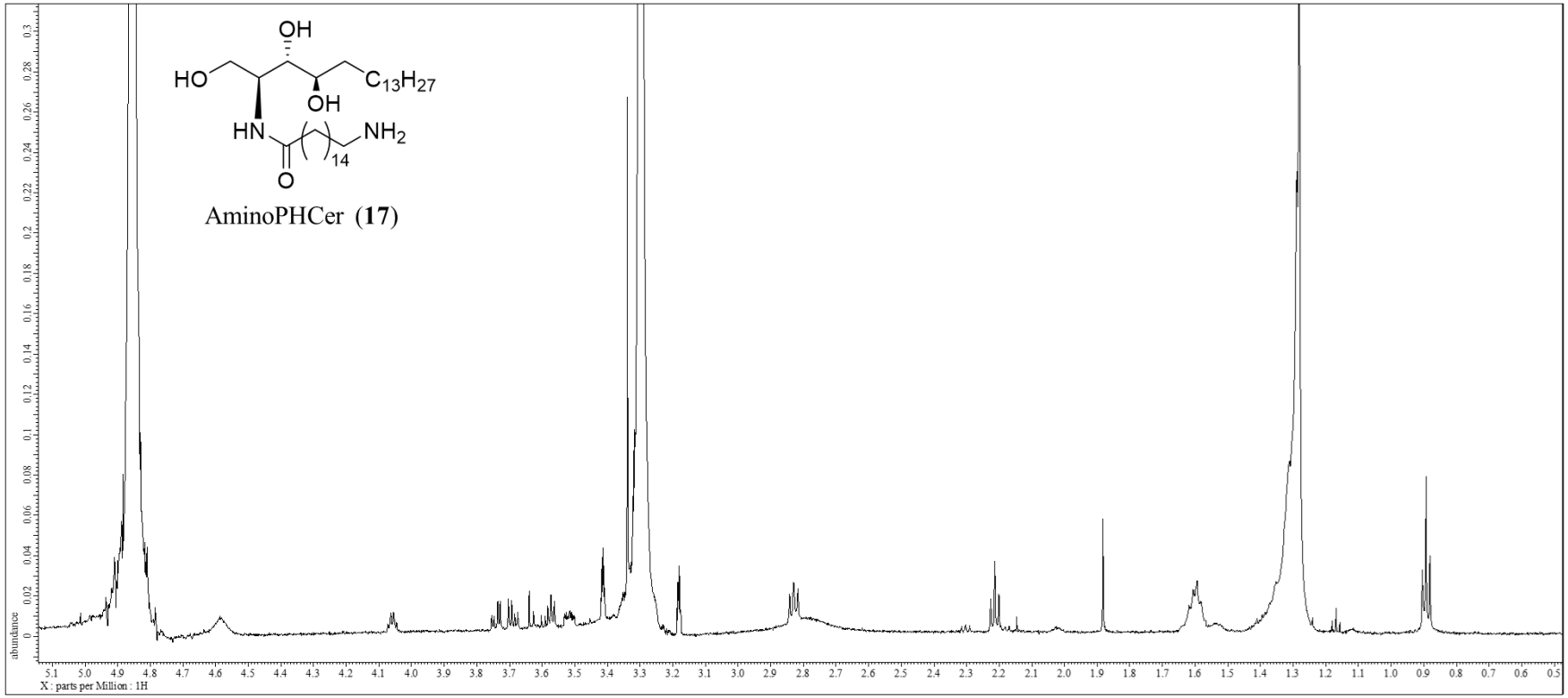

Figure S1.17. 600 MHz ^{1}H NMR spectrum of aminoPHCer (**17**)

S2. Supporting Information in Chapter 2

Table S2.1. Identified lipid binding proteins from Neuro2a cells in each band.

#1 Cer

Protein name	*Score*	*Mass*	*Number of peptides*
Keratin, type I cytoskeletal 42	123	50444	4
Bone marrow stromal antigen 2	91	19311	3
Nesprin-2	87	787997	5

#2 SM

Protein name	*Score*	*Mass*	*Number of peptides*
Proline-, glutamic acid- and leucine-rich protein 1	99	119306	4
YLP motif-containing protein 1	80	155146	4
GRB10-interacting GYF protein 2	79	149387	3

#3 SM

Protein name	*Score*	*Mass*	*Number of peptides*
Tumor protein D54	805	24085	32
MICOS complex subunit Mic19	229	26546	6
Vimentin	222	53712	11
Peptidase inhibitor 16	179	54243	5
14-3-3 protein gamma	178	28456	11
Iron-sulfur protein NUBPL	169	34402	5
Mitochondrial import inner membrane translocase subunit TIM44	165	51401	6
MICOS complex subunit Mic27	157	29356	5
Beta-actin-like protein 2	155	42319	7
HAUS augmin-like complex subunit 1	154	31416	8
MICOS complex subunit Mic25	153	30175	6
Bone marrow stromal antigen 2	153	19311	5

60S ribosomal protein L24	139	17882	3
Calcium-binding mitochondrial carrier protein SCaMC-1	134	53096	4
Transcription initiation factor TFIID subunit 9B	133	27269	5
Single-strand selective monofunctional uracil DNA glycosylase	127	31091	4
Dynamin-like 120 kDa protein, mitochondrial	126	111783	5
14-3-3 protein sigma	124	27803	7
Glutamate--cysteine ligase regulatory subunit	124	30858	4
Coiled-coil domain-containing protein 127	120	30661	7
Peripherin OS=Mus musculus	117	54349	5
Cytosolic Fe-S cluster assembly factor NUBP2	114	29898	3
Heat shock protein HSP 90-beta	113	83571	3
ADP/ATP translocase 1	112	33111	6
Proteasome subunit alpha type-3	107	28615	4
Ras suppressor protein 1	95	31531	8
B-cell receptor-associated protein 31	94	27996	7
Neurosecretory protein VGF	94	68248	4
Myeloid leukemia factor 2	93	28094	3
Epimerase family protein SDR39U1	91	31496	3
Keratin, type II cytoskeletal 79	90	57802	3
Isocitrate dehydrogenase [NADP], mitochondrial	87	51330	3
D-beta-hydroxybutyrate dehydrogenase, mitochondrial	85	38617	4
Isocitrate dehydrogenase [NADP] cytoplasmic	83	47044	3
40S ribosomal protein S17	80	15571	3
X-linked lymphocyte-regulated protein PM1	77	24711	3
Peroxisomal membrane protein PEX16	75	38710	5
Tubulin alpha-1A chain	75	50788	4

tRNA selenocysteine 1-associated protein 1	74	32744	5
60S acidic ribosomal protein P0	73	34366	3
IgE-binding protein	72	63221	5
Cytochrome c1, heme protein, mitochondrial	67	35533	3
Myosin light polypeptide 6	65	17090	3
Proteasome subunit alpha type-1	54	29813	3

#4 Cer

Protein name	***Score***	***Mass***	***Number of peptides***
Protein FAM3C	200	25022	8
Protein SCO2 homolog, mitochondrial	183	29097	7
Bone marrow stromal antigen 2	167	19311	4
Membrane-associated progesterone receptor component 2	139	23434	3
Major prion protein	133	28131	4
Keratin, type II cytoskeletal 2 epidermal	126	71336	6
Bcl-2 homologous antagonist/killer	123	23394	7
Peroxisomal membrane protein 11C	122	27533	3
Retinol dehydrogenase 11	119	35525	4
Keratin, type I cytoskeletal 15	112	49278	7
4F2 cell-surface antigen heavy chain	105	58414	6
RNA transcription, translation and transport factor protein	99	28249	7
MICOS complex subunit Mic60	98	84247	5
Keratin, type II cytoskeletal 5	95	61957	7
Peptidase inhibitor 16	92	54243	3
Tubulin beta-5 chain	90	50095	3
Melanoregulin	90	25450	3
Alpha-internexin	85	55520	3
m-AAA protease-interacting protein 1, mitochondrial	83	33249	6
ZW10 interactor	81	28866	3

Endoplasmic reticulum chaperone BiP	76	72492	4
Adenine nucleotide translocase lysine N-methyltransferase	75	25009	3
Alpha-enolase	74	47453	3
Keratin, type II cytoskeletal 2 oral	70	63319	4
Tubulin beta-4B chain	63	50255	3
Acyl-protein thioesterase 2	58	25120	3
Peroxisomal membrane protein PEX16	53	38710	3

#5 SM

Protein name	***Score***	***Mass***	***Number of peptides***
ATP synthase subunit g, mitochondrial	273	11417	13
Dynein light chain 1, cytoplasmic	160	10530	4
ATP synthase subunit e, mitochondrial	144	8230	6
Tubulin beta-5 chain	137	50095	3
ADP/ATP translocase 2	133	33138	8
Enhancer of rudimentary homolog	127	12422	4
ADP/ATP translocase 1	124	33111	10
Keratin, type II cytoskeletal 1	124	66079	4
Keratin, type I cytoskeletal 16	114	51973	5
Ubiquitin-like protein 5	107	8655	4
Small integral membrane protein 4	106	9740	5
Keratin, type I cytoskeletal 15	104	49278	5
Histone H4	90	11360	4
40S ribosomal protein S18	85	17708	4
Cytochrome c oxidase subunit NDUFA4	61	9321	4

S3. Supporting Information in Chapter 3

Supporting File 3.1: Full list of identified proteins in proteomics analysis; and list of binding proteins for each lipid (Tables S3.1.1–S.3.1.8 in Excel file)

Supporting File 3.2: Enriched GO terms and clusters of the BP category (Tables S3.2.1–S.3.2.14 in Excel file)

Supporting File 3.3: Enriched GO terms and annotation clusters of the CC category (Tables S3.3.1–S.3.3.12 in Excel file)

Supporting File 3.4: Enriched GO terms and annotation clusters of the MF category (Tables S3.4.1–S.3.4.14 in Excel file)

S4. Supporting Information in Chapter 4

Table S4.1. Identified lipid binding proteins from yeast cells in each band.

#1 DHCer

Protein name	*Score*	*Mass*	*Number of peptides*
Fumarate reductase 2	98	55202	5
Exocyst complex component EXO70	83	71534	3
Sphingosine-1-phosphate lyase	49	66037	2
Protein transport protein TIP20	41	81401	2

#2 DHCer

Protein name	*Score*	*Mass*	*Number of peptides*
Eukaryotic translation initiation factor 3 subunit A	198	110333	9
Aspartate aminotransferase, mitochondrial	151	52219	7
Cruciform cutting endonuclease 1, mitochondrial	140	41430	5
Pyruvate dehydrogenase E1 component subunit alpha, mitochondrial	140	46712	7
V-type proton ATPase subunit C	119	44218	5
Protein SBE22	72	96850	3
Exocyst complex component SEC10	68	100508	4
Farnesyl pyrophosphate synthase	67	40800	3
ADP,ATP carrier protein 2	63	34632	3
Fumarate reductase 2	54	55202	2
NADH-cytochrome b5 reductase 2	48	34144	2
Carbamoyl-phosphate synthase arginine-specific large chain	48	124465	2
Mitochondrial phosphate carrier protein	45	32962	2
Vacuolar protein sorting-associated protein 9	42	52735	2
Isocitrate dehydrogenase [NADP], mitochondrial	33	48331	2

#3 DHCer

Protein name	*Score*	*Mass*	*Number of peptides*

Glucose-6-phosphate 1-epimerase	269	34048	12
NADH-cytochrome b5 reductase 2	185	34174	11
Regulator of Ty1 transposition protein 103	134	46517	3
N-terminal acetyltransferase A complex catalytic subunit ARD1	116	27700	7
Mitochondrial phosphate carrier protein	114	32962	4
Protein BMH1	99	30187	2
ADP,ATP carrier protein 2	106	34632	4
Phosphoinositide phosphatase SAC1	96	71308	4
Protein TBF1	90	63127	2
Nucleolar pre-ribosomal-associated protein 1	55	204014	3
Inorganic phosphate transporter PHO86	55	34917	2
External NADH-ubiquinone oxidoreductase 1, mitochondrial	51	62849	2
Midasin	50	561182	2

#4 PHCer

Protein name	***Score***	***Mass***	***Number of peptides***
Regulator of Ty1 transposition protein 103	96	46517	4
Pyruvate dehydrogenase E1 component subunit alpha, mitochondrial	82	46712	3

#4 DHCer

Protein name	***Score***	***Mass***	***Number of peptides***
Regulator of Ty1 transposition protein 103	231	46517	9
Transcription initiation factor IIB	167	38746	4
54S ribosomal protein L3, mitochondrial	143	44257	5
Protoporphyrinogen oxidase	136	60064	8
Pyruvate dehydrogenase E1 component subunit alpha, mitochondrial	128	46712	5
Phosphoglucomutase 2	126	63391	6
Protein PET54	95	34616	4
V-type proton ATPase subunit D	88	29176	4

Eukaryotic translation initiation factor 3 subunit A	85	110333	2
Uncharacterized vacuolar membrane protein SCY_4679	83	74263	2
Sideroflexin FSF1	77	35506	3
40S ribosomal protein S19-A	73	15907	4
Trehalose-phosphatase	70	103539	3
Cytochrome P450 61	68	61979	2
eIF-2-alpha kinase activator GCN1	66	297995	2
V-type proton ATPase subunit H	61	54781	2
Alpha-1,2-mannosyltransferase MNN5	59	67609	2
Protein SCD6	59	39223	2
NADH-cytochrome b5 reductase 2	55	34144	2
Transposon Ty1-DR6 Gag polyprotein	53	49151	3
Aspartate aminotransferase, mitochondrial	48	52219	2
40S ribosomal protein S9-B	48	22285	2

#5 PHCer

Protein name	***Score***	***Mass***	***Number of peptides***
Transcription initiation factor IIB	93	38746	2
SRP-independent targeting protein 3	61	21180	2
Ribonucleoside-diphosphate reductase large chain 1	61	100296	2
Cyclin-dependent kinase 1	58	34268	2
Mitochondrial oxaloacetate transport protein	45	35302	2
Tyrosine--tRNA ligase, cytoplasmic	44	44220	2
Adenylosuccinate synthetase	38	48420	2

#5 DHCer

Protein name	***Score***	***Mass***	***Number of peptides***
Glyceraldehyde-3-phosphate dehydrogenase 1	194	35842	9
Transcription initiation factor IIB	115	38746	3
SRP-independent targeting protein 3	106	21180	4
UPF0674 endoplasmic reticulum membrane protein YNR021W	101	47234	3
Uncharacterized protein YDR476C	79	25421	2

Ribonucleoside-diphosphate reductase large chain 1	75	100296	2
Cyclin-dependent kinase 1	73	34268	2
Mitochondrial oxaloacetate transport protein	69	35302	3
Tyrosine--tRNA ligase, cytoplasmic	68	44220	2
Adenylosuccinate synthetase	64	48420	2
Mitochondrial dicarboxylate transporter	60	33141	2
54S ribosomal protein L3, mitochondrial	59	44257	2
Nuclear control of ATPase protein 2	57	71273	2
3-keto-steroid reductase	52	39757	2
ARF guanine-nucleotide exchange factor 2	51	166534	3
Protein transport protein SEC7	49	228227	2
Essential nuclear protein 1	46	55217	2
Transposon TyH3 Gag-Pol polyprotein	41	199337	2
Mitochondrial GTPase 1	40	42232	3
Cystathionine gamma-lyase	39	42516	2
ADP-ribosylation factor 1	36	20574	2

#6 PHCer

Protein name	***Score***	***Mass***	***Number of peptides***
SRP-independent targeting protein 3	190	21180	6
Mitochondrial phosphate carrier protein	118	32962	4
Elongation factor 1-gamma 2	74	46605	2

#6 DHCer

Protein name	***Score***	***Mass***	***Number of peptides***
SRP-independent targeting protein 3	249	21180	9
Mitochondrial phosphate carrier protein	171	32962	6
Pyruvate dehydrogenase E1 component subunit alpha, mitochondrial	146	46712	8
Signal peptidase complex catalytic subunit SEC11	107	18807	3
Epsin-3	99	45064	2
Protein kinase MCK1	86	43450	2

UPF0674 endoplasmic reticulum membrane protein YNR021W	79	47234	3
V-type proton ATPase subunit D	79	29176	5
Elongation factor 1-gamma 2	77	46605	2
Replication factor C subunit 3	69	38465	2
Peroxisomal membrane protein PMP27	68	27029	2
Nuclear control of ATPase protein 2	68	71273	3
Uncharacterized mitochondrial membrane protein FMP10	68	27681	4
Tyrosine--tRNA ligase, cytoplasmic	65	44220	2
Golgi to ER traffic protein 2	64	31474	2
Guanine nucleotide-binding protein alpha-1 subunit	64	54498	2
Dolichol-phosphate mannosyltransferase	60	30514	4
3-hydroxy-3-methylglutaryl-coenzyme A reductase 2	55	116701	2
Mitogen-activated protein kinase FUS3	54	41088	2
Endoplasmic reticulum transmembrane protein 1	43	23559	2

#7 DHCer

Protein name	***Score***	***Mass***	***Number of peptides***
eIF-2-alpha kinase activator GCN1	150	297995	4
Regulator of Ty1 transposition protein 103	135	46517	3
SRP-independent targeting protein 3	121	21180	5
Pyruvate dehydrogenase E1 component subunit alpha, mitochondrial	119	46712	7
MICOS subunit MIC26	112	27009	4
Elongation factor 1-gamma 2	111	46605	5
Uncharacterized mitochondrial membrane protein FMP10	94	27681	7
3-hydroxy-3-methylglutaryl-coenzyme A reductase 2	91	116701	2
Signal peptidase complex catalytic subunit SEC11	88	18807	2
Guanine nucleotide-binding protein alpha-1 subunit	87	54498	2
V-type proton ATPase subunit D	87	29176	4
ARS-binding factor 2, mitochondrial	80	21548	3

External NADH-ubiquinone oxidoreductase 1, mitochondrial	79	62849	2
Vacuolar protein sorting-associated protein 70	74	92131	2
Golgi to ER traffic protein 1	71	27075	3
Tyrosine--tRNA ligase, cytoplasmic	67	44220	2
mRNA-decapping enzyme subunit 2	64	108818	2
Protein SUR7	63	34093	2
Non-classical export protein 2	62	19240	4
Nucleolar protein 56	61	57057	2
UPF0674 endoplasmic reticulum membrane protein YNR021W	60	47234	2
Essential nuclear protein 1	58	55217	3
Mitogen-activated protein kinase FUS3	56	41088	2
Guanosine-diphosphatase	55	57413	2
FAD-linked sulfhydryl oxidase ERV2	54	22469	2
NADH-cytochrome b5 reductase 2	52	34144	3
Signal peptidase complex subunit SPC2	51	20789	2
Glucose-signaling factor 2	51	45955	2
Trehalose-phosphatase	47	103539	3
Protein SOP4	41	26609	2
Mitochondrial GTP/GDP carrier protein 1	39	33252	3
Nucleus-vacuole junction protein 1	37	36570	2
Vesicular-fusion protein SEC18	36	84289	2
GTP-binding nuclear protein GSP1/CNR1	35	24966	2

Table S4.2. Intensity of GFP-tagged V-ATPase and ATTO594neg lipid in vacuole membranes.

+ DHCer		+ DPPC		Control
GFP-V-ATPase	ATTO594neg-lipid	GFP-V-ATPase	ATTO594neg-lipid	GFP-V-ATPase
46.7 ± 0.9	41.3 ± 0.9	49.9 ± 0.9	67.6 ± 1.2	50.6 ± 0.8

Data are presented as mean ± *SE* (GFP: $n > 100$, ATTO594: $n > 25$)

S5. Supporting Information in Chapter 5

Table S5.1. Affinities K_A and theoretical maximum response R_{max} of lipids toward wt-KcsA, as determined using SPR method.[a] Related to Figure 5.3.

Lipid	pH 4.0 (active state)		pH 7.5 (resting state)	
	K_A	R_{max}	K_A	R_{max}
PG	$(6.06 \pm 0.35) \times 10^4$	11.0 ± 0.3	$(4.29 \pm 0.33) \times 10^4$	15.5 ± 2.1
	$(1.40 \pm 0.15) \times 10^5$	78.9 ± 0.5	$(8.83 \pm 5.89) \times 10^3$	1.13 ± 0.66
PC	$(1.18 \pm 0.06) \times 10^5$	58.7 ± 1.2	$(9.55 \pm 2.29) \times 10^4$	31.6 ± 2.8
	$(7.26 \pm 1.54) \times 10^3$	14.8 ± 2.0	$(4.03 \pm 3.63) \times 10^4$	$(1.38 \pm 0.98) \times 10^{-3}$
PA	$(1.28 \pm 0.04) \times 10^5$	24.1 ± 0.4	$(9.33 \pm 3.36) \times 10^4$	37.9 ± 1.8
	$(2.45 \pm 0.33) \times 10^5$	96.1 ± 0.6	$(3.97 \pm 1.74) \times 10^4$	1.48 ± 0.98
CL	$(9.86 \pm 4.56) \times 10^8$	93.7 ± 10.1	$(5.49 \pm 2.11) \times 10^4$	44.3 ± 3.6
	$(4.60 \pm 0.30) \times 10^4$	167 ± 3	$(3.68 \pm 2.07) \times 10^4$	2.86 ± 1.70

[a] Data are presented as mean ± *SD* ($n = 3$). The affinity is shown as the binding constants K_A (M^{-1}). Each value was calculated from the sensorgram by fitting to a 1:2 heterogeneous ligand model. R_{max} was corrected for number of immobilized proteins as 1000 RU. The heterogeneous ligand binding model assumes the following two competitive equilibriums.

$$A + B \underset{k_{off1}}{\overset{k_{on1}}{\rightleftharpoons}} AB \qquad K_{A1} = k_{on1} / k_{off1},\ R_{max1}\text{: maximum capacity 1}$$

$$A + C \underset{k_{off2}}{\overset{k_{on2}}{\rightleftharpoons}} AC \qquad K_{A2} = k_{on2} / k_{off2},\ R_{max2}\text{: maximum capacity 2}$$

In this study A is lipid, and B and C are different binding sites in KcsA, one of which was assumed specific and the other non-specific.

Table S5.2. Kinetic data of the interaction between wt-KcsA and lipids at pH 4.0.[a] Related to Figure 5.3.

	k_{on}	k_{off}
PG	$(9.39 \pm 0.29) \times 10^2$	$(1.55 \pm 0.07) \times 10^{-2}$
PC	$(6.36 \pm 0.12) \times 10^1$	$(5.39 \pm 0.37) \times 10^{-4}$
PA	$(9.51 \pm 0.55) \times 10^2$	$(7.44 \pm 0.23) \times 10^{-3}$
CL	$(2.09 \pm 0.16) \times 10^3$	$(2.56 \pm 1.44) \times 10^{-6}$

a Kinetic data were obtained from the larger kon values. Data are presented as mean ± *SD* ($n = 3$).

Table S5.3. Affinities KA and theoretical maximum response R_{max} of lipids toward ΔM0-KcsA at pH 4.0, as determined using SPR method.[a] Related to Figure 5.4.

Lipid	K_A	R_{max}
PG	$(5.58 \pm 0.74) \times 10^4$	112 ± 8
	$(1.20 \pm 0.58) \times 10^4$	48.2 ± 4.7
PC	$(1.03 \pm 0.24) \times 10^5$	65.6 ± 14.8
	$(1.43 \pm 0.60) \times 10^3$	92.9 ± 32.7
PA	$(5.89 \pm 0.74) \times 10^4$	174 ± 3
	$(4.83 \pm 0.48) \times 10^4$	32.7 ± 1.4
CL	$(1.58 \pm 0.25) \times 10^9$	94.1 ± 33.4
	$(3.95 \pm 1.11) \times 10^4$	169 ± 12

[a] Data are presented as mean ± *SD* ($n = 3$). The affinity is shown as the binding constants K_A (M^{-1}). Each value was calculated from the sensorgram by fitting to a 1:2 heterogeneous ligand model. R_{max} was corrected for amount of immobilized proteins as 1000 RU. For heterogeneous ligand model, refer to Table S5.1 caption.

Table S5.4. Affinities K_A and theoretical maximum response R_{max} of lipids toward ΔM0-KcsAs with Arg mutation, as determined using SCK method.[a] Related to Figure 5.7.

	K_{A1}	R_{max1}	K_{A2}	R_{max2}
+ E71A	$(4.60 \pm 0.03) \times 10^6$	34.0	$(6.18 \pm 0.01) \times 10^6$	248.5
+ E71A/R52Q	$(6.90 \pm 0.09) \times 10^6$	33.9	$(1.37 \pm 0.03) \times 10^{10}$	168.6
+ E71A/R64Q	$(2.47 \pm 0.02) \times 10^6$	35.6	$(6.45 \pm 0.01) \times 10^6$	84.5
+ E71A/R89Q	$(7.08 \pm 0.05) \times 10^5$	91.8	$(2.96 \pm 0.02) \times 10^6$	184.5
+ E71A/R64Q/R89Q	$(4.97 \pm 0.01) \times 10^5$	85.8	$(1.95 \pm 0.01) \times 10^6$	419.4

[a] Kinetic parameters were extracted by a global fit in SCK with *SE* ($n = 3$). The affinity is shown as the binding constants K_A (M^{-1}). K_{A1} was derived from specific binding, and K_{A2} was derived from non-specific binding. Each value was calculated from the sensorgram by fitting to a 1:2 heterogeneous ligand model. R_{max} was corrected for amount of immobilized proteins as 2000 RU. For heterogeneous ligand model, refer to Table S5.1 caption.